# THE INFLUENCE OF MICROSTRUCTURE ON THE CREEP PROPERTIES OF 441 FERRITIC STAINLESS STEEL

March 2003

A thesis submitted to the Faculty of Engineering and the Built Environment in fulfillment of the requirements for the degree of Master of Science in Engineering.


Prepared by:

MICHAEL J DOLLMAN

Supervised by:

ASSOCIATE PROFESSOR ROB KNUTSEN

# ABSTRACT

The objectives of this report were to determine the influence of microstructure on the creep properties of 441 stainless steel. Of particular interest was the effect of grain size and of the niobium content. A further requirement of this investigation was to design and manufacture two lever-arm type, constant load creep rigs in response to the need for a high quality creep test facility. These rigs were to be used to satisfy the initial objective and to evaluate an industry benchmark test used for determining the creep resistance of a particular alloy, known as the sag test.

The creep test rigs were designed in accordance with the ASTM E139-00 standard for creep testing of metallic materials. Extension, temperature and load data can be logged as a function of time and plotted in any spreadsheet program. The time necessary for building and calibrating the creep rigs was a major limiting factor. As a result, it was decided to begin calibration of the rigs with the 441 stainless steel test matrix samples. The integrity of much of the data was compromised, due to some 'teething' problems with the rigs involving the controlling and measuring of the applied load. Eventually, reliable tests could be run on the rigs, however, the results proved to be highly dependant on the way in which the user set up the test. The ideal situation is to be able to consistently run reliable, reproducible tests, regardless of who the user is. For this reason, certain recommendations have been made for minor modifications to the design, which should result in significant improvements in data quality.

Sag tests were conducted in a laboratory furnace. The results of these tests, although showing some variation, showed the expected trends of increasing creep resistance with increasing annealing temperature. Unfortunately, it was not possible to determine whether it was the increase in grain size or the increased amount of niobium in solid solution that resulted in the increased resistance to creep.

Important qualitative conclusions were drawn from the trends shown in the data and from literature. The possible mechanism of deformation was discussed in the light of microstructural observations and the applied conditions of stress and temperature during testing.

# ACKNOWLEDGEMENTS

I would like to acknowledge the following people/ organisations for their assistance and support during the course of my MSc (Eng) degree:

Columbus Stainless and the National Research Foundation (NRF) for their financial assistance with this project.

My supervisor, Associate Professor Rob Knutsen for his guidance and support throughout the duration of the project.

The entire Mechanical Engineering workshop staff at the University of Cape Town for their assistance with the commissioning of the creep test rigs. In particular I would like to thank Glen Newins for his guidance with respect to the mechanical design and manufacturing of the rigs.

Mr Andrew Semple, from UniTemp, who gave me regular advice regarding installation of the furnaces and temperature measurement.

All the staff and my colleagues at the Centre for Materials Engineering at the University of Cape Town, who made my time during the course of this project thoroughly enjoyable.

Finally, I would like to acknowledge my wife, Hazel, and my parents, Quentin and Judy, for their continued support and encouragement.

# TABLE OF CONTENTS

# CHAPTER 1

# INTRODUCTION

## 1.1 BACKGROUND TO THE PROJECT

Ferritic stainless steels, such as AISI 409, have been used extensively in automotive exhaust components. These steels exhibit excellent thermal fatigue resistance and good oxidation, condensate corrosion and creep resistance. Although the oxidation and creep resistance are not as good as that of the austenitic grades, the cost saving offered by using ferritic stainless steels is substantial. Components at the hot end of the exhaust, such as the catalytic converter, require better oxidation and creep resistance than AISI 409 can provide. Currently, 18wt% Cr ferritic steels, such as AISI 430 and 441 are in use for these components[1,2].

Columbus Stainless, a local stainless steel producer, produces 441 stainless steel for use in the manufacture of automotive catalytic converters. The bulk of the steel is exported to manufacturers of catalytic converters overseas. Certain of these manufacturers require that the steel meet stringent standards with respect to creep resistance. The industry benchmark test, which is used for ranking and comparing alloys in terms of creep resistance, is known as the sag test. This test is simple and cost effective when compared with creep testing, however, the data obtained from such a test is only really useful for comparative testing.

In order for Columbus Stainless to meet the standard that their customers require and to be able to guarantee the consistent quality of their product, it is important that they understand the effect of the thermo-mechanical processing and the resulting microstructure on the final creep properties of the alloy. It has been found in alloys stabilised with niobium that the niobium results in a substantial increase in the creep strength of the material if the final annealing temperature is high. Further research into this effect as well as the effect of grain size and other microstructural features will enable Columbus Stainless to optimise the thermomechanical processing of this alloy.

## 1.2 PROJECT OVERVIEW

The purpose of this project is to characterise the effects of the microstructure of 441 ferritic stainless steel on the creep properties. It is of specific interest to conduct creep tests and compare and evaluate the sag test results obtained to date with these results. Despite the reported reliability of the sag test results, much irregularity has been found in data collected previous to this investigation.

Different heats of 441 will be tested in order to better characterise the effect of niobium on the creep properties. The material has been supplied in the cold rolled condition (before final annealing on the plant) and the effect of changing the final annealing temperature will be investigated.

The condition of stress and temperature under which creep occurs largely determines the mechanism of creep that is operative within the material. Each mechanism is unique in its working and the way in which the microstructure relates to the creep properties will be determined by the mechanism of creep. It is therefore an important aim of this investigation to identify the operative creep mechanism in 441 under conditions similar to the service environment. This will enable a meaningful discussion of the role of various microstructural features in resisting deformation during the creep of the alloy.

A large portion of this project has been dedicated to the design, manufacture and commissioning of two lever-arm type, constant load creep testing rigs. The rigs were designed to conform to the ASTM E139-00 standards for creep testing of metallic materials[3]. The purpose of designing and building the creep rigs was to provide a high quality creep testing facility for the Centre for Materials Engineering at the University of Cape Town and for Columbus Stainless.

## 1.3 PROJECT CONSTRAINTS

This investigation aims to characterise the effect of the microstructure on the creep properties of 441 stainless steel. This objective has, however, been limited by the time used in designing, manufacturing and commissioning of the creep test rigs. Thus, the experimental matrix has been designed such that the rigs can be evaluated and the results used to obtain specific objectives with respect to the broad aim of characterising the effects of the microstructure on the creep properties.

Specifically, the test matrix was designed to allow the reliability of the sag testing to be evaluated and compared with actual creep test results. Furthermore, the effect of final annealing temperature (and hence the initial microstructure) on the creep strength will be evaluated by comparing the creep rates of the alloys after various annealing treatments.

Other limitations imposed on this project, included the lack of suitable equipment to conduct high temperature (>1050°C) isothermal annealing treatments, time taken by certain suppliers to deliver parts and materials required for manufacturing the creep test rigs and the availability of certain high temperature alloys required for the creep test apparatus.

# CHAPTER 2

# LITERATURE REVIEW

## 2.1 FERRITIC STAINLESS STEELS

### 2.1.1 Introduction to Ferritic Stainless Steels

Chromium (Cr) greatly enhances the corrosion resistance of steels by combining with oxygen ($O_2$) to form a protective passive film of chromium oxide ($Cr_3O_2$) on the steel's surface. This film prevents the iron (Fe) in the steel from oxidising, or what is more commonly known to be rusting. Should some form of mechanical damage result in penetration of the film, more $Cr_2O_3$ will form, thus the film is in a sense self-repairing. The term 'stainless' steel has arisen from the ability of chromium bearing steels to resist oxidation and other forms of corrosion in this manner. An alloy is *generally* considered to be stainless if it contains at least 11% of Cr by weight. Stainless steels can be divided into a few broad categories of alloys, namely: austenitic, ferritic, martensitic and duplex stainless steels. These are categorized according to their crystallographic structure. The structure of a particular alloy is largely dependant on the composition of that alloy. Various alloying elements are added to stainless steels to control the microstructure and hence the mechanical and/ or physical properties. Certain of these alloying elements will have a tendency to promote the formation of an austenitic, face-centred-cubic structure (austenite formers), whereas others will promote the formation of a ferritic, body-centred-cubic structure (ferrite formers)[4]. The most common austenite and ferrite forming elements are listed in table 2.1.

| Ferrite Formers | Austenite Formers |
|---|---|
| Chromium (Cr) | Nickel (Ni) |
| Molybdenum (Mo) | Carbon (C) |
| Silicon (Si) | Manganese (Mn) |
| Niobium (Nb) | Cobalt (Co) |
| Tantalum (Ta) | |
| Titanium (Ti) | |
| Tungsten (W) | |
| Vanadium (V) | |
| Aluminium (Al) | |

**Table 2.1:** Common ferrite and austenite forming elements present in stainless steel alloys.

In order to take into account the combined effect of each of these elements, relative to the effect of the primary alloying additions, namely Cr (a ferrite former) and Ni (an austenite former), the concept of Cr and Ni equivalent compositions was developed. These equivalent compositions are plotted on a set of axes known as a Schaeffler diagram (figure 2.1) allowing the compositional ranges of each of the main categories of stainless steel to be superimposed onto one diagram[4].

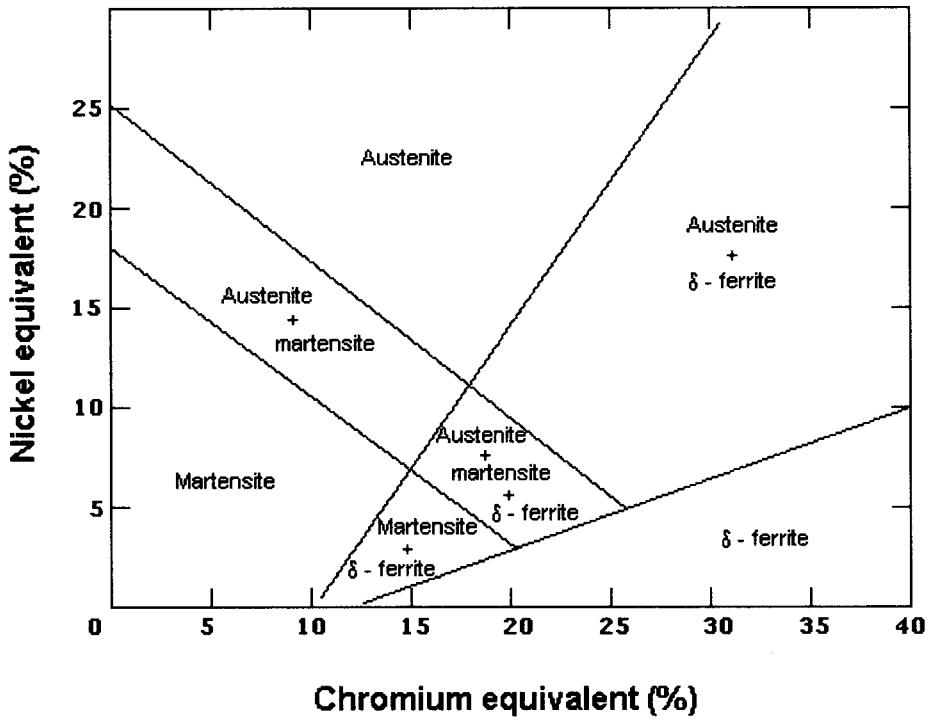


**Figure 2.1:** Schaeffler Diagram.

The Cr and Ni equivalent compositions of a particular alloy can be calculated using equations 2.1 and 2.2[4].

$$Cr_{eq} = \%Cr + \%Mo + 1.5(\%Si) + 0.5(\%Nb) + 0.5(Ta) + 2(\%Ti) + \%W + \%V + \%Al \qquad (2.1)$$

$$Ni_{eq} = \%Ni + 30(\%C) + 0.5(\%Mn) + 0.5(\%Co) \qquad (2.2)$$

The most common (or well known) of the stainless steels are the austenitic grade stainless steels. These include the AISI 304 and 316 grades often referred to as 18-8 stainless steel. The austenitic grades are non-magnetic and exhibit excellent corrosion resistance, but are more expensive than the other grades owing mainly to the higher percentage of Ni that they contain.

Ferritic stainless steels contain strong ferrite forming elements to ensure a completely ferritic structure, even in the presence of carbon (note the pronounced effect of C as an austenite former

in equation 2.2). The mechanical properties of the ferritic grades are generally inferior to those of the austenitic grades. The yield strength is relatively low (±300MPa) in the annealed condition and they generally exhibit poor toughness. This, combined with the poor weldability due to a susceptibility to experience intergranular corrosion (see § 2.1.2) in the heat-affected zone (HAZ), is not favourable for fabrication purposes[4].

### 2.1.2 Sensitisation and Stabilisation in Ferritic Stainless Steels

The susceptibility of stainless steels to intergranular corrosion after welding or thermomechnical processing is known as *sensitisation*. This sensitisation can generally be attributed to the formation of Cr depleted zones as Cr precipitates out of solution in the form of unfavourable Cr carbonitrides ($Cr_{23}C_6$ and $Cr_2N$). This precipitation generally occurs along the grain boundaries when the steel is heated to above 900°C. Ferritic stainless steels in particular are susceptible to this type of attack since the solubility of carbon (C) and nitrogen (N) in the ferrite matrix is low[4]. In order to overcome this problem, the amount of C and N in the steel could be kept to below the limit of solubility. However, by refining the steel to achieve these levels of C and N would substantially increase production costs and negate one of the primary benefits of using ferritic stainless steels (viz. cost effectiveness). Certain elements that combine with C and N to form stable carbonitrides in preference to Cr are therefore added. This technique of preventing the precipitation of Cr carbonitrides is commonly known as *stabilisation*[5].

Alloying elements that have been found to best stabilise ferritic stainless steels are titanium (Ti), niobium (Nb) and zirconium (Zr)[5].

The addition of Ti results in the formation of very stable titanium carbonitrides, Ti(C,N). In order for full stabilisation to occur, a slightly larger amount of Ti than is stoichiometrically required (in terms of the amount of C and N) must be added. Reasons for this are because some Ti may react with sulphur (S) in the steel and some may remain in solid solution. The amount of Ti usually added to ferritic stainless steel is given by equation 2.3[6].

$$\%Ti = 5 \times (\%C + \%N) \tag{2.3}$$

Ti is effective as a stabilising element, because besides forming carbonitrides, it also raises the temperature at which sensitisation occurs since Ti(C,N) only dissolves at very high temperatures. There are, however, certain disadvantages associated with the addition of Ti. For example, the toughness of the steel is lowered since Ti(C,N) precipitates are large and blocky in shape.

Sensitisation may occur in ferritic stainless steel stabilised with Ti at high temperatures, where Ti(C,N) can dissolve[5].

Nb is a more expensive alloying element than Ti. Although Nb carbonitrides, Nb(C,N), are less stable than Ti(C,N), stabilising with Nb does offer the advantage of forming fine, equiaxed precipitates that do not decrease the toughness of the steel. Nb is added to steel in the amount given by equation 2.4[6].

$$\%Nb = 9 \times (\%C + \%N) \tag{2.4}$$

It has been found that stabilisation with both Ti and Nb (known as dual stabilisation) effectively stabilises the steel by binding all the C and N into stable Ti,Nb(C,N). The toughness of the steel is not decreased as extensively as with stabilisation using Ti, since fewer large Ti(C,N) precipitates are formed because a smaller proportion of Ti is added[5].

The effect of adding Zr as a stabilising element to ferritic stainless steels is similar to those experienced when adding Ti. Zr is more expensive than Ti, although alloys stabilised with Zr are reported to exhibit excellent high temperature oxidation resistance. Zr is generally not used as a stabilising element in practice- probably due to the high cost[5].

### 2.1.3 High Temperature Applications of Ferritic Stainless Steels

As was mentioned earlier, the low Ni content in ferritic stainless steels results in these alloys being far cheaper than austenitic alloys. For this reason, ferritic stainless steels are often preferred for high temperature applications, despite the generally better corrosion resistance and mechanical properties of the austenitic grades. In terms of mechanical properties at elevated temperatures, ferritic stainless steels do have the advantage of exhibiting better thermal fatigue resistance than austenitic grades due to a higher thermal conductivity and lower coefficient of thermal expansion. A high resistance to liquid metal attack makes these alloys good candidates for use in the lead and copper metal industries[4].

Some common high temperature applications include automobile exhaust components, steam turbine rotors, boiler tubing, heating elements and components for nuclear reactors and petroleum refineries[7].

The recent legislature in certain countries[8,9] requires that emissions from automobile exhausts be significantly reduced. Therefore, the use of catalytic converters (which were developed in the

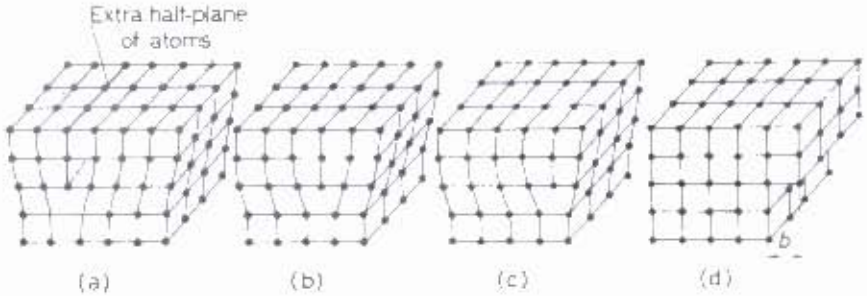


**Figure 2.2:** Glide of an edge dislocation through crystal lattice. After Smallman[14].

A dislocation may move through an entire crystal, resulting in the upper portion of the crystal having slipped a certain distance relative to the lower portion. The direction and magnitude of this slip is given by the Berger's vector, *b*, as shown in figure 2.2 (d). For an edge dislocation, *b* is parallel to the slip direction and perpendicular to the dislocation line. The converse is true of a screw dislocation, where *b* is perpendicular to the slip direction and parallel to the dislocation line[15]. This is illustrated in figure 2.3 (c).

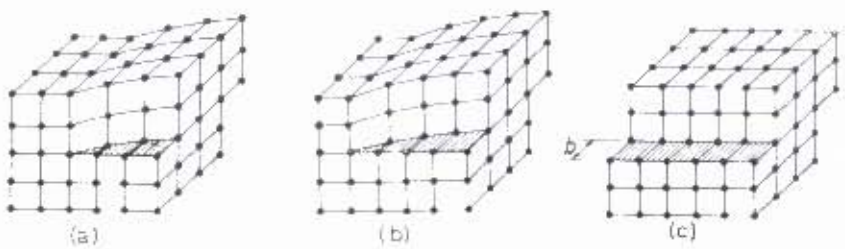


**Figure 2.3:** Glide of a screw dislocation through the crystal lattice. The slip direction is to the left. After Smallman[14].

Figures 2.2 and 2.3 illustrate the glide of dislocations in a simple cubic structure. Most metals, however, have a face-centred cubic (FCC), body-centred cubic (BCC) or hexagonal close packed (HCP) structure. The mechanism of glide in these structures is not different to that in a simple cubic structure, however, the slip planes in each structure will be unique. The combination of a preferred slip plane (usually a close packed plane) and a slip direction is known as a slip system. Ferritic stainless steel has a BCC structure, the unit cell of which is illustrated in figure 2.4.

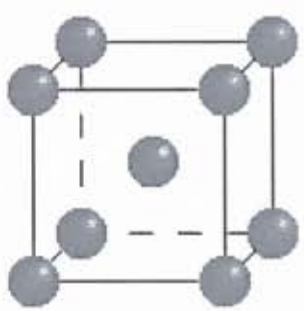

**Figure 2.4:** Unit cell of a body-centred cubic crystal structure.

It is important to realize that shear stresses arise under loading conditions where the applied stress is not a shear stress. A dislocation will only move in a particular direction along a given slip plane if the shear stress on that slip system exceeds a critical value. This value of shear stress is known as the critical resolved shear stress (CRSS) and is also known as the Peierls stress (in a perfect crystal). Therefore, the slip system that experiences the highest resolved shear stress will be the first system on which slip will occur. As the stress increases, or as crystals in the material rotate relative to the tensile axis, other slip systems may become active[14].

The CRSS can be determined by considering a single, cylindrical crystal of area, $A$, under a tensile load, $P$, as shown in figure 2.5 below.

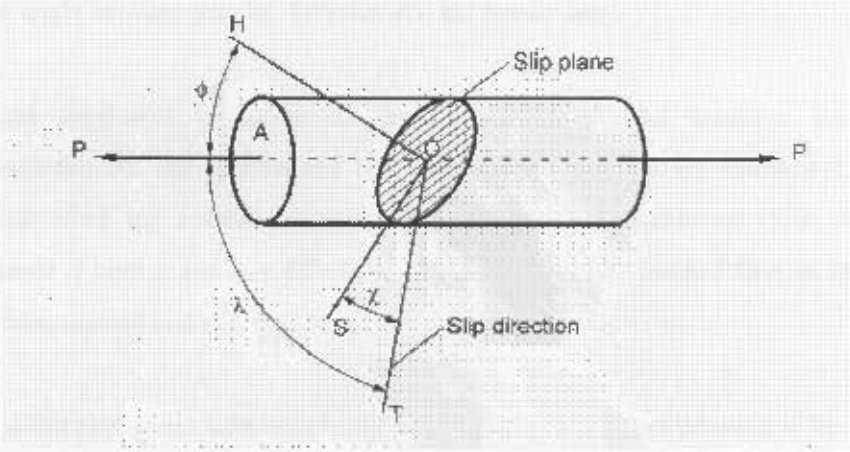


**Figure 2.5:** Single, cylindrical crystal indicating slip plane, slip direction and tensile axis. After Smallman[14].

The area of the slip plane can be given by equation 2.5:

$$A_{slipplane} = \frac{A}{\cos\phi} \tag{2.5}$$

where $\phi$ is the angle between the slip plane normal (OH) and the tensile axis. The applied load, $P$, may be resolved into a normal force (along OH) and a shear force along the line of greatest slope in the slip plane (viz. OS). These forces are given by the following equations:

$$P_{Normal} = P\cos\phi \tag{2.6}$$

$$P_{Shear} = P\sin\phi \tag{2.7}$$

The corresponding stresses can be calculated by dividing by the slip plane area, $A_{slipplane}$.

$$\sigma_{Normal} = \frac{P\cos\phi}{A/\cos\phi} = \left(\frac{P}{A}\right)\cos^2\phi \tag{2.8}$$

$$\tau = \frac{P\sin\phi}{A/\cos\phi} = \left(\frac{P}{A}\right)\cos\phi\sin\phi \tag{2.9}$$

The line of greatest slope (OS) is generally not coincident with the slip direction, therefore the resolved shear stress (RSS) on the slip plane in the slip direction can be calculated using:

$$\tau_{RSS} = \left(\frac{P}{A}\right)\cos\phi\cos\lambda \tag{2.10}$$

where $\lambda$ is the angle between the slip direction and the tensile axis.

The expression $\cos\phi.\cos\lambda$ is known as the Schmid factor and describes the geometrical relationship between the slip system and the tensile axis. Considering equation 2.10, the RSS will be greatest when the Schmid factor is a maximum. The maximum value of the Schmid factor is obtained if both $\phi$ and $\lambda = 45°$. Thus the CRSS will be reached first on the slip system with its slip plane normal and slip direction closest to 45°[14].

The glide of dislocations and subsequent slip of crystal planes is not possible if the CRSS is not exceeded. If, however, the CRSS is exceeded, dislocation movement may still be impeded by the presence of obstacles such as solute atoms and precipitate particles. In order for dislocations to pass these obstacles, they must climb (edge dislocations) or cross-slip (screw dislocations)[12].

In the process of dislocation climb, vacancies diffuse to the dislocation line (with mechanical stress being the driving force) causing the dislocation line to '*climb*'. Figure 2.6 illustrates the diffusion of a vacancy to the dislocation line resulting in climb of the dislocation by one lattice position.

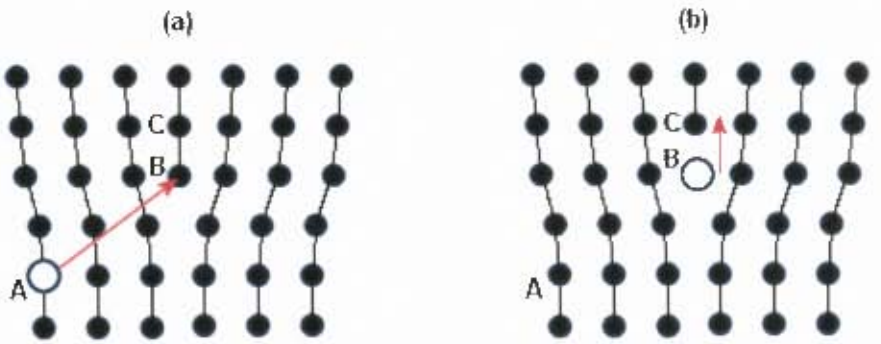


**Figure 2.6:** (a) A vacancy diffuses from A to the dislocation line at B, resulting in (b), the climb of the dislocation by one lattice position from B to C[16].

This climb allows dislocations to move around obstacles, such as precipitate particles, resulting in continued dislocation glide as illustrated in figure 2.7[16]. Thus although plastic deformation may occur by the glide of dislocations, the rate at which it occurs is determined by the rate of diffusion, which is largely dependent on the temperature (see § 2.2.2).

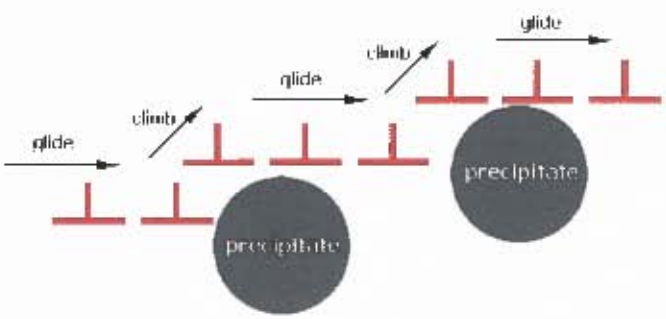


**Figure 2.7:** Glide and climb of dislocations around precipitate particles[16].

The glide of a screw dislocation is not restricted to a single slip plane, as with an edge dislocation. This means that the dislocation can 'cross-slip' into another slip plane and thus move around an obstacle in the lattice in this manner.

Dislocations may dissociate into one or more *partial* dislocations. Consider the top view of an edge dislocation in figure 2.8 (a). In order for slip to continue, the dislocation must glide a distance described by the Burger's vector, *b*. The Burger's vector may be resolved into two components, *c* and *d*, which describe an easier path for slip to occur, since this lowers the total strain energy. Thus the dislocation dissociates into two partial dislocations (figure 2.8 (b)). This process may continue as shown by figure 2.8 (c), resulting in a larger separation between the partial dislocations.

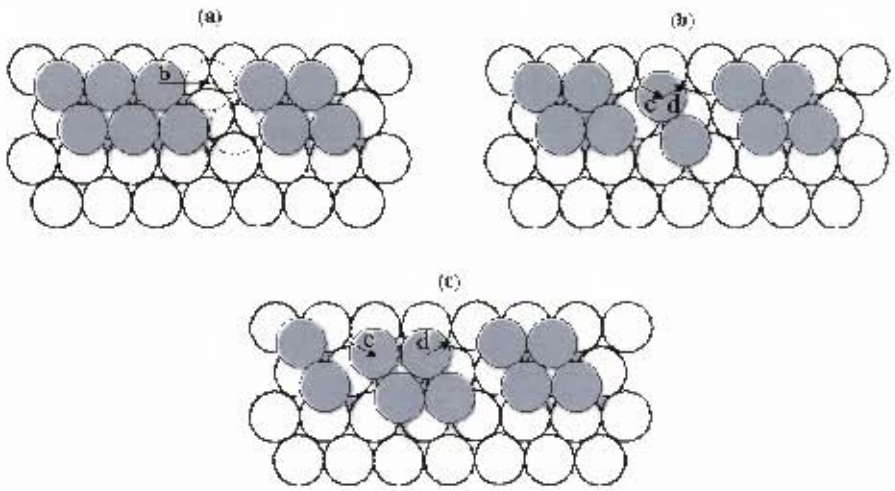


**Figure 2.8:** Formation of a partial dislocation and the resulting stacking fault in a FCC crystal. After Stouffer and Dame[17].

The atoms between the partial dislocations are no longer stacked in the correct sequence, resulting in a so-called *stacking fault*. The distortion energy associated with this fault is known as the stacking fault energy and the magnitude of this energy determines the width of the core (i.e. the separation distance between partial dislocations)[17]. The stacking fault energy will be described further in § 2.2.3.1.

When glide occurs, dislocations may interact with other dislocations as they intersect one another's glide planes. The interaction of dislocations in the lattice can result in discontinuities within those dislocations. These discontinuities can be in the form of kinks or jogs. A kink is a discontinuous step in the dislocation line in the slip plane of that dislocation (figure 2.9 (a)). A jog is similar discontinuity, however the step in the dislocation line is onto a different slip plane (figure 2.9 (b)).

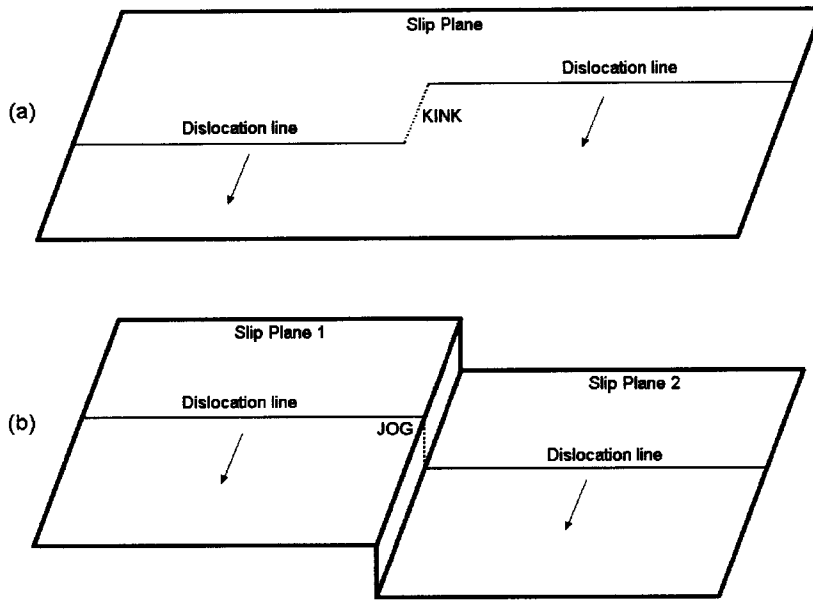


**Figure 2.9:** (a) A kink in an edge dislocation. (b) A jog in an edge dislocation. After Stouffer and Dame[17].

Because kinks lie in the slip plane, little impediment to dislocation glide is provided. Jogs, however, can impede the motion of dislocations or even pin them. By pinning, it is meant that the dislocation is prevented from gliding by the jog[17].

### 2.2.2 Diffusion in Metallic Materials

Diffusion becomes significant in metals at high temperatures (generally greater than 0.4 times the melting temperature) and thus a sound understanding of the fundamental principles of diffusion is necessary to gain a good understanding of the behaviour of metals at elevated temperatures. Self-diffusion is defined as being the transport of matter in an elemental substance (e.g. Fe atoms diffusing through Fe metal). The exact mechanisms of diffusion in solids due to temperature or concentration gradients are not certain, however, it is generally accepted that the self-diffusion of atoms is equivalent to the diffusion of vacancies through the lattice in the opposite direction[15]. At high temperatures, there is sufficient thermal energy for diffusion to progress through bulk material in grain interiors, whereas at lower temperatures, diffusion occurs along paths offering less resistance such as grain boundaries[14].

Diffusion occurs in response to the existence of a concentration gradient of the diffusing species. In the case of vacancy diffusion, a difference in the concentration of vacancies at one point with respect to another will result in a migration of vacancies down the concentration gradient. This will obviously only occur when temperatures are high enough for diffusion to be possible. The

rate at which this diffusion occurs is defined by a quantity termed the flux, $J$. Under steady state conditions, the flux is proportional to the concentration gradient (equation 2.11)[18].

$$J = -D\frac{dc}{dx} \tag{2.11}$$

This is known as Fick's first law of diffusion. The proportionality constant, $D$ in this equation is the diffusion coefficient and is characteristic of the material through which diffusion is occurring. $dc/dx$ is the concentration gradient, where $c$ is the concentration and $x$ the distance over which the gradient is calculated. The diffusion coefficient can be calculated using equation 2.12:

$$D = D_0 e^{\left(-Q_0/RT\right)} \tag{2.12}$$

where, $D_0$ is a constant, $Q_0$ is the activation energy, $R$ is the universal gas constant and $T$ is the absolute temperature. It has been found that the values of $D_0$ for different materials with the same crystal structure are very similar, indicating that the rate of diffusion is largely dependent on the crystal structure of the material. $Q_0$ is dependant on the bonding in the material and has a significant effect on the rate of diffusion.

Thus, from equations 2.11 and 2.12, it can be seen that the rate of diffusion is dependent on the concentration gradient of diffusing species, the crystal structure and possibly most significantly on the temperature (since $R$ is a constant and $D_0$ and $Q_0$ are constant for a particular material).

### 2.2.3 Recovery and Recrystallisation

#### 2.2.3.1 Stacking Fault Energy

The stacking fault energy ($\gamma_{SFE}$) is a material dependent quantity and determines the degree to which dislocations will dissociate into partial dislocations. The lower the value of $\gamma_{SFE}$, the easier it is for this dissociation to occur (i.e. the distance between 2 partial dislocations will be large). This is significant, because the formation of partial dislocations will hinder the climb and cross-slip of dislocations. Two partial dislocations must recombine before climb or cross-slip is possible. Therefore, the climb and cross-slip of dislocations occurs readily in materials with a high value of $\gamma_{SFE}$ (where the distance between 2 partial dislocations is small) if there is sufficient thermal energy available. Approximate values of $\gamma_{SFE}$ for various materials are tabulated in table 2.2[19].

| Material | $\gamma_{SFE}$ (mJm$^{-2}$) |
|---|---|
| Aluminium | 166 |
| Copper | 78 |
| Nickel | 128 |
| AISI304 Stainless Steel | 21 |

**Table 2.2:** Approximate values of $\gamma_{SFE}$ for various metals[19].

Ferritic stainless steels are known to have a high value of $\gamma_{SFE}$. Thus the rate of dislocation climb and cross-slip in these materials occurs more readily than in materials having lower $\gamma_{SFE}$.

### 2.2.3.2 Recovery

The stored energy in the lattice of a plastically deformed metallic material is high due to the formation and movement of dislocations in the microstructure. As a result of this, there is a driving force to reduce the amount of stored energy in the microstructure in accordance with the second law of thermodynamics. Recovery is the process by which dislocations rearrange themselves into low energy configurations, forming a subgrain structure in the lattice. Subgrains are defined as grains whose relative misorientation is less than 15°[19]. In order for this dislocation rearrangement to occur, the climb and cross-slip of dislocations must be made possible by the availability of thermal energy[13]. Thus recovery is likely to occur during elevated temperature processes such as annealing and hot rolling, where diffusion is possible. Figure 2.10 is a schematic diagram illustrating how dislocations in a deformed material are rearranged into sub grains, which represent a lower energy configuration due to the reduction in stored energy in the lattice.

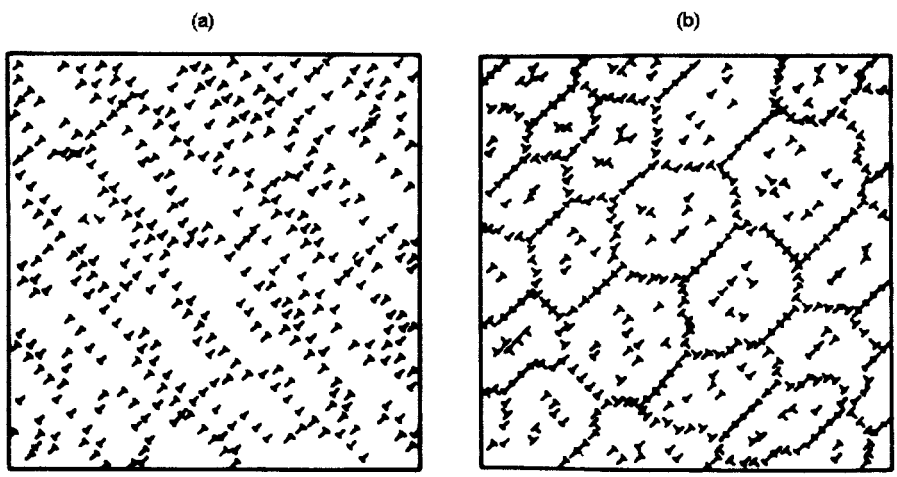


**Figure 2.10:** Plastic deformation results in the multiplication of dislocations (a). With sufficient thermal energy, dislocations form subgrains (a lower energy configuration) by climb and cross-slip (b).

Since the dislocation rearrangement occurs by the climb and cross-slip of dislocations, and the $\gamma_{SFE}$ controls the rate of climb and cross-slip (by determining the stability of partial dislocations), the $\gamma_{SFE}$ of a particular material will greatly influence the rate of recovery of that material. A material having a high $\gamma_{SFE}$ will therefore recover readily with sufficient thermal energy. For this reason, ferritic stainless steels exhibit high rates of recovery.

As mentioned before, it is important to consider recovery in high temperature processes. This includes high temperature creep. Recovery plays an important role in the creep of metallic materials at high temperatures under moderate to high stresses[20].

#### 2.2.3.3 Recrystallisation

The process of recrystallisation involves the nucleation of new strain-free grains and the growth of these grains by means of high-angle (>15°) grain boundary migration. The term 'nucleation' is however used loosely, as nucleation does not occur in the classic thermodynamic sense, but rather from small, recovered volumes (subgrains or cells) that are already present in the microstructure. The process of recrystallisation is illustrated schematically in figure 2.11. The driving force for recrystallisation is the same as that for recovery – lowering of the stored energy in the microstructure – therefore recovery and recrystallisation can be seen as competing processes. Both processes, however, can and do occur simultaneously, especially considering that a recrystallised grain with a low dislocation density must nucleate from some sort of substructure. Hence an amount of recovery is necessary for recrystallisation to proceed. If the $\gamma_{SFE}$ of a material is low, recovery will be limited and recrystallisation will be the dominant process. The converse is also true[19].

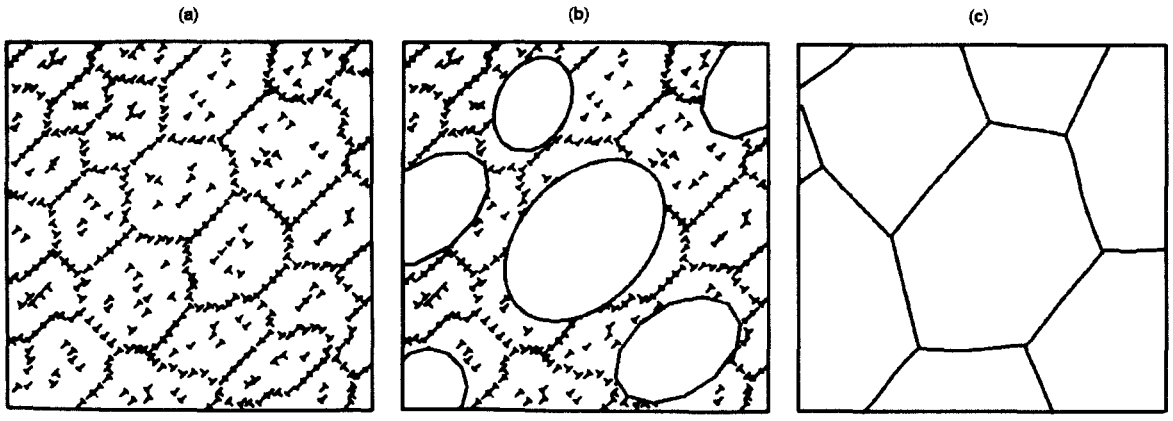


**Figure 2.11:** Progression from a recovered microstructure (a) to a fully recrystallised microstructure (c).

The coalescence of subgrains during high temperature exposure can result in a microstructure with a low dislocation density. In this case, there is no longer a driving force for recrystallisation and hence it does not occur and the shape of the grains is not changed from the deformed condition. This process is often termed continuous recrystallisation or extended recovery. It is likely that extended recovery will only occur in materials with a high $\gamma_{SFE}$, where the process of recovery can occur readily[19].

Although the $\gamma_{SFE}$ of ferritic stainless steels is high, they do undergo recrystallisation at high temperatures. It has also been found that ferritic stainless steels exhibit extended recovery at moderate (600 - 800°C) temperatures where the available thermal energy is insufficient for high-angle grain boundary migration[19].

## 2.3 HIGH TEMPERATURE CREEP IN METALLIC MATERIALS

Creep is defined as the time-dependent deformation of a material under a given stress. The rate at which this creep occurs is dependent on the external conditions of temperature and stress (equation 2.13) and on the particular microstructural characteristics of the material in question (discussed in following sections).

$$\dot{\varepsilon} = f(t, \sigma, T) \tag{2.13}$$

where $\dot{\varepsilon}$ is the creep strain rate, $t$ is the time, $\sigma$ is the applied stress and $T$ is the temperature. In metals, creep becomes noticeable at approximately $0.4T_m$, where $T_m$ is the melting point. Creep is therefore a major limitation in designing components for use at elevated temperatures[13,20]. Figure 2.12 shows a characteristic creep strain versus time curve at high temperture and constant load.

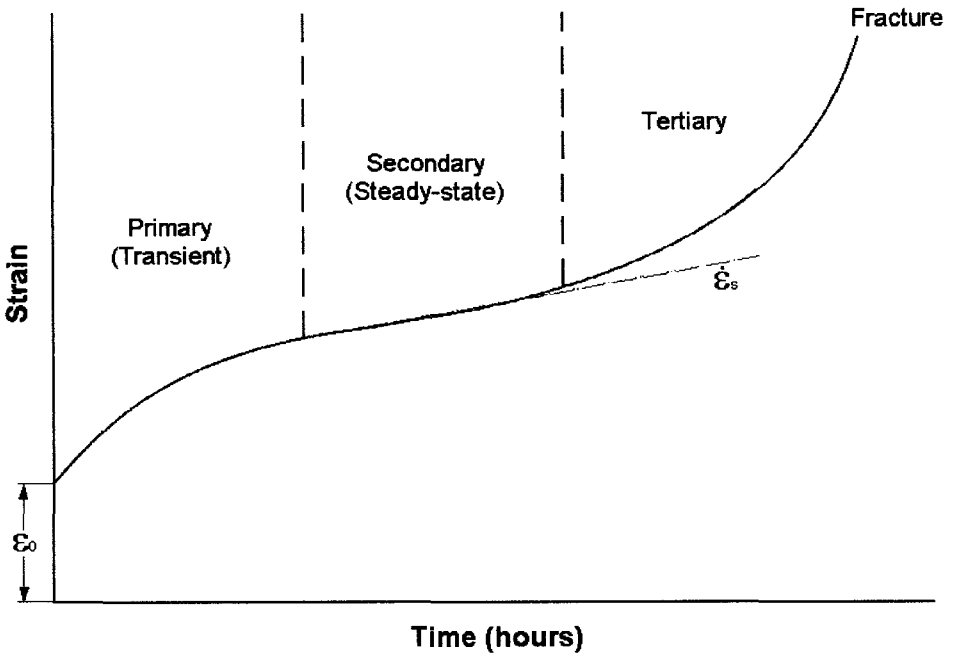


**Figure 2.12:** Characteristic creep curve showing primary, secondary and tertiary stages. $\varepsilon_0$ is the instantaneous strain on loading and $\dot{\varepsilon}_s$ is known as the steady-state creep rate.

Three distinct stages of creep are observed in this plot and each stage can be distinguished by investigating the creep rate within that stage. The primary (or transient) stage following application of the load is characterised by a decreasing creep rate with time. The creep rate then attains a minimum value as a state of equilibrium is reached. This minimum rate is maintained resulting in the secondary (or steady-state) stage. Void and crack formation result in an increase in the creep rate (tertiary stage) eventually resulting in fracture[20].

Not all materials exhibit a characteristic creep curve[21]. The mechanisms of creep deformation (discussed in the following section) vary, depending on the nature and condition of the material, the temperature and the applied stress. In a single creep test, a few different deformation mechanisms may be operating either in succession, or simultaneously, yielding a non-characteristic creep curve[6].

## 2.4 MECHANISMS OF CREEP DEFORMATION

### 2.4.1 Introduction to Creep Deformation Mechanisms

The deformation of polycrystalline materials is known to occur by the movement of lattice defects such as vacancies or dislocations through the crystal lattice[22]. High temperatures associated with creep provide substantial thermal energy for the movement of these defects.

Mechanisms of deformation differ with respect to the type of defect that is moving and how the defect moves through the lattice. There is, however, considerable disagreement in past and current literature as to the exact workings of certain of these mechanisms during creep and to the existence of certain other well established theoretically based mechanisms. These theories will be presented in the following sections as they are generally accepted. Debate surrounding these theories will be dealt with in sections thereafter.

There are two primary categories of creep deformation mechanisms that are proposed, namely: diffusional creep and dislocation creep. Temperature and stress are the primary factors that determine which mechanism operates, resulting in creep. Deformation mechanism maps, devised by Ashby[23], plot the different proposed mechanisms as a function of normalised stress (with respect to the shear modulus) and normalised temperature (with respect to the melting temperature) (figure 2.13).

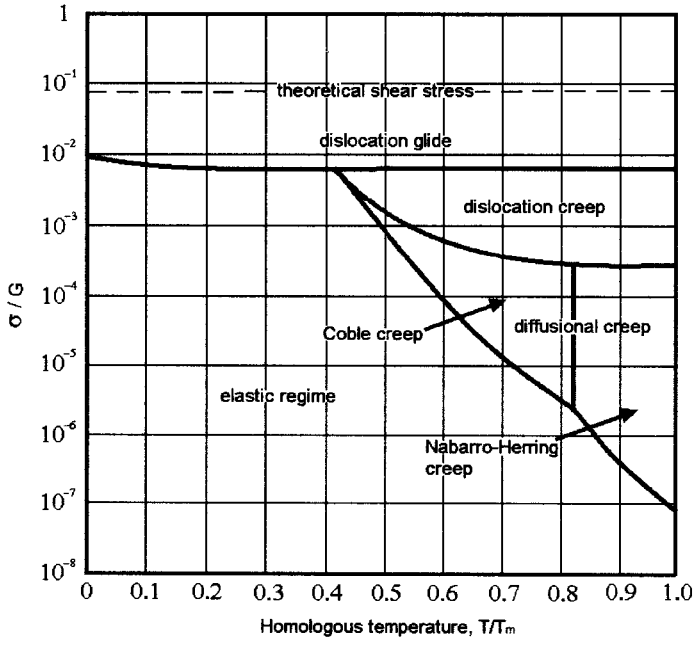


**Figure 2.13:** Example of a deformation mechanism map. After Ashby[23].

Each material will have a unique deformation mechanism map. The stress and temperature range over which particular deformation mechanisms operate depend largely on the microstructure of the material concerned. As can be seen in figure 2.13, creep occurs at elevated temperatures. Diffusional creep is usually prevalent at high temperatures and low stresses due to the availability of thermal energy for diffusion to occur. As the stress is raised and the temperature lowered, dislocation creep takes over as the dominant deformation mechanism.

### 2.4.2 Diffusional Creep Mechanisms

Nabarro[24] was the first to propose self-diffusion as a mechanism of creep deformation. He proposed that a shear stress applied to a polycrystalline material would result in an excess of vacancies along those grain boundaries under tension and a decrease in the number of vacancies along those grain boundaries under compression. A stress-directed flow of vacancies would therefore proceed down the concentration gradient from the grain boundaries under tension to those under compression. This flux of vacancies can be viewed as a flux of atoms in the opposite direction (figure 2.14), resulting in an elongation of the grains in the direction of the tensile axis. Herring[25] consequently extended this theory to high temperature creep and the mechanism became known as Nabarro-Herring creep.

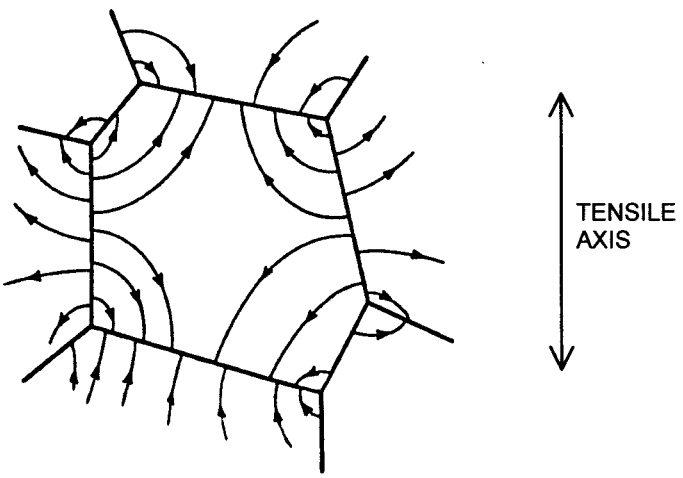


**Figure 2.14:** Arrows indicate the flux of atoms in a polycrystalline material from boundaries under compression to those under tension. After Herring[25].

The steady-state creep rate can be expressed as:

$$\dot{\varepsilon} = \frac{AD_l Gb}{kT}\left(\frac{b}{d}\right)^p \left(\frac{\sigma}{G}\right)^n \tag{2.14}$$

where, $A$ is a dimensionless constant, $D_l$ is the coefficient for lattice self-diffusion, $G$ is the shear modulus, $b$ is the burger's vector, $k$ is Boltzmann's constant, $T$ is the absolute temperature, $d$ is the grain size, $p$ is the inverse grain size exponent, $\sigma$ is the applied stress and $n$ is the stress exponent. For Nabarro-Herring creep, $A = 9.3$[26], $p = 2$ and $n = 1$[27].

Both Nabarro and Herring considered the self-diffusion of vacancies (or atoms) through the crystal lattice in the grain interiors, but neglected diffusion along grain boundaries. Coble[28], while investigating the diffusional creep of alumina ($Al_2O_3$) found that the oxygen ion ($O^{2-}$) diffusion coefficient was several orders of magnitude lower than that for the Al ion ($Al^{3+}$). The

diffusion coefficient of $O^{2-}$ is enhanced when the oxygen ion diffusion occurs along the grain boundaries. Coble therefore proposed that the boundary diffusion of oxygen might control the overall creep rate. This proposal led to the theory of Coble creep. The fundamental concepts of Coble creep are the same as for Nabarro-Herring creep, except that Coble suggested that diffusion takes place along grain boundaries. It is likely that both grain boundary and lattice diffusion occur, however the contribution of grain boundary diffusion to the total strain should increase with increasing grain size as the lattice diffusion distances increase[28]. Also, if the grain boundaries provide easier diffusion paths than the lattice, Coble creep should be more pronounced at lower temperatures where there is less thermal energy available for the movement of defects. The strain rate for Coble creep can also be expressed by equation 2.6, however, $A$ = 33.4, $p$ = 3 and the diffusion coefficient is now $D_{GB}$, the coefficient for grain boundary diffusion[27].

The elongation of grains in the direction of the tensile axis in diffusional creep requires that grains in the polycrystalline material slide past one another to a certain degree as an accommodating process. This is known as Lifshitz sliding and should not be confused with the deformation mechanism of grain boundary sliding known as Rachinger sliding. In diffusional creep, the grains retain their relative positions in the matrix, whereas in Rachinger sliding, the grains slide past one another, with no grain elongation, resulting in an increased number of grains along the tensile axis of the material (figure 2.15)[27].

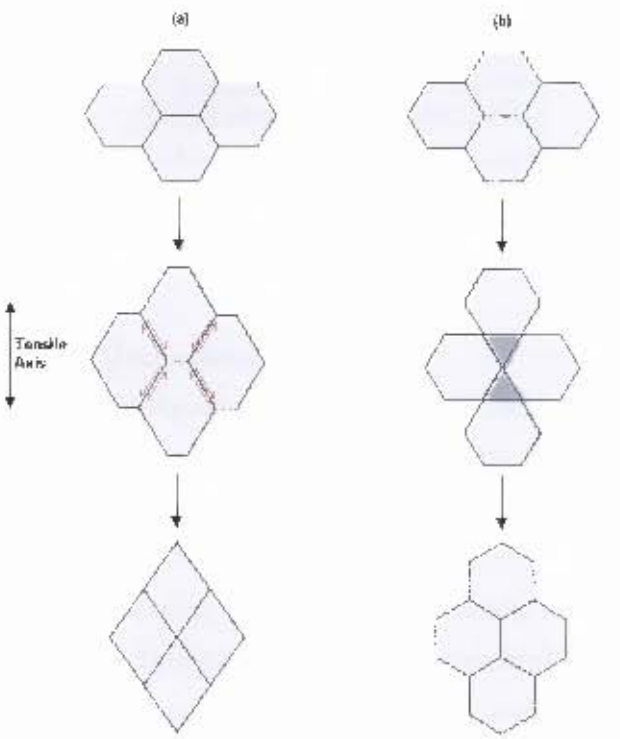


**Figure 2.15:** Schematic showing (a) Lifshitz sliding, characteristic of diffusional creep and (b) Rachinger sliding where grain boundaries slide relative to one another with no grain elongation. After Langdon[27].

The red arrows in figure 2.15 (a) indicate the direction of Lifshitz sliding as diffusional creep is taking place. This physical distinction in grain boundary sliding mechanisms can provide an important method of distinguishing between deformation mechanisms[27]. This is discussed further in § 2.5.5.

The elongation of grains in diffusional creep is achieved by the deposition of bulk material at those grain boundaries experiencing a tensile stress. The implication of this for materials that contain precipitate particles is that the material deposited at these grain boundaries should be particle-free. Figure 2.16 shows a micrograph of Mg-0.55%Zr alloy after diffusional creep. The presence of these particle-free areas, known as denuded zones, are clearly seen on the grain boundaries perpendicular to the applied tensile stress[29].

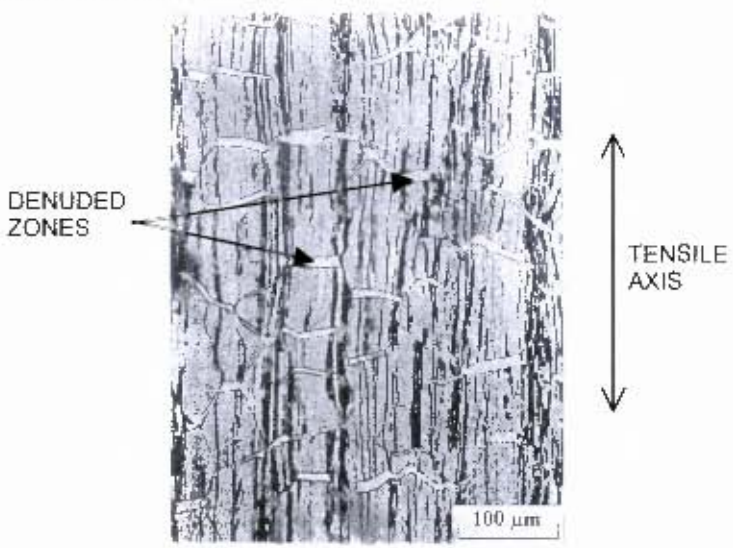


**Figure 2.16:** Mg-0.55%Zr Alloy after diffusional creep. Denuded zones are clearly visible on grain boundaries perpendicular to the applied tensile stress. After Langdon[29].

### 2.4.3 Dislocation Creep Mechanisms

The creep rates predicted by diffusional processes at intermediate and high stresses are too low by orders of magnitude when compared with experimentally obtained values. Changes in the dislocation density and arrangement during creep have been confirmed by electron microscopy indicating the operation of dislocation deformation mechanisms. There are three main deformation mechanisms of dislocation creep that are generally recognised. These are the glide of dislocations leading to slip (glide-controlled creep), the climb and cross-slip of dislocations leading to subgrain formation (recovery-controlled creep) and grain boundary sliding (GBS). The conditions of temperature and stress, as well as certain material characteristics, will determine the contribution of each of these mechanisms to the total creep strain[14,30]. Materials

exhibiting glide-controlled creep, such as solid solution alloys, are known as class I materials. Those materials exhibiting recovery-controlled creep, such as pure metals and single-phase alloys, are known as class II materials[31]. Dislocation creep is also commonly known as power law creep and can be expressed using the power law expression (equation 2.15)[21].

$$\dot{\varepsilon}_s = A\sigma^n \left(\frac{1}{d}\right)^p e^{\left(-Q_c/RT\right)} \tag{2.15}$$

where $A$ is a constant, $\sigma$ is the applied stress, $n$ is the stress exponent, $d$ is the grain size, $p$ is the inverse grain size exponent, $Q_c$ is the activation energy, $R$ is the universal gas constant and $T$ is the absolute temperature. If equations 2.12 and 2.14 are combined, it can be seen that the equations for diffusional and dislocation creep are of the same form. Dislocation creep mechanisms are generally accepted to be insensitive to grain size (this is discussed further in § 2.5.1.) and therefore $p = 0$. The creep rate in diffusional creep processes is linearly proportional to the stress and hence $n = 1$ for these mechanisms. Each creep mechanism can be characterised by particular values of $n$ and $Q_c$ for a particular material, however, using these values as a means for identifying creep mechanisms may not be reliable[32] (this is discussed in § 2.5.5.).

Harper-Dorn (H-D) creep is also recognised as a creep mechanism operating by the movement of dislocations through the lattice at low stresses. At higher stresses, H-D creep gives way to power law creep. H-D creep will be dealt with separately in § 2.4.4.

Glide-controlled creep occurs by the glide of dislocations through the crystal lattice. It will occur if the stress is high enough for the dislocations to overcome obstacles and generally occurs at lower temperatures and higher stresses than recovery-controlled creep. The creep rate will be determined by the rate at which dislocations move through the lattice[22]. The glide of dislocations is normally controlled by shear stress, as discussed in § 2.2.1. In the case of glide-controlled creep, the increased lattice vibrations due to thermal energy affect the value of the critical shear stress required for dislocation mobility. Thus dislocations glide on slip planes by the action of thermal energy assisted by the shear stress on those planes and therefore, the controlling factor in glide-controlled creep is the activation energy required by a dislocation in order to pass an obstacle. The larger the amount of thermal energy introduced (i.e. the higher the temperature), the easier it is for the dislocation to overcome the activation energy barrier[17].

Evans and Wilshire[20] state that the processes of work hardening, recovery and internal stress provide a general framework for individual dislocation mechanisms operating during recovery-

controlled creep. The fundamentals of this dislocation creep process as described by Evans and Wilshire are presented.

The rate of work hardening, $h$, in metal can be defined by the rate of change of stress as a function of strain (equation 2.16).

$$h = \frac{\partial \sigma}{\partial \varepsilon} \tag{2.16}$$

A material with a high dislocation density that is heated sufficiently will undergo recovery (and possibly recrystallisation). Recovery occurs by the rearrangement of dislocations into lower energy sub-structures and results in the softening (or lowering of the yield stress) of a material as described in § 2.1.3. The extent of recovery in a material at a particular temperature is a function of the time for which the material is heated. Therefore the rate of recovery, $r$, can be given by equation 2.17.

$$r = -\left(\frac{\partial \sigma}{\partial t}\right) \tag{2.17}$$

The processes of work hardening and recovery occur simultaneously at high temperatures, resulting in a flow stress that is dependent on both strain and time (equation 2.18).

$$\sigma = f(\varepsilon, t) \tag{2.18}$$

In order to find an expression for the strain rate, consider a strain increment, $d\varepsilon$ over a period of time, $dt$. This yields a change in the flow stress as follows:

$$d\sigma = \frac{\partial \sigma}{\partial \varepsilon} d\varepsilon + \frac{\partial \sigma}{\partial t} dt \tag{2.19}$$

Rearranging equation 2.19 for a situation of steady state creep when the change in flow stress is zero (i.e. $d\sigma = 0$), the following expression for steady-state creep strain rate, $\dot{\varepsilon}_s$ is obtained:

$$\dot{\varepsilon}_s = \frac{d\varepsilon}{dt} = -\frac{\partial \sigma / \partial t}{\partial \sigma / \partial \varepsilon} = -\frac{r}{h} \tag{2.20}$$

where $r$ is the rate of recovery and $h$ is the rate of work hardening. This expression can be written in terms of dislocation density, $\rho$, since the flow stress, $\sigma$ is a function of $\rho$ (equation 2.21).

$$\dot{\varepsilon}_s = \frac{d\varepsilon}{dt} = -\frac{\partial\rho/\partial t}{\partial\rho/\partial\varepsilon} = -\frac{r}{h} \tag{2.21}$$

Therefore, during high temperature creep, both work hardening and recovery contribute to the overall strain rate. The three stages of creep (illustrated in figure 2.12) can now be reviewed and described in terms of these processes. Primary creep is characterised by a decreasing creep rate with time, which would correspond to a high rate of work hardening. As the creep rate becomes steady and secondary creep proceeds, the rate of work hardening and the rate of recovery reach a state of dynamic equilibrium of generation and annihilation of dislocations[33]. The formation of voids and cracks in the material results in an acceleration of the creep rate (i.e. tertiary creep) culminating in fracture[14].

In glide-controlled creep, the thermal energy coupled with the applied stress provided dislocations with enough energy to overcome obstacles in the lattice. In recovery-controlled creep, dislocations may pile up against obstacles with larger activation energies than that which is available. The high temperature at which this mechanism predominates allows diffusion to become significant. Thus dislocations are able to move around obstacles by means of climb as vacancies diffuse to the dislocation line. It is therefore not necessary for a dislocation to overcome the activation energy associated with the particular obstacle. The climb of dislocations around obstacles was discussed in greater detail in § 2.2.1.

The mechanism of grain boundary sliding (GBS) involves the sliding of grains over one another by the glide of grain boundary dislocations. Grain boundary migration also occurs by means of dislocation climb[26]. GBS always operates in conjunction with other mechanisms such as diffusion, which act as accommodating processes, maintaining the coherency of the grains within the lattice and preventing the formation of voids. Equation 2.14 can be rewritten for GBS accommodated by lattice diffusion as follows[34]:

$$\dot{\varepsilon}_{GBS} = \frac{417 D_{GB} G w}{kT}\left(\frac{b}{d}\right)^3\left(\frac{\sigma}{G}\right) \tag{2.22}$$

$w$ indicates the grain boundary width. Notice that the stress exponent is equal to unity indicating Newtonian viscosity (as with diffusion creep). Also, the strain rate is proportional to the inverse of the cube of the grain size as is the case with Coble creep.

Dislocations result in stress fields within the lattice surrounding them. The rearrangement of dislocation structures during creep therefore results in an inhomogeneous distribution of internal

stress. The driving force causing dislocation movement is therefore not the same everywhere in the lattice, since this driving force is given by the difference between the applied stress and the internal stress. This inhomogeneity has been observed by means of transmission electron microscopy (TEM) and it is therefore necessary for any dislocation creep theory to account for these observations[35].

Although much work has been done and much progress made in developing dislocation creep theories, there is still a lack of understanding on the effects of particle hardening and of the dislocation processes of dynamic recovery[33].

### 2.4.4 Harper-Dorn Creep

At high temperatures and low stresses, two possible mechanisms of deformation are thought to be possible, namely diffusional creep (N-H creep or Coble creep) or deformation resulting from the glide and climb of dislocations (i.e. recovery-controlled creep). The activation energy for creep for both of these general mechanisms has been found to be equal to that for self-diffusion, indicating that the controlling factor in both of these processes is diffusion. The mechanism, by which they proceed, is however distinctly different[36].

Harper and Dorn[36] attempted to distinguish between the operations of these two mechanisms at low stresses in pure aluminium. Their results showed that even at stresses as low as 0.028MPa, primary creep (decreasing creep rate with time) was observed, followed by conventional secondary creep. Diffusional creep would not exhibit an initially decreasing creep rate, but rather a constant or increasing rate. The creep rate that they observed was also more than two orders of magnitude greater than that predicted by the Nabarro-Herring theory for diffusional creep[37]. Harper and Dorn therefore deduced that at high temperatures and low applied stresses, creep of pure aluminium proceeds by a dislocation climb process. The secondary creep rate was found to vary linearly with stress in the low stress range (viscous flow), but gave way to power law dependence at higher values of stress (figure 2.17). Materials that exhibit this linear dependence of the creep rate on stress are said to undergo Newtonian or viscous deformation. For this reason, H-D creep is also known as Newtonian viscous dislocation creep. The value of the stress exponent, $n$, for H-D creep is therefore equal to 1 (see equation 2.15), as is the case with diffusion creep. Although they confirmed the operation of a mechanism of creep other than diffusional creep at low stresses, the question as to whether the existence of differing low stress and intermediate stress dependencies pointed towards the existence of two distinct *dislocation* mechanisms for creep[38].

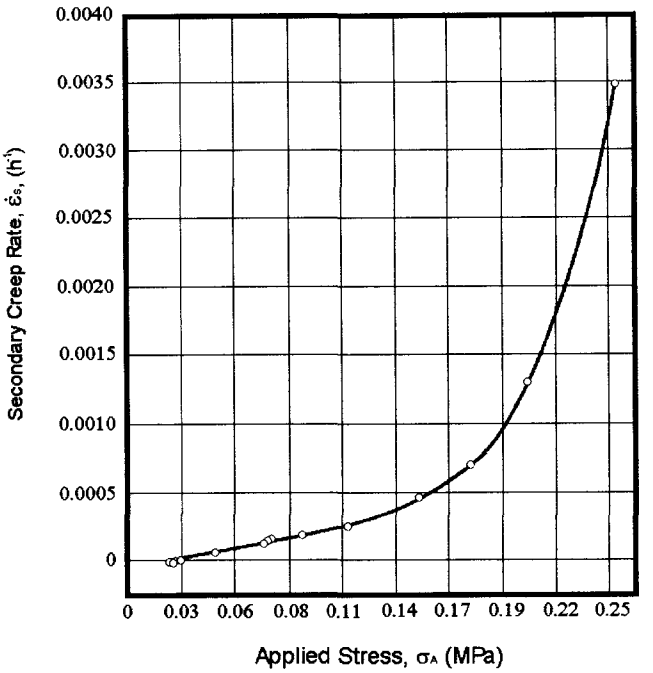


**Figure 2.17:** Effect of low stresses on the secondary creep rate of high-purity aluminium at 920K. After Harper and Dorn[36].

In order to investigate this possibility, they studied the effect of stress on the grain boundary shearing or sliding (as a secondary or accommodating creep process). Harper and Dorn referenced the work of Fazan et al[39] and McLean[40,41] in order to justify this method of investigation. These authors showed that the ratio of grain boundary shearing to the total creep strain, $\varepsilon_{gb}/\varepsilon_t$, is constant throughout a single test. Additionally, the grain boundary shearing was shown to be controlled by the deformation mechanisms within the adjacent grains. This was justified by the observation that the activation energy for the shearing was found to be the same as that for creep within the grains. They postulated therefore that changes observed in grain boundary shearing could reflect changes in crystallographic deformation mechanisms[38].

The ratio, $\varepsilon_{gb}/\varepsilon_t$, was shown to be independent of strain and time by the same authors as quoted by Harper and Dorn[39,40,41] and was calculated at various stresses and found to be a function of the stress. This stress dependence is illustrated in figure 2.18, where $\alpha$ designates the deformation mechanism operating in the low stress range and $\beta$ the mechanism operating in the intermediate stress range. It can be clearly seen that the stress dependence of this ratio changes dramatically between the low and intermediate stress ranges. This, together with the observation that subgrain formation occurred in the intermediate stress range and not in the low stress range gave evidence supporting the view of two distinct deformation mechanisms[38].

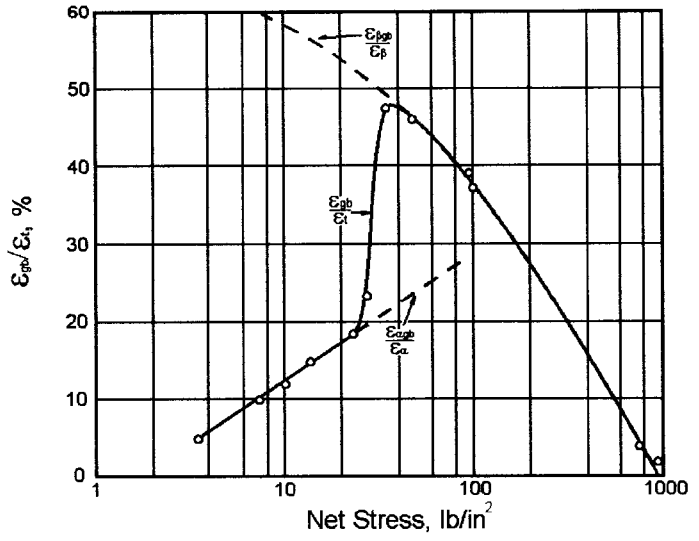


**Figure 2.18:** Stress dependence of $\varepsilon_{gb}/\varepsilon_t$ ratio indicating two distinct deformation mechanisms operating in low and intermediate stress ranges respectively. After Harper and Dorn[38].

Harper and Dorn[38] proposed that the deformation mechanism operating at intermediate stresses was recovery-controlled creep. This was supported by the observed presence of subgrains and calculating the value of activation energy to be equal to that for self-diffusion. The creep deformation resulting from the mechanism proposed at low stresses was reported to be caused by the glide of jogged screw dislocations, however little detail is given as to the precise mechanism[38].

Many authors[38,42,43,44] have attempted to investigate the physical mechanism by which H-D creep proceeds. Despite these attempts, H-D creep is still the subject of much speculation[45]. Ardell[42] used the dislocation network model to predict the transition stress from H-D to power law creep. This model indicates that creep occurs by means of constrained dislocation motion (glide and climb) as the dislocation network is coarsened. Nabarro[43] pointed out the main characteristics of H-D creep as observed by experiment. The most significant of these are perhaps the linear dependence of strain rate on the applied stress, the independence of strain rate on grain size, the general disagreement between authors as to the presence of subgrains[37] and the initially high and decreasing dislocation density which reaches a constant value during steady state creep and is independent of the applied stress. The presence of heavily stepped (jogged) dislocations indicating cross-slip or climb (and hence possibly recovery) was also observed. Nabarro suggested a dislocation climb process at constant dislocation density, which is controlled by the Peierls stress (or CRSS).

Wang[44] developed a microphysical model similar to that of Nabarro, with a few important differences, which will be detailed further. The model, which agrees very well with experimental

data, proposes that creep occurs by means of dislocation glide and climb at constant dislocation density, $\rho_s$. $\rho_s$ is determined by the Peierls stress; however, H-D creep is found to occur at stresses lower than the Peierls stress. This is made possible, since dislocations can move by the migration of thermally activated kinks. The stress required for the migration of kinks is only a fraction of the Peierls stress, which is required for dislocation glide under normal conditions. Creep strain in Nabarro's climb model was produced by the climb of dislocations, whereas Wang has suggested that strain results from dislocation glide and that the climb of dislocations controls only the *rate* of strain[44].

### 2.4.5 Debate Over the Theory of Diffusional Creep

The mechanisms of creep deformation at very low stresses have generally been accepted to be the mechanisms of diffusion creep and H-D creep. Certain authors[29] accept both mechanisms as being viable for producing strains in materials at high temperatures and accept the theory for diffusion creep as being sound[46]. However, the validity of the experimental evidence for the theory of diffusion creep has been seriously questioned by authors such as Ruano et al.[47,48,49] and Wilshire[50]. A major point of contention is the observed presence of denuded zones (see § 2.4.2) in particle-strengthened materials that have crept under conditions of high temperature and low stress. Ruano and coworkers have rejected the presence of such zones as conclusive evidence for the existence of diffusion creep. The basis of this rejection is the observation of denuded zones under conditions where the stress exponent was greater than unity (the required stress exponent for diffusion creep), indicating the operation of dislocation creep mechanisms. An alternative mechanism involving either the dissolution or 'sweeping' of precipitates at moving grain boundaries was proposed for the formation of denuded zones. The presence of denuded zones on grain boundaries parallel to the applied stress have added weight to this view[49]. Although Ruano does not accept the theory of diffusional creep, he admits that the Nabarro-Herring model is the most elegant and sound of all creep theories[49]. This model (as described in § 2.4.2) accounts for the creation of vacancies at grain boundaries. It also serves as a foundation for other creep theories involving the glide and climb of dislocations. However, Ruano and coworkers[49] do not accept that grain boundaries are good sources and sinks for vacancies.

Nabarro[51] acknowledges the objections against diffusional creep processes, but maintains that diffusional creep represents a substantial part of the total strain in a creep test performed under the appropriate conditions of stress and temperature. He claims the evidence used to prove that denuded zones are not the result of diffusional creep is flawed. Specifically, the particles near a grain boundary could not be 'swept' by the grain boundary during migration since the particles would be accumulated on one side of the boundary and this is not observed. Also, as has been

shown in the case of Mg hardened by precipitates of $ZrH_2$, the precipitates could not have gone into solution, since the denuded zones have been observed to be denuded of zirconium (in, or out of solution)[51].

At the time, Nabarro stated that it was clear that the theory of diffusional creep, although sound in principle is still very incomplete[51]. However, McNee[70] et al. recently published fairly conclusive evidence for the theory of diffusion creep, using surface scratch measurements and observations of denuded zones.

### 2.4.6 Debate over the Theory of Harper-Dorn Creep

The debate surrounding the theory of H-D creep is centred on the unconvincing evidence proposed for this theory. Although the mechanism is supposedly well established, there are authors[45], who have questioned the existence of H-D creep as a unique creep mechanism because of the experimental uncertainty. The stress exponent for H-D creep should be unity (indicating Newtonian viscosity). Blum and Maier[45] found in their investigation of pure Al that this exponent was much larger than unity. This was used as confirmation for rejecting the mechanism of H-D creep.

Nabarro[52] pointed out that the stress levels at which Blum and Maier conducted their tests was beyond the transition stress at which H-D creep gives way to power law creep. He noted further that the quantitative model for H-D creep has been very successful when compared with experimental data. In a more recent paper[51], he noted that there is strong evidence for and against the theory, which, as with all creep theories to date, is incomplete.

## 2.5 MICROSTRUCTURAL EFFECTS ON HIGH TEMPERATURE CREEP BEHAVIOUR

The high temperature creep strength of a particular material under given conditions is influenced by the microstructure of the material. The degree to which the various microstructural characteristics influence the creep strength will, in turn, depend on the operating mechanism of deformation. The creep deformation mechanism active in the material will be largely determined by the external conditions such as stress and temperature[14]. The effects of grain size, solid solution particles, precipitate particles and the dislocation sub-structure on the creep properties will be discussed with respect to diffusional and dislocation creep.

### 2.5.1 Grain Size

In diffusion creep, the grain size is of great significance, since a larger grain size means that the distances over which diffusion must take place are greater. This significance is clear when considering equation 2.14 with the appropriate factors and exponents[27]. Equations 2.23 and 2.24 describe the relationship between creep strain rate, grain size and stress for N-H and Coble creep respectively[26].

$$\dot{\varepsilon}_{N-H} = \frac{9.3 D_l G b}{kT}\left(\frac{b}{d}\right)^2\left(\frac{\sigma}{G}\right) \tag{2.23}$$

$$\dot{\varepsilon}_C = \frac{33.4 D_{GB} G b}{kT}\left(\frac{b}{d}\right)^3\left(\frac{\sigma}{G}\right) \tag{2.24}$$

As can be seen, in N-H creep, the creep rate is proportional to the inverse of the square of the grain size ($d$)[24], whereas in Coble creep, the creep rate is proportional to the inverse of the cube of $d$ [28]. In the case of Coble creep, where diffusion occurs along grain boundaries, the dependence on the grain size is stronger.

The dependence of the creep rate on grain size for dislocation creep mechanisms is not very well agreed upon[53]. In general, based on investigations of pure Al, it is assumed that dislocation creep is grain size independent[36]. However, it has been found that the creep rate may increase, decrease or remain insensitive to grain size during dislocation creep as the grain size is varied. This grain size dependence is influenced by the nature of the material, the range of grain sizes tested and the external conditions of stress and temperature[32]. In an investigation into the creep of copper[32], it was found that the stress exponent, $n$, decreased with decreasing grain diameter while $p$ increased over the same range. Thus, even if the value of $p$ is assumed to be zero for dislocation creep, as it generally is, the grain size will still influence the value of $n$ and hence the creep rate.

### 2.5.2 Solid Solution Atoms

The rate of self-diffusion in pure metals and solid solution alloys is nearly identical; therefore, it seems clear that solute atoms do not offer any hindrance to vacancy diffusion[54]. However, it has been found that a change in the concentration of solute atoms in dilute solid solution alloys can result in a change in the activation energy for self-diffusion, and hence the diffusion coefficient, by affecting the atomic mobility in the lattice. This change in activation energy could be either positive or negative, depending on the lattice and the solute atoms present. A positive change

could result from an increased vacancy concentration resulting from the presence of the solute atoms in the lattice[55]. The effects of large amounts of alloying elements on the creep properties is difficult to determine, since other factors, such as lowering of the melting point, have a large effect[56]. An example is in α-titanium, where it has been found that self-diffusion is enhanced by the presence of small concentrations of interstitial impurities such as Fe, Co and Ni[57]. Unfortunately little information could be found on the self-diffusion in ferrite (iron) in the presence of interstitial and substitutional impurities. Obviously, this effect of solute atoms on the rate of diffusion will result in a proportional effect on the creep rate during diffusional creep, since the steady-state creep rate is directly proportional to the diffusion coefficient (see equation 2.14).

Solute atoms strain the lattice of the material in which they are present. The magnitude of this strain field is related to the difference in size between the solute and the solvent atoms. The strain field can be minimised if the solute atoms position themselves near a dislocation. For this reason, there is an attractive interaction that exists between solute atoms and dislocations. The clusters of solute atoms around dislocations are known as solute *atmospheres*. Because of these internal lattice strains due to the presence of solute atoms, the ability of dislocations to propagate is reduced, thus, the material is strengthened[56].

The attraction between solute atoms and dislocations results in solute atmospheres being dragged by dislocations as they glide through the lattice. The rate at which a dislocation can move is therefore dependent on how fast it can *drag* its solute atmosphere (due to the attractive interaction)[20]. This strengthening effect is not usually effective at high temperatures, since the solute atoms can diffuse faster than the dislocations can move[14]. Distinction should be made between solid solution hardening (produced by randomly distributed, immobile solute atoms) and Cottrell locking (the resistance to glide produced by a dislocations solute atmosphere). The creep rate in this case can be given by equation 2.25:

$$\dot{\varepsilon} = \rho b \bar{v} \tag{2.25}$$

where $\rho$ is the density of mobile dislocations, $b$ is the Burger's vector and $\bar{v}$ is the average dislocation velocity[20].

The presence of solute atoms in the lattice can also greatly reduce the stacking fault energy resulting in large partial dislocation separations. Since climb and cross-slip cannot occur unless partial dislocations recombine, the process of recovery, and hence recovery-controlled creep, is inhibited to a large extent[54].

### 2.5.3 Precipitate Particles

Most commercial creep resistant alloys rely on strengthening by means of a fine dispersion of precipitate or insoluble particles[54,58]. Precipitate particles should provide very little if any hindrance to diffusion through the lattice, however the effects of precipitation on diffusional creep can still be large when considering the accommodating process of grain boundary sliding. Since grain boundaries parallel to the tensile axis in diffusion creep must slide past one another, an accumulation of precipitate particles on these boundaries will impede the sliding and reduce the creep rate[14,51]. Should the grain boundaries become pinned, the premature formation of cavities and intergranular cracking is more likely, thus reducing the creep ductility of the material[54]. Another disadvantage of precipitation at grain boundaries is that it can lead to room temperature embrittlement[58].

Precipitates are effective at obstructing the movement of dislocations at high temperatures in the same manner as they do at ambient temperatures. Dislocations must overcome these obstacles by climb and cross-slip as shown in figure 2.7 in §2.2.1. Thus under conditions of stress and temperature where dislocation creep is predominant, precipitate particles are effective at reducing the creep rate[20,59]. In order for this method of strengthening to be the most effective, the precipitates should be small and finely dispersed. A fine dispersion will ensure that the distance between two adjacent precipitates is not large enough for a dislocation to bow between them and continue to glide through the lattice[54].

### 2.5.4 Optimal Microstructure for Creep Resistance

In order to optimize the microstructure for high creep resistance, certain guidelines should be followed. The following are a summary of the guidelines set out by Honeycombe[54].

Certain alloys are able to resist stresses at particular temperatures better than others simply because they have a higher melting point than others. Thus for a particular application, the melting point of the alloy should be higher than the service temperature by a sufficient amount in order to minimise the creep rate. Table 2.3 lists the ratio of recommended maximum service temperature, $T_s$, to the melting temperature, $T_m$, for various alloys[14].

| Base metal | Alloy | $T_s/T_m$ |
|---|---|---|
| α - iron | Complex ferritic alloy | 0.48 |
| γ - iron | Austenitic alloy containing cobalt | 0.59 |
| Aluminium | Complex alloy | 0.56 |
| Nickel | Nimonic 90 | 0.68 |
| Magnesium | Complex alloy | 0.62 |

**Table 2.3:** Ratio of $T_s/T_m$ for various creep resistant alloys. After Smallman[14].

A material with a low stacking fault energy will have a high resistance to creep deformation, since most of the dislocations exist as partial dislocations with large separation distances, which cannot climb or cross-slip past obstacles easily.

Solute particles that have a large difference in atomic size to the atoms in the matrix will result in large lattice strains, which significantly impede dislocation motion. A solute such as this will however probably not have a very high solid solubility. It is useful for solid solutions to have long range order, since dislocations in such ordered alloys (known as super-dislocations) are paired in a similar fashion to partial dislocations, which inhibits their ability to climb and cross-slip.

As has been previously mentioned, precipitation strengthening is very effective, especially in reducing the rate of dislocation creep. The problem encountered at high temperatures is that diffusion becomes significant and the precipitates coarsen resulting in the possibility of dislocations bowing between precipitates. In order to reduce the amount of coarsening that takes place at high temperatures, elements that diffuse slowly and are less soluble in the matrix than other elements should be chosen for the formation of precipitates.

Precipitation on grain boundaries and dislocations is also advantageous, since it impedes grain boundary sliding and dislocation movement.

### 2.5.5 Practical Identification of Creep Mechanisms

Various methods of determining the creep deformation mechanism operating in a particular alloy under particular conditions exist. In order to accurately determine the mechanism, it is sometimes necessary to use more than one of these methods. Certain methods make use of calculating particular material parameters, whereas others involve the direct observation and interpretation of microstructural features such as precipitates and subgrain structure.

In general, the creep rate measured during a creep test is proportional to the applied stress raised to some power (the stress exponent, $n$). The value of $n$ allows some distinction to be made, since its value depends on the operative mechanism[60,61] of deformation. The values of $n$ tabulated in table 2.4 are approximate and may vary considerably depending on the microstructure and other external factors. For example, creep by dislocation glide in a solid solution alloy (class I material) yields a value for $n$ of approximately 3 [61] (as opposed to >5 as indicated in table 2.4). Also, as has been discussed in § 2.5.1, certain mechanisms are more dependent on grain size than others. For this reason, the inverse grain size exponent, $p$, may also be calculated and used as a distinguishing factor. These values (both $n$ and $p$) should however be used with caution, since variations in the grain size can result in changes to the value of $n$. For this reason, Wilshire and Palmer[32] state that it is not possible to *reliably* identify the creep mechanism by considering only the values of $n$ and $p$.

| Mechanism | Stress exponent, $n$ |
|---|---|
| Diffusional Creep | 1.0 |
| Dislocation Glide | > 5.0 |
| Dislocation Climb | 4.5 |
| Grain Boundary Sliding | 2.0 |
| Harper-Dorn Creep | 1.0 |

**Table 2.4:** Values of stress exponent, $n$, for various creep deformation mechanisms.

A careful evaluation of the dislocation structure after a creep test can help in identifying the operative mechanism. The presence of a dislocation substructure after creep would indicate that recovery has taken place and that the rate controlling process was probably the climb and cross-slip of dislocations. If, on the other hand, dislocations are observed randomly arranged and bowed between precipitate particles, it is likely that glide-controlled creep has been the dominant mechanism[61].

The various modes of dislocation creep are relatively easy to detect by inspection of the stress- and inverse grain size exponent together with an observation of the microstructure. Diffusional creep and H-D creep however both yield a stress exponent of unity. Langdon[27,29,62] devised a method using marker lines scribed on the specimen surface to distinguish between these mechanisms, which will be outlined below.

Consider the arrangement of three rectangular grains illustrated in figure 2.19 (a) with vertical marker lines AA' and BB' scribed on the surface. Diffusion creep requires that grain boundary

sliding (Lifshitz sliding – see §2.4.2) occurs as an accommodating process, whereas H-D creep occurs by the movement of dislocations within the grain interiors and no grain boundary sliding. Thus, if the array of three grains deforms by diffusion creep, the marker lines will be offset at the grain boundary transverse to the applied stress (figure 2.19 (b)). If deformation occurs by H-D creep, no offset will be observed, because the marker lines should retain their original position as depicted in figure 2.19 (c). Similar offsets should be observed with marker lines scribed transverse to the applied stress[27].

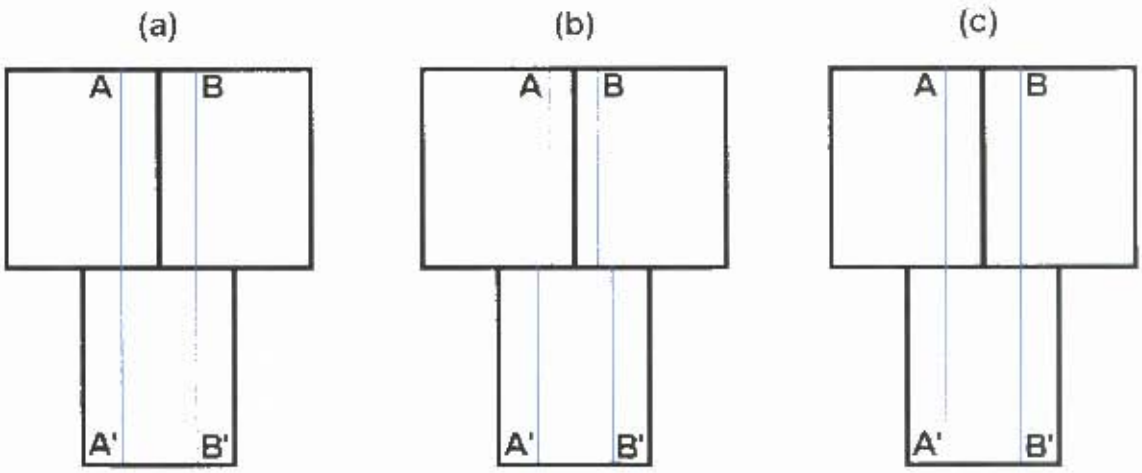


**Figure 2.19:** (a) Three grains with marker lines AA' and BB': (b) deformed by diffusional creep and (c) deformed by H-D creep. After Langdon[27].

It is important to keep in mind that grain boundary sliding (GBS) as a primary dislocation mechanism will also result in marker line offsets at grain boundaries. The physical distinction between these two processes lies in the fact that during diffusion creep grains elongate, but retain their original position within the matrix, whereas during GBS, the grains are displaced with respect to one another, but retain their original shape. Therefore a simple measurement of the grain aspect ratio in the initial condition and after testing will allow a distinction to be made between these two processes[62].

## 2.6 INFLUENCE OF NIOBIUM ON THE HIGH TEMPERATURE CREEP OF FERRITIC STAINLESS STEELS

Niobium is added to stainless steels as a stabilising element (as described in §2.1.2). In addition to this, Nb is a ferrite forming element, which aids in stabilising the ferrite phase in the steel at all temperatures[63].

It has been reported that the amount of 'uncombined' Nb (i.e. Nb in solid solution that has not formed precipitates with other elements) has a profound effect on the creep strength of ferritic stainless steels[6]. This effect is shown in figure 2.20 where the stress required to cause a 2% total strain in 100 hours is plotted against the amount of uncombined Nb present at the beginning of the test.

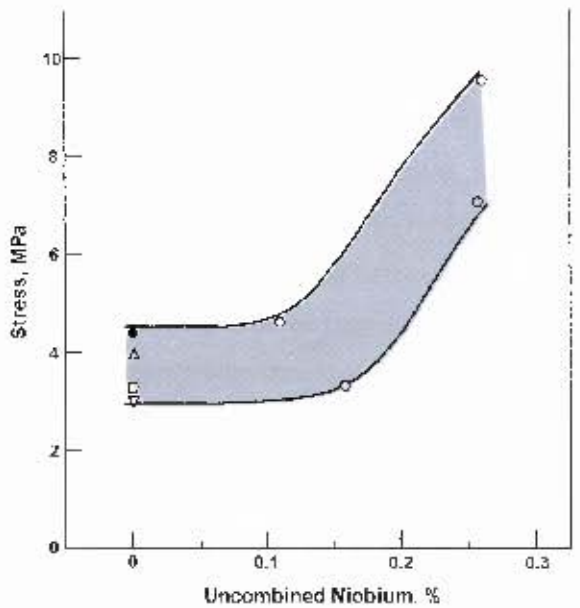


**Figure 2.20:** Stress required to cause 2% total strain in 100 hours plotted against uncombined Nb content. After Johnson[6].

The results in figure 2.20 are of materials that have been annealed prior to creep testing. The effect of this annealing treatment is to produce an equiaxed grain structure as well as to dissolve all the precipitates (primarily Ti and Nb carbonitrides in dual-stabilised grades)[6].

The combination of an amount of uncombined Nb and a high final annealing temperature has also been found to improve the high temperature *tensile strength* of ferritic stainless steels. This strengthening has been attributed to solid solution strengthening by uncombined Nb in solution, possibly aided by dynamic precipitation of a Laves phase during testing[11]. The Laves phase is a hexagonally structured intermetallic precipitate having the general formula $Fe_2M$, where M in this case is usually Nb, but could also represent Mo, Cr, Mn or Si. $Fe_2Nb$ may precipitate in ferritic stainless steels during slow cooling from high annealing temperatures or by holding at constant temperature between approximately 820°C and 930°C [65].

The effect obtained by the addition of Nb on the creep strength has been attributed mostly to the precipitation of the Laves phase[6,11,65], however, solid solution strengthening is equally likely, especially if dislocation creep is the dominant mechanism and the service temperature is not too

high so as to allow solute diffusion (see § 2.5.2). A high final annealing temperature ensures solution of any Laves phase present after thermomechanical processing and enables precipitation to occur on grain boundaries and within grains as creep proceeds[6].

## 2.7 CREEP TESTING OF METALLIC MATERIALS

### 2.7.1 General Methodology

A creep test measures the time dependent deformation of a material under predetermined conditions of temperature and stress. Two similar tests, which can usually be conducted on the same or similar rigs, are the stress-rupture and the stress-relaxation test. The stress-rupture test is simply a creep test in which only the time to rupture is measured at constant temperature and stress. In a stress-relaxation test, the specimen is strained to a predetermined value and the stress on the specimen is measured as a function of time[66].

A creep test rig is designed to measure the deformation of a particular material with respect to time under conditions of constant temperature[66]. Two primary types of rigs are available, namely: constant load and constant stress creep test rigs. The most common of these is the constant load rig, where a constant load is applied to a specimen in uniaxial tension, either directly (by suspending the load from the specimen), or by means of a lever-arm. A schematic of a lever-arm type, constant load creep rig is shown in figure 2.21.

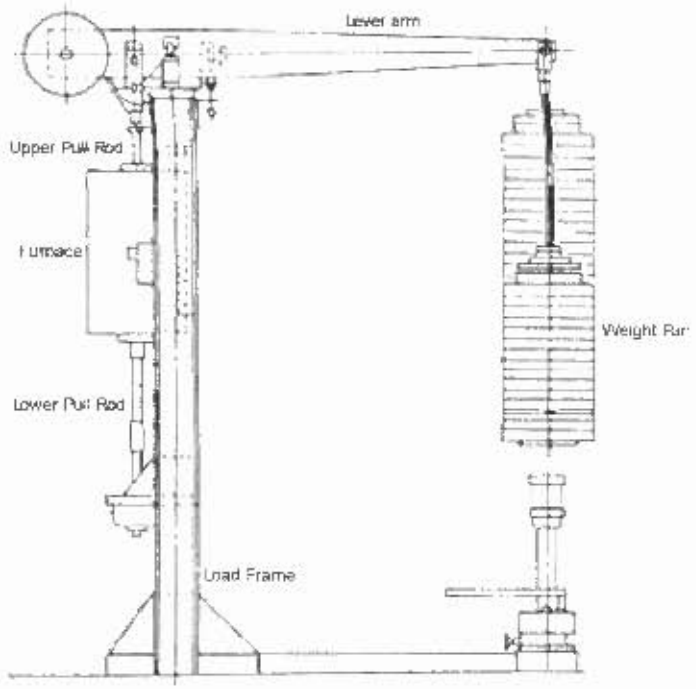


**Figure 2.21:** Lever-arm type constant load, uniaxial tension creep test rig.

A constant stress creep test rig makes use of precision machined cams to reduce the load (and hence keep the stress constant) as the specimen increases in length and decreases in cross-sectional area[66].

In order to measure the extension of the specimen, an extensometer system is used that attaches directly onto the specimen gauge length and transmits the extension to a strain measuring device such as a linear variable differential transformer (LVDT) outside the furnace[66].

### 2.7.2 Review of ASTM Standards

ASTM Standard E139-00[3] outlines the standard practice for conducting creep, creep rupture and stress rupture tests of metals. The standard includes methodology for determining the amount of time dependent deformation a material undergoes during a creep test as well as outlining the minimum requirements for creep testing equipment. Given that an objective of this project is to design, build and commission a set of creep testing machines, the aspects of this standard relating to the requirements for creep testing will be reviewed.

*Creep testing equipment:*

Precaution should be taken to ensure that load is applied to the specimens as axially as possible (the maximum bending strain should not exceed 10% of the axial strain).

The machine should incorporate means of taking up the extension of the specimen so that the load will be maintained within the required limits and the extension of the specimen should not introduce any eccentricity of loading. The take-up mechanism should avoid introducing shock loads, overloading or torque to the system.

The machine should be erected in such a way as to minimise the transmission of shock due to external causes.

For materials tested at high temperatures, which are attacked by their environment (e.g. oxidation), it may be desirable to enclose the specimen in an inert capsule.

*Heating apparatus:*

The heating apparatus should be an electric resistance or radiation furnace that allows a constant temperature to be maintained in air at atmospheric pressure. This apparatus should be able to control temperature to within the limits given in table 2.5:

| Temperature Range | Temperature Limits |
|---|---|
| ≤ 1000 °C | ± 2 °C |
| > 1000 °C | ± 3 °C |

**Table 2.5:** ASTM prescribed temperature limits for creep testing of metallic materials.

*Temperature measuring equipment:*

The temperature measurement devices must be sufficiently sensitive to ensure temperature control according to the limits tabulated in table 2.5.

The appropriate thermocouples, depending on the temperature range being measured, should be used for temperature measurement. These thermocouples should be kept clean and should be regularly calibrated. Other temperature measuring, controlling and recording instruments should also be calibrated regularly.

*Extensometer system:*

The sensitivity and accuracy of the strain measuring system should be suitable to define the creep characteristics with the precision required for the application of the data.

The extensometer should be attached directly to opposite sides of the specimen and the reported strain should be the average of strains on the two sides (obtained mechanically or electrically) or, the average of two separate readings.

The extensometer should be attached to the reduced region of the specimen (gauge length) itself and not to any load carrying parts joined to the specimen (e.g. grips), however, for materials with low ductility, it is satisfactory to attach the extensometer to the specimen shoulders.

The extensometer should be well enough secured to the specimen that it does not slip due to a reduction in specimen area.

### 2.7.3 Sag Testing Techniques

The sag test has been developed as a less time consuming and more cost effective means of comparing the creep strength of various alloys. The specimens used for sag testing are strips of material 1" wide and 11 ½" long with a ½", 90° locating bend at one end (figure 2.22)[67].

# CHAPTER 3

# CONSTANT LOAD CREEP TEST RIG

## 3.1 BACKGROUND TO THE DESIGN

### 3.1.1 Design Statement

To design a creep test rig capable of accurately measuring the extension of various materials under a range of conditions of stress and temperature as a function of time.

### 3.1.2 Creep Test Rig Design Requirements

There are certain requirements that must be met by the design of the creep rig. Specifically, the design must:

- meet the criteria set out in the ASTM E139-00[3] standards for the creep testing of metallic materials (see § 2.7.2).
- be able to accurately measure the extension of a specimen as a function of time.
- be able to be used for stress relaxation testing as well as creep testing.
- be able to be used for testing a wide range of materials having different creep characteristics.

### 3.1.3 Creep Test Rig Design Constraints

There are certain factors that constrain the design of the creep test rig. The rig should:

- be able to be manufactured within a reasonable timeframe.
- *be as cost effective as possible, without compromising on any of the requirements set out above.*
- be of such a quality that it will be able to be used for numerous years with minimal maintenance. This requires the use of specialised materials such as nickel superalloys.

## 3.2 DESIGN CONCEPT FORMATION

It was decided from the start that the design of a constant *stress* creep test rig would be too complex, given the time and other resources available. Also, there is no significant advantage to using a constant stress rig that would warrant its use for this application.

The initial design concept of the rig, illustrated in figure 3.1, is similar to any commercially available constant load creep test rig.

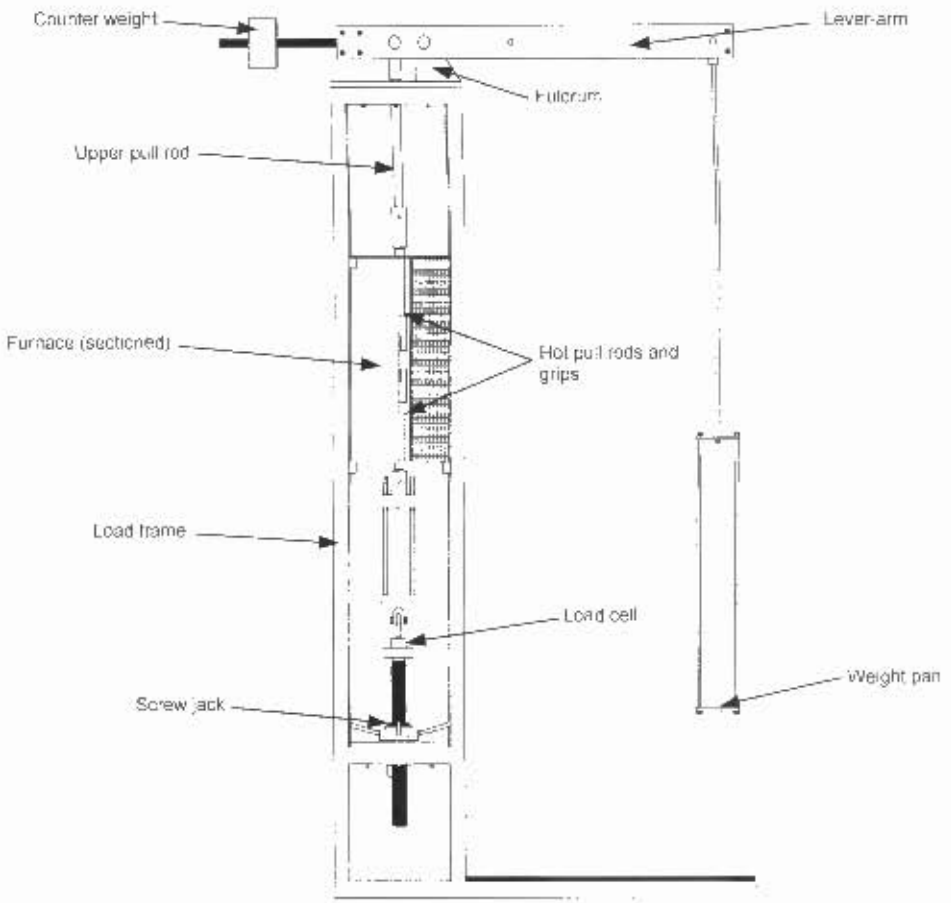


**Figure 3.1:** Concept design of lever-arm type, constant load creep test rig.

The specimen is held between the grips in the furnace. In order to apply a constant load to the specimen, weights must be placed on the weight pan. This load is transmitted to the specimen by the lever in proportion with the lever ratio. The temperature is maintained at a constant level by the furnace, which encloses the specimen and grips. An extensometer system (not shown in figure 3.1) is made up of rods that extend into the furnace and attach directly to the specimen gauge length. The relative displacement of the rods is measured outside the furnace and the data is logged using a suitable data-logging package.

## 3.3 SPECIFICATION OF CREEP TEST RIG DESIGN

The constant load creep test rig, shown in figure 3.2, has been designed to conform to the requirements and criteria set out in § 3.1. Two identical rigs were built to enable simultaneous

tests to be run, since creep tests are by nature long in duration. A set of technical drawings of the main components of the rigs has been included in Appendix A. The final design has the following capabilities and features:

- A testing temperature range from ambient temperature to 1200°C.
- A vertical tube furnace with three independently controlled heating zones to maintain temperature within limits prescribed by ASTM standard E139-00[3] (see table 2.5).
- An adjustable lever-arm ratio (1:3, 1:5 or 1:10) to allow loads between ±10kg and 1000kg to be applied to the specimen in uniaxial tension.
- Self-aligning rod-end bearings at the top and bottom of the load train ensure that the load is applied as axially as possible.
- Design of the hot pull rods and grips allow both pinned and threaded specimens to be tested.
- A screw jack at the base of the load train enables the vertical positioning of the lower pull rod to allow various length specimens to be tested and is used for load application during stress relaxation tests.
- A data acquisition system, which allows load, extension and specimen temperature to be logged as a function of time.

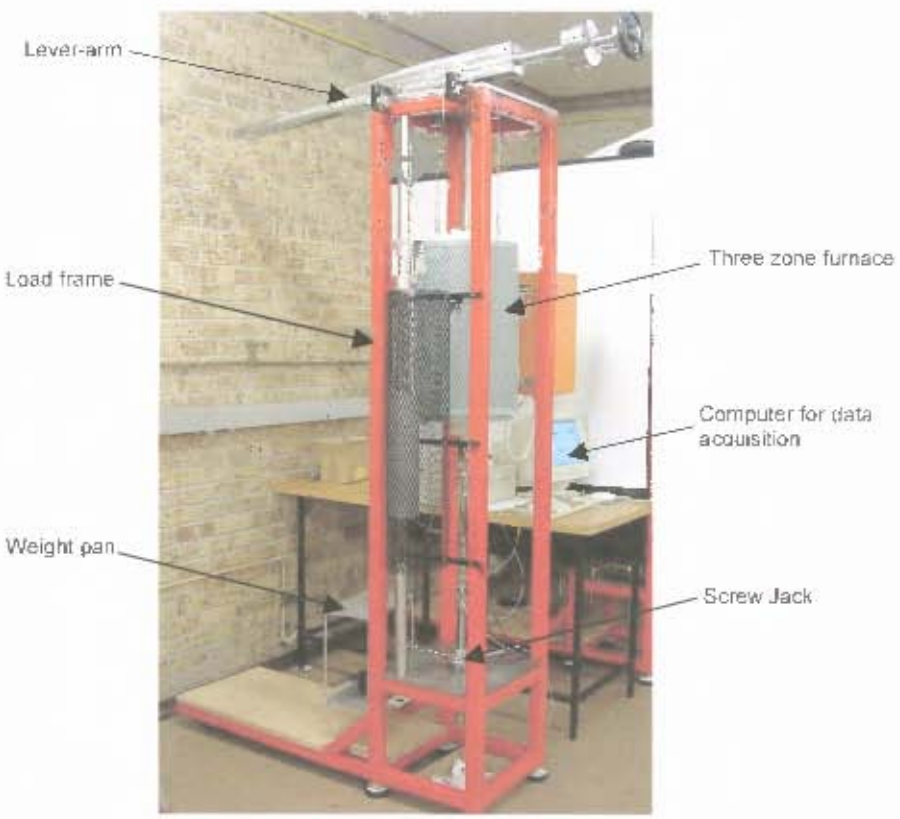


**Figure 3.2:** Photograph of the constant load creep test rig.

The materials selected for construction of the rig were selected to provide sufficient properties to ensure a good service life for the rig. Below is a list of the materials used for the manufacture of the main components of the creep test rig.

| Components | Materials Used |
|---|---|
| Frame | Mild steel (painted) |
| Base plates | 3CR12 Corrosion resistant steel |
| Lever-arm | 3CR12 Corrosion resistant steel |
| Upper and lower puff rods | 316 Stainless steel |
| Pull rod connectors | 316 Stainless steel |
| Hot puff rods | Haynes 230® alloy |
| Threaded specimen grips | Haynes 230® alloy |
| Extensometer clamps and rods | Inconel 601 alloy |
| Screw jack components | 304 Stainless steel |

**Table 3.1:** Materials used for the manufacture of the main components of the rig.

The data acquisition system (figure 3.3) consists of various sensors, a control unit and data acquisition software programmed in Microsoft Visual Basic 6.0®.


**Figure 3.3:** The control unit and computer of the creep test rig data acquisition system.

This software has the capability to log data at user defined time intervals. Each rig has a channel for logging load and another for logging the specimen extension. Two channels are set-aside on each rig to log the temperature on the top and bottom of the specimen. This allows any vertical temperature distribution to be monitored.

The sensors being used on each rig include a load cell, a linear variable differential transducer (LVDT) and two type-K thermocouples. The specifications of each sensor are given in table 3.2.

| Sensor | Specification |
|---|---|
| GEFRAN TU Compact Load Cell | 0.2% accuracy; 0 - 100kg load range |
| GEFRAN TU Compact Load Cell | 0.2% accuracy; 0 - 1000kg load range |
| SOLARTRON LVDT | ± 25mm measurement stroke |
| Type-K thermocouples (2 x) | ± 1°C |

**Table 3.2:** Creep test rig sensors.

It was decided to purchase two load cells for use in different load ranges. With a load accuracy of 0.2% of the full-scale load, the accuracy of a reading of 50kg with the 0 - 1000kg load cell would only yield an accuracy of 50kg ±1kg (i.e. ± 2%). Depending on the chosen load, the load cells can be interchanged accordingly.

## 3.4 DISCUSSION OF CREEP TEST RIG DESIGN

### 3.4.1 Structural Components

The structural components of the creep test rig include the load frame and the base plates. The frame, constructed from welded box section mild steel tube (50 × 50 × 4.5 mm), provides the backbone of the rig. Figure 3.2 clearly shows a labelled photograph of the rig indicating the frame and other main components.

There are two base plates; (upper and lower) between which the load is applied. Each plate was machined from 16mm thick 3CR12 corrosion resistant steel. These plates are bolted to the load frame and have been designed to be able to withstand the maximum applied load of 1000 kg. 3CR12 corrosion resistant steel was selected as it offers good oxidation resistance and is more cost-effective than other corrosion resistant steels such as austenitic stainless steel.

### 3.4.2 Load Application Components

As has been previously described, the load is applied to a specimen by means of a lever through the pull rods. The lever consists of two 3CR12 corrosion resistant steel plates that have been bolted together with spacing blocks between them. Two deep groove ball bearings (SKF 6006-2Z) allow the lever to move freely about the fulcrum. Figure 3.4 illustrates the assembly of the lever, fulcrum and upper base plate.

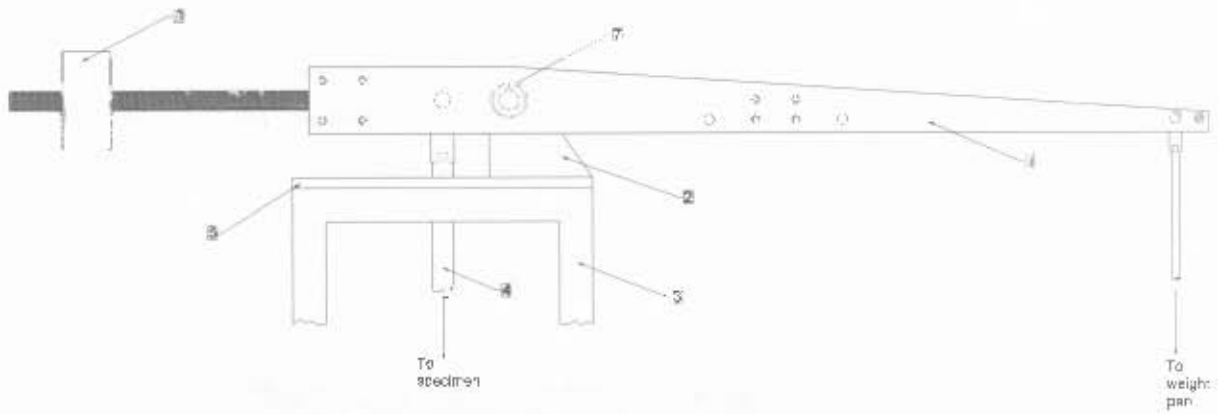


| LEGEND | | | |
|---|---|---|---|
| 1 | Lever-arm | 5 | Upper base plate |
| 2 | Fulcrum | 6 | Counter weight |
| 3 | Top of load frame | 7 | SKF 6006-2Z bearing |
| 4 | Upper pull rod | | |

**Figure 3.4:** Assembly of lever, fulcrum and upper base plate.

The counter weight (No. 6 in figure 3.4) is threaded onto the end of the lever. This allows the load to be adjusted by small increments by screwing the weight in the appropriate direction. This is important to allow the load to be zeroed while the furnace is being heated.

The ASTM E139-00 standard[3] requires that the load be applied as axially as possible to the specimen. In order to ensure this, the upper and lower pull rods are attached by means of self-aligning rod-end bearings to the lever and the load cell respectively.

The pull rods and specimen grips required a careful materials selection, because of the need for good strength and oxidation resistance at high temperatures. The cost and availability of alloys meeting these requirements also added to the difficulty of selecting a suitable alloy. The alloys identified as candidates for this application were Nimonic 115, Inconel MA256 (mechanically alloyed with $Y_2O_3$) and Haynes 230[4] alloys. Table 3.3 lists the compositions of these materials.

| Nimonic 115 | | Inconel MA 256 | | Haynes 230 | |
|---|---|---|---|---|---|
| Ni | 60.0 | Ni | 78.0 | Ni | 57.0 |
| Cr | 14.2 | Cr | 20.0 | Cr | 22.0 |
| Co | 12.5 | Fe | 1.0 | W | 14.0 |
| Al | 4.9 | Al | 0.3 | Co | 5.0 |
| Ti | 3.8 | Ti | 0.5 | Fe | 3.0 |
| Mo | 3.2 | $Y_2O_3$ | 0.6 | Mo | 2.0 |

**Table 3.3:** Table showing comparative compositions (in wt%) for candidate materials for pull rods and grips.

Initially, the materials selection was only between the Nimonic and Inconel alloys, since these materials were apparently going to be available at a reduced price. The Haynes 230® was included as a candidate material when it was found that the other alloys could not be obtained at a reduced price. The Haynes alloy, although not as good as the Nimonic and Inconel alloys, offers excellent high temperature strength and oxidation resistance and is more cost effective. The manufacturers of the alloy (Haynes International) claim that it can be used for continuous service in an oxidising environment at temperatures up to 1150°C. Some of the properties of the Haynes alloy are tabulated in table 3.4.

| PROPERTY | VALUE |
|---|---|
| Yield Strength | 395 MPa |
| 1000 hr Rupture Stress (870°C) | 66 MPa |
| 1000 hr Rupture Stress (1150°C) | 4.1 MPa |
| 1000 hr Oxidation Metal Loss (1205°C) | 7.1mm* |
| Melting Range | 1300 - 1370°C |

**Table 3.4:** Properties of Haynes 230® alloy. *AISI 316 stainless steel exhibits a metal loss of >140.4mm in the same test[6].

The Haynes alloy contributed to a large portion of the cost of the rigs. The price of the alloy was exacerbated by the fact that it had to be acquired from the United Kingdom with an unfavourable Rand – Pound exchange rate.

### 3.4.3 Heating System

The furnaces used for the creep test rigs are electrical tube furnaces manufactured by Custom Furnaces CC. Each furnace has three independently controlled heating zones to ensure excellent temperature distribution along the vertical length of the furnace and hence the specimen being tested. The maximum operating temperature of the furnaces is 1200°C, however, most creep tests will be conducted at temperatures below this. The furnace is insulated at either end during testing. Ceramic fibre blanket is used to plug the lower end of the furnace and specially cast refractory brick inserts seal the top end.

Each furnace is suspended by means of a pulley and counter weight system. The furnace can be moved up and down easily, allowing easy access to the specimen when setting up or dismantling a test.

### 3.4.4 Extensometer System

The nature of creep testing means that measuring the extension of the specimen directly from the gauge length is difficult. It is, however, accomplished by using a high temperature extensometer consisting of rods that extend from the gauge length of the specimen inside the furnace to outside the furnace. Measuring the displacement between small plates attached to the rods outside of the furnace allows the extension of the gauge length to be accurately measured. As mentioned previously, a 50mm stroke (25mm either side of the electronic zero point) LVDT is used to measure this displacement. Figure 3.5 shows a schematic representation of the extensometer system. The dashed red line in the illustration indicates the position of the furnace relative to the extensometer.

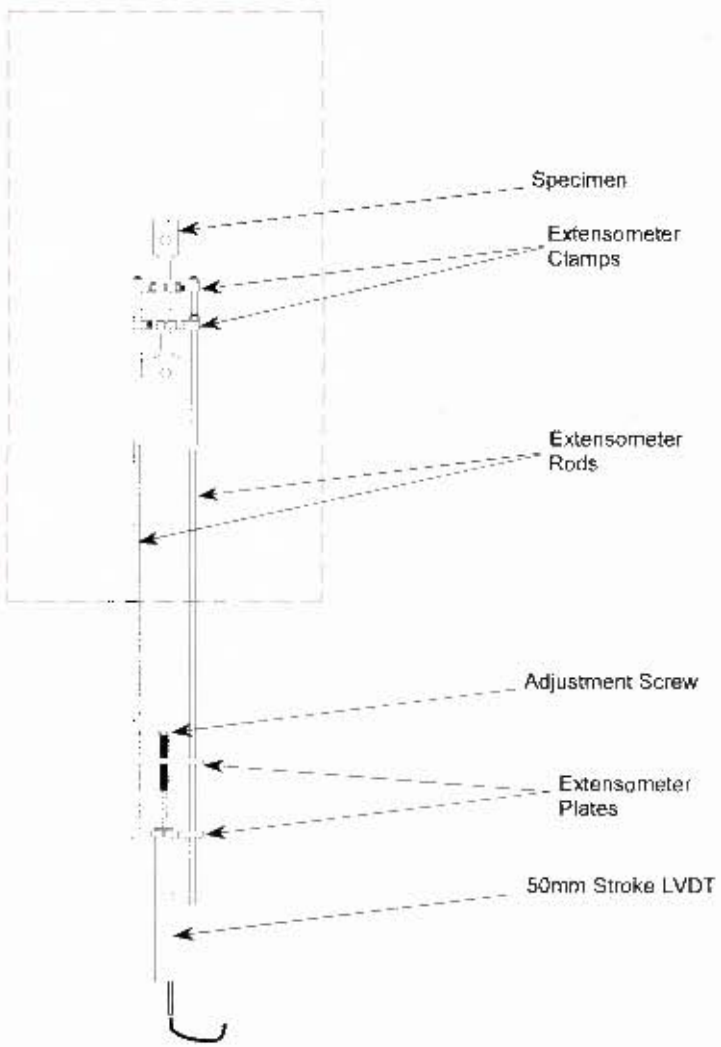


**Figure 3.5:** Schematic of creep test rig extensometer system

Figure 3.6 (a) and (b) show close up photographs of the LVDT and extensometer plates, and the extensometer clamps respectively.

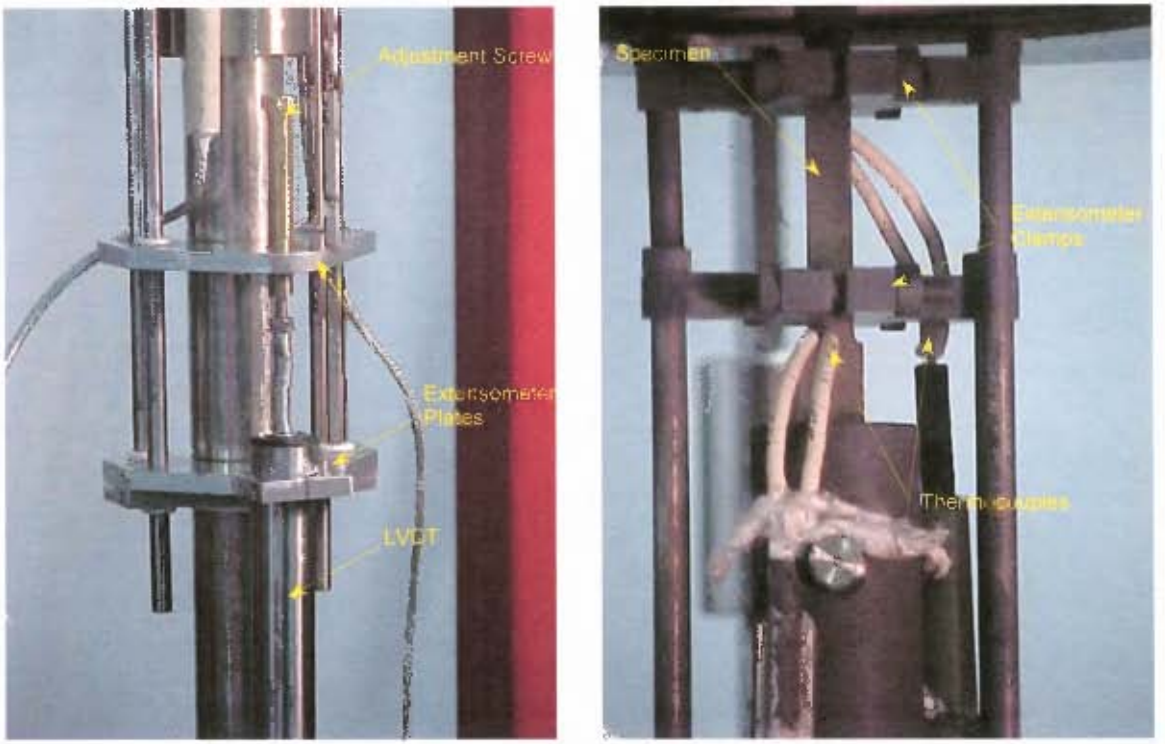


**Figure 3.6:** (a) Extensometer system; (b) Extensometer clamps visible beneath furnace. During a test, the furnace would enclose the clamps and specimen.

In order for the extension measurements to be made accurately, the LVDT should only be zeroed when the furnace reaches its set temperature. This will ensure that any expansion of the extensometer components, load train components and the specimen is complete and will not influence the measurements.

A nickel-based alloy, Inconel 601, was chosen for manufacturing the extensometer rods and clamps. The nominal composition of this alloy is 60wt% Ni, 22wt%Cr and 13wt% Fe. It has excellent oxidation resistance properties with fair high temperature strength, although, since there is no appreciable force acting on the extensometer, strength was not a major selection criterion.

### 3.4.5 Data Acquisition System

The voltage outputs from the various sensors are transmitted to the control unit, where these voltages are adjusted to read meaningful values of load, extension and temperature. These are then transmitted to the computer via an analogue to digital card (Eagle Technologies PCI703S), where they may be logged at user-defined time intervals. Figure 3.7 shows the creep data acquisition software user interface (The code for the data acquisition software is included in Appendix B).

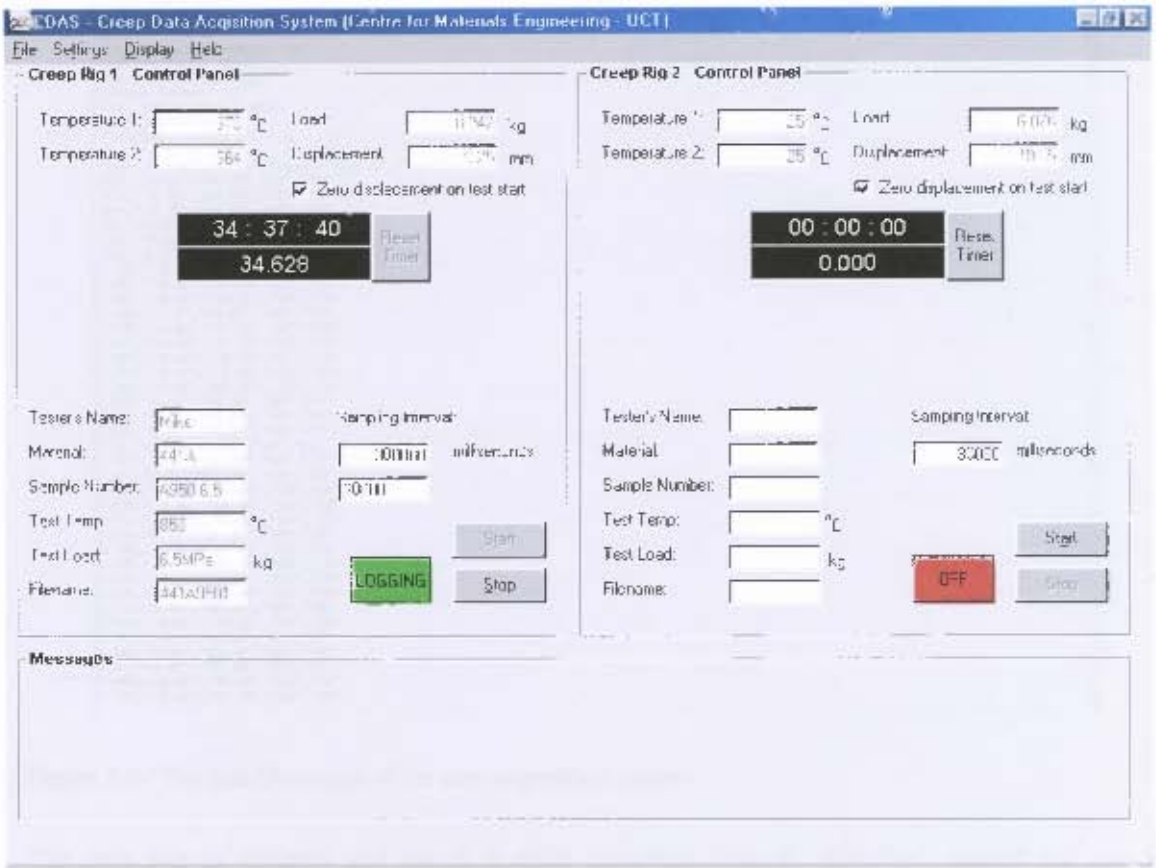


**Figure 3.7:** Creep data acquisition system user interface.

The measured values from each rig are displayed and continuously updated in the text boxes (Temperature 1, Temperature 2, Load, Displacement) indicated in figure 3.7. When the user starts the logging process for a particular rig, the test information and the data are logged to a text file (figure 3.8), which can later be opened and graphed in a spreadsheet program such as Microsoft Excel®.

Should any information, such as a warning, need to be communicated to the user during the course of a test or the setting up of a test this information is displayed in the frame at the bottom of the screen labelled 'Messages'. An example of such a warning is a confirmation message, which displays when the user stops a test, prompting the user to confirm his/ her actions.

The user is able to set the calibration factors of each channel, so that regular calibration of the test rigs is made simple. The sensors, however, should be first calibrated by adjusting the calibration screws within the control unit.

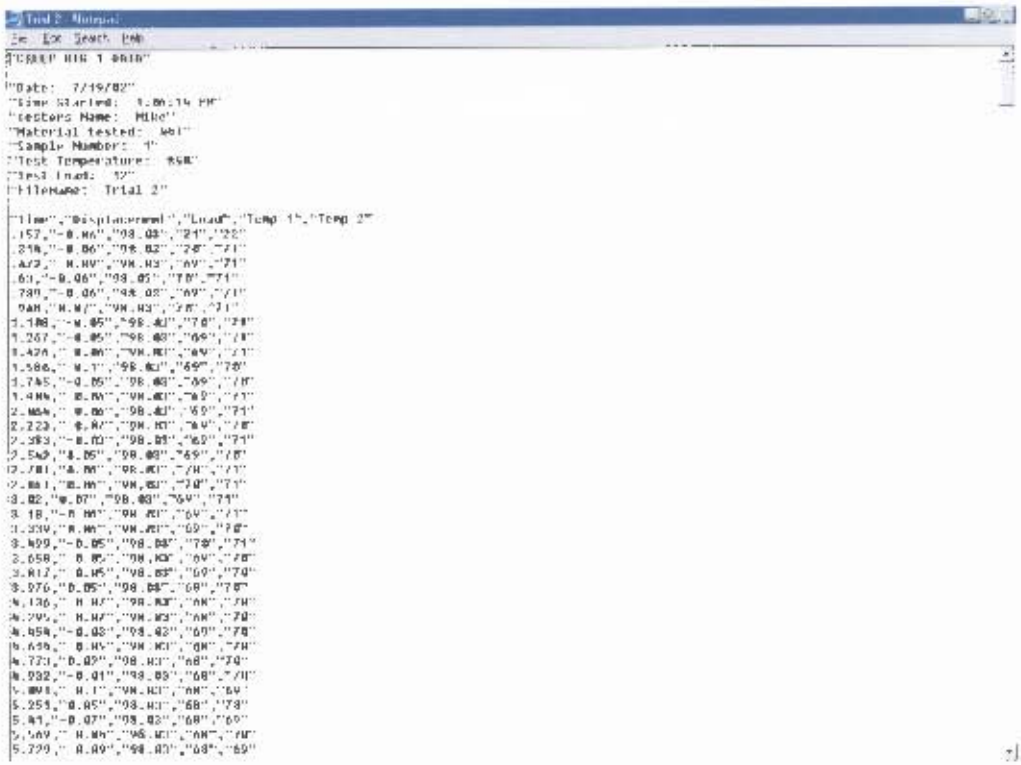

**Figure 3.8:** The text file output of the data acquisition system.

The data file is updated and saved at each sampling interval, therefore, should the test be interrupted by an unforeseen event, such as a power failure, no data will be lost.

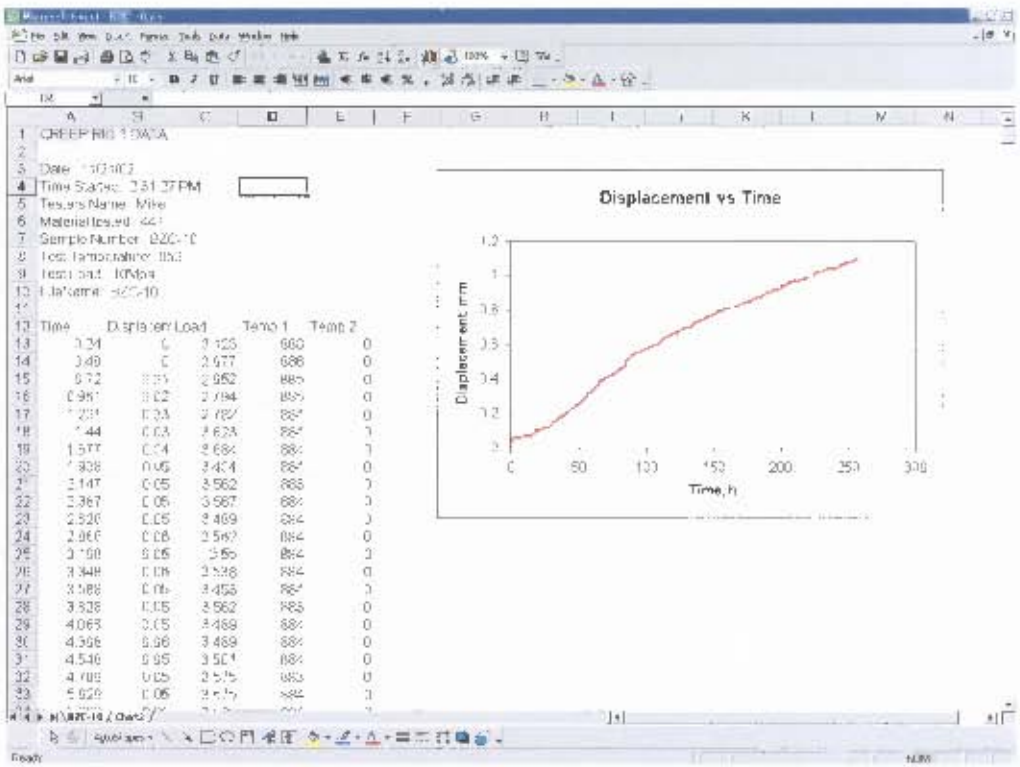


**Figure 3.9:** Data can be exported into a spreadsheet for analysis.

## 3.5 EVALUATION OF THE CREEP TEST RIG DESIGN

Creep tests conducted on certain materials at low stresses may exhibit creep rates of the order of $1 \times 10^{-8}$ $s^{-1}$ (i.e. about 0.15mm extension of a 50mm gauge length specimen in 100 hours). The accuracy of the displacement reading is therefore of great significance if the creep rate of such tests is to be determined accurately.

Data was logged using the data acquisition system while the LVDT was held at a constant position. It was found that over a 24-hour period, the displacement reading did not fluctuate from the zero position at all. The data is being logged to the second decimal place, which shows that the system can accurately detect changes in displacement of 0.01mm. This was confirmed by using a micrometer gauge set-up as shown in figure 3.10. This same set-up was used for calibration of the LVDT's.

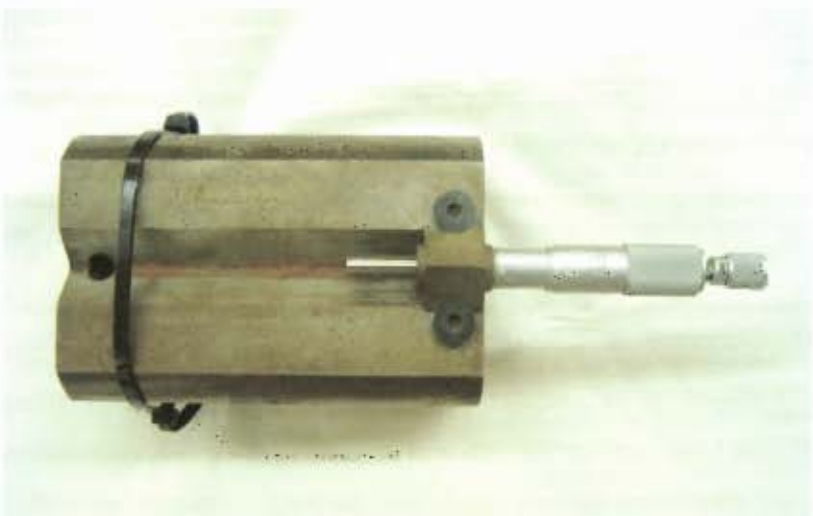

**Figure 3.10:** Micrometer gauge set-up used for LVDT calibration and evaluation.

It is not essential to log temperature and load data for creep testing, however, should a significant fluctuation of either the load or temperature occur during the course of a test, it would be important for the user to be aware of this. For this reason, load and temperature readings are also logged as a function of time. Figure 3.11 shows a typical plot of displacement and load versus time.

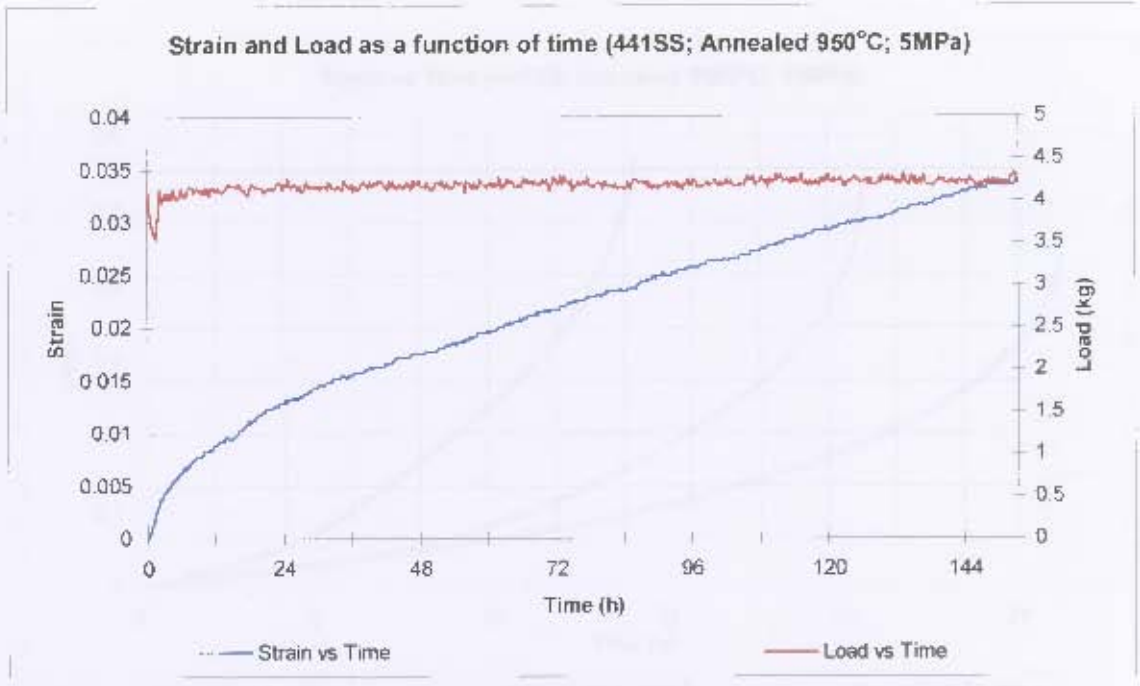


**Figure 3.11:** Typical plot of displacement and load as a function of time.

It is clear from the figure above that the load is maintained at a constant value for the duration of the test, except for the slight drop in load during the first hour. Such a change in load would not be detected without logging the load readings as a function of time.

It is also of significance to note that the results obtained from each of the two rigs are consistent. However, this reproducibility of results was only achieved after many teething problems with the rigs. Unfortunately, much of the experimental matrix (as detailed in chapter 4) was completed before this reproducibility was achieved; hence it is difficult to draw solid conclusions from the test data (see following chapters). Despite this, it can now be stated with certainty that tests conducted independently on each of the rigs on the same material in the same condition will yield the identical results, provided the that the user understands the technique required for properly setting up a test.

In testing the reproducibility of results, three identical samples were tested to fracture under the same conditions of stress and temperature (15MPa and 850°C respectively). Two samples were tested on rig 1 and one sample was tested on rig 2. Initial tests showed great variability in the test data as can be seen in the strain – time curves in figure 3.12.

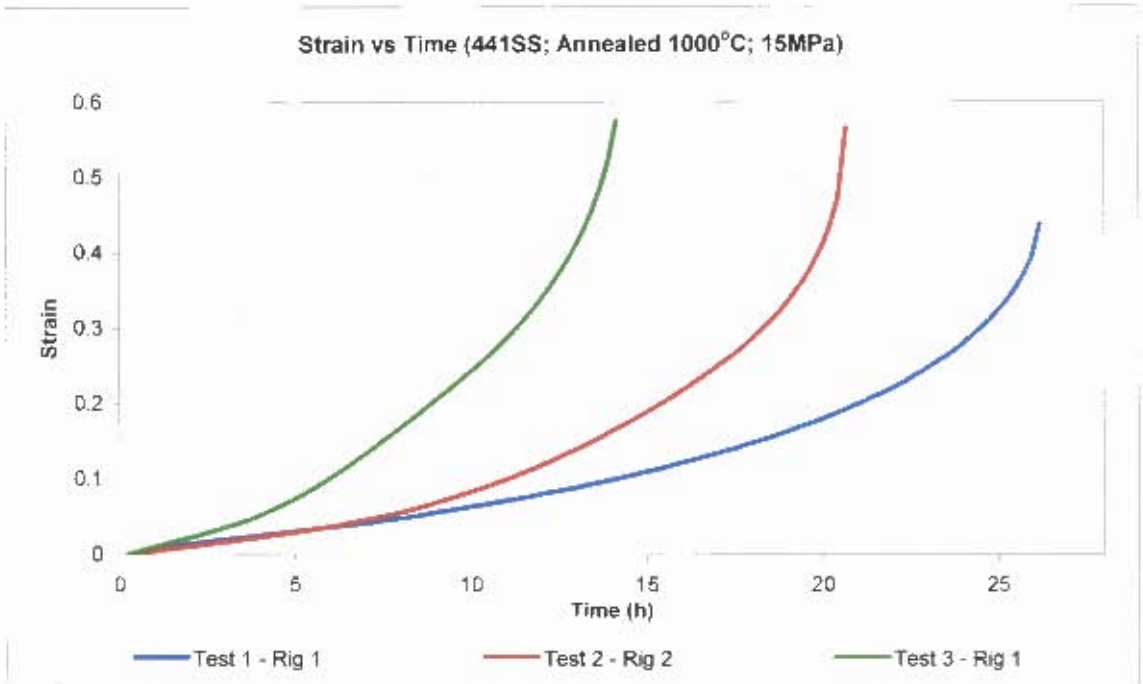


**Figure 3.12:** Strain – time plots for 3 identical creep tests used to try and determine reproducibility of test data.

The time to fracture ranged from approximately 14 to 26 hours, with tertiary creep (increasing creep rate with time) being dominant. Possible reasons for the variability of data involved specimen design, the test set-up and the nature of tertiary creep (necking and void formation). Figure 3.13 shows the three samples after testing. It is clear, in sample 3, that some amount of necking took place outside of the gauge length.

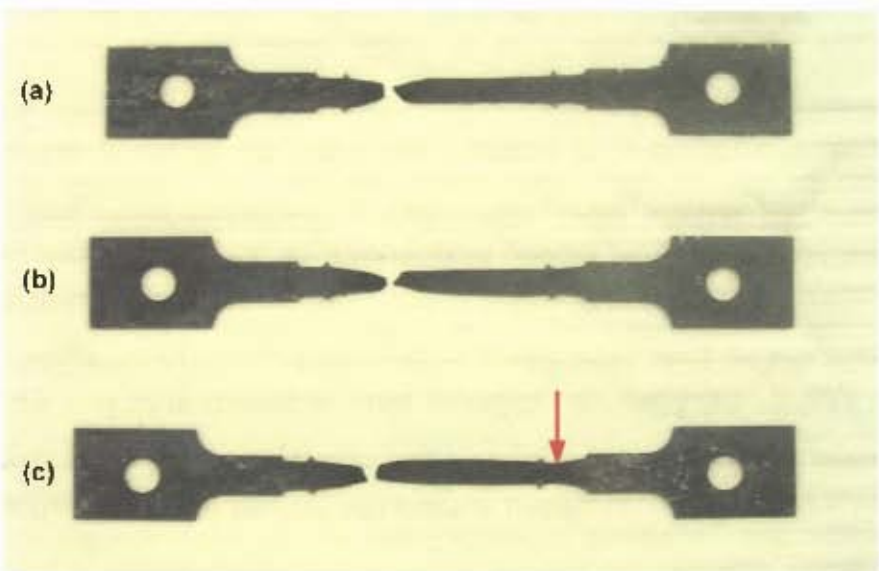


**Figure 3.13:** Creep test samples after testing. (a) Test 1 - rig 1, (b) test 2 - rig 2 and (c) test 3 - rig 1. Notice plastic deformation outside of gauge length on sample (c) indicated by red arrow.

A further set of tests was conducted, where it was decided to change the test set-up slightly. The only significant change made was to pack the insulation more lightly in an attempt to minimise any friction in the system. This was only done on one of the rigs (rig 2) and the other rig (rig1) was set-up in the same manner as all previous tests had been. For convenience, the set-up on rig 1 has been referred to as the 'standard' set-up and on rig 2 as the 'new' set-up. It can be seen in figure 3.14 that the effect of the new set-up on the results is significant.

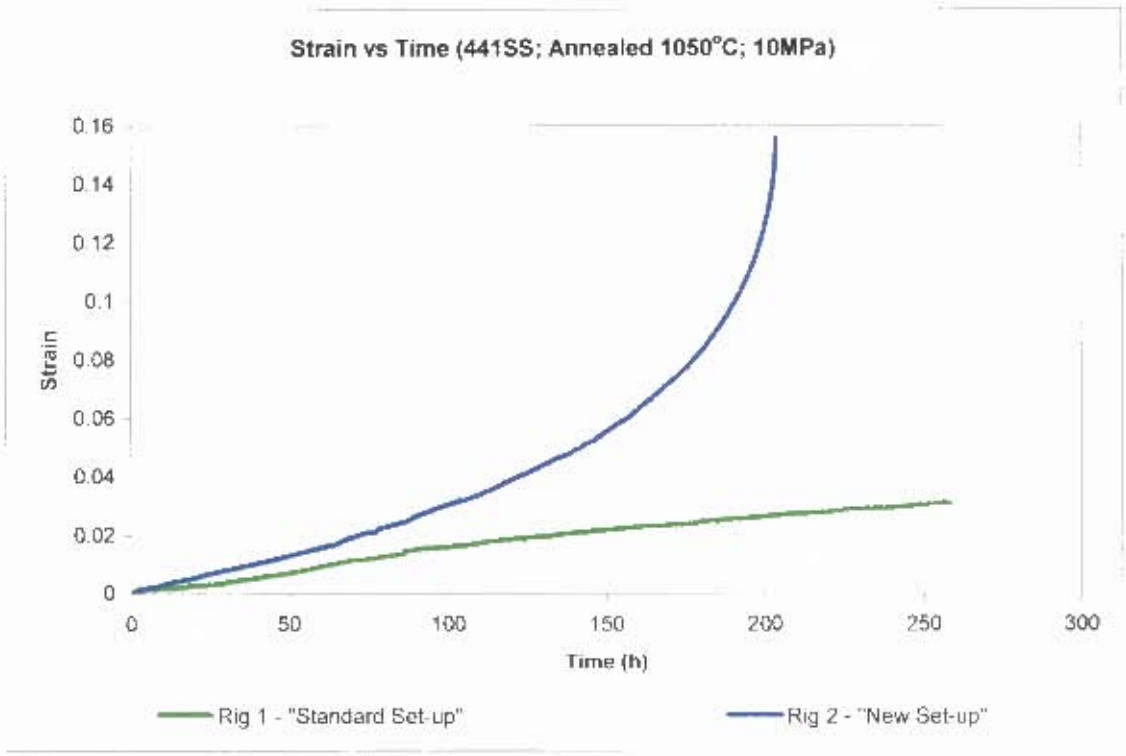


**Figure 3.14:** Differences in test data obtained by making minor changes to the test set-up in one test.

A marked difference in test data can be observed. Where the creep rate of the green curve (rig 1; standard set-up) is decreasing, the blue curve, indicating the new test set-up, shows a great increase in creep rate with increasing time. Most of the test data obtained for the experimental matrix shows results similar to the green curve above (see § 5.3). Unfortunately, there were no samples remaining to verify that the blue curve is in fact correct; therefore further tests were conducted on another set of two samples. Both tests were set-up using the new method in this case. Also, the samples used were modified by slightly increasing the width of the sample outside the gauge length. The samples were both annealed at 950°C and the test conditions were 850°C and 10MPa. The results are presented below in figure 3.15.

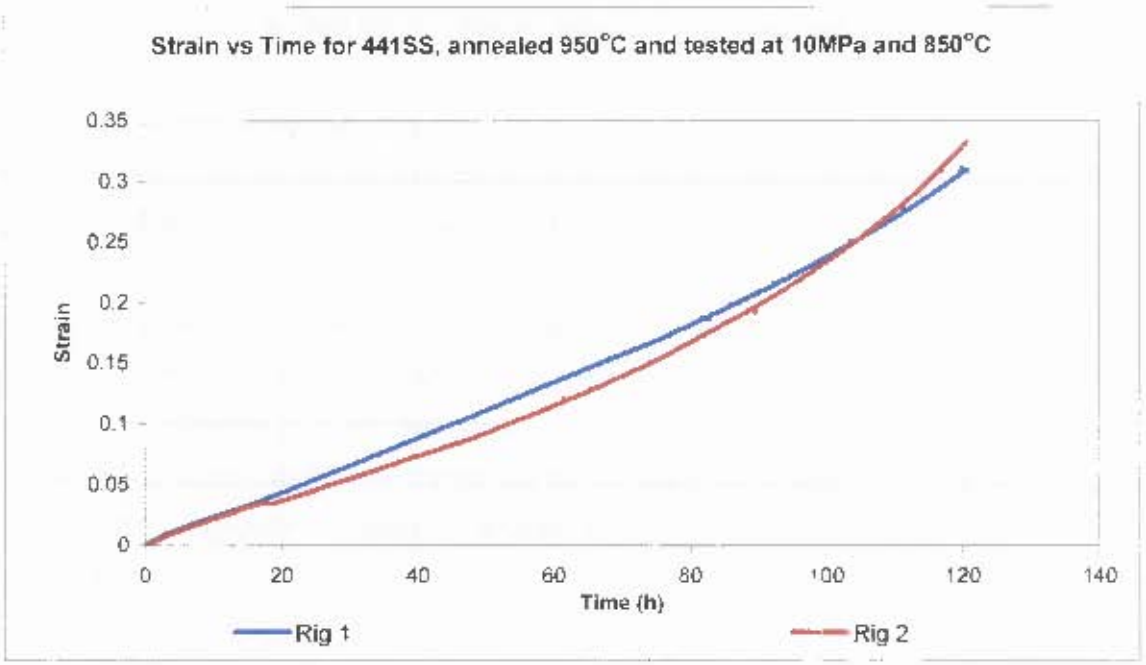


**Figure 3.15:** Strain - time plot for 441 stainless steel annealed at 950°C and tested at 850°C and 10MPa.

It can be seen that a much greater degree of reproducibility has been obtained by using the new test set-up. The agreement of the two curves above was excellent up until about 18 hours where the red curve (rig 2) showed a sharp drop in the creep rate. Subsequent to this, the rate accelerated until it exceeded that of the blue curve. The only possible explanation for the observed variation in strain against time must be a corresponding variation in the loading conditions as a function of time. Factors such as friction between the pull rods and the insulation could be resulting in such anomalies.

Given the results shown in figure 3.14, it is evident that the reliability of test data is very dependent on the way in which a user sets up the test rig. For a set of identical samples, the only factors that could result in a difference in the creep behaviour are load and temperature. In terms of the design of the creep test rigs, the more likely factor to alter during the course of a test (or to be incorrectly determined prior to a test) is the load. Three separate temperature controllers independently control each zone of the three-zone furnace, ensuring excellent temperature uniformity and despite certain temperature differences due to convection; the furnaces have shown to be consistently stable. The load train on the other hand could be problematic for two reasons. Firstly, there could be friction in the system caused by misalignment of the lever arm bearings, tight packing of the furnace insulation, bowing of the extensometer rods or some component within the furnace touching the wall of the furnace tube. Secondly, the load on the sample is meant to be zero during heating. If some factor, such as friction, should cause the load

to be wrongly indicated on the load cell, there would be no way of determining the loading conditions during testing since the reference set during heating (zero load) would be false.

Taking the above explanation, the green curve in figure 3.14 would represent a condition of lower test load than that of the blue curve. This seems to have been the case in much of the experimental matrix testing as can be seen in § 5.3.

If the user is careful in setting up a test, it is possible to obtain accurate results, however, this is not the most desirable situation. Any user should, within reason, be able to conduct a reliable creep test by following a set test procedure. For this reason, certain recommendations are made in chapter 8 to slightly modify the current test rigs to lessen the influence of user technique on the test results. Appendix C contains detailed technical information regarding these minor modifications.

# CHAPTER 4

# EXPERIMENTAL METHODS

## 4.1 MATERIALS AND HEAT TREATMENT

Columbus Stainless supplied two heats of 441 ferritic stainless steel for this investigation. The difference between the two heats is the amount of Nb present in the alloy. The nominal composition of each alloy is given in table 4.1.

| HEAT | MPO No. | Composition (wt%) | | | | | | | |
|---|---|---|---|---|---|---|---|---|---|
| | | Cr | Ni | Mn | Si | V | C | Ti | Nb |
| A | 3271730 | 17.96 | 0.19 | 0.56 | 0.50 | 0.14 | 0.02 | 0.20 | 0.47 |
| B | 330758 | 17.63 | 0.33 | 0.47 | 0.54 | 0.13 | 0.01 | 0.18 | 0.74 |

**Table 4.1:** Chemical compositions of 441 heats supplied by Columbus Stainless.

The materials were supplied as cold rolled sheet with a gauge thickness of approximately 1.4mm. The materials were supplied cold rolled so that the effects of changing the final annealing treatment parameters could be observed. Because of the time limitation, it was decided to only vary the annealing temperature and maintain the same annealing time throughout the test matrix. The heat treatment matrix was the same for both alloys and was carried out by Bohler Steel in Cape Town. The matrix is shown in table 4.2.

| Temperature (°C) | Time (seconds) |
|---|---|
| 950 | 200 |
| 1000 | 200 |
| 1050 | 200 |

**Table 4.2:** Annealing matrix for Heats A and B. Both sag and creep test specimens were annealed according to this matrix.

Sag test specimens and creep test specimens were annealed according to the matrix above to ensure that a reasonable comparison of results could be made. Furthermore, the annealing treatments were conducted isothermally in a barium chloride salt bath to ensure accuracy and consistency of the treatment.

## 4.2 METALLOGRAPHY

Optical light microscopy was performed on a REICHERT MeF3A polarised light microscope. Nomarski interference contrast mode was used to enable good contrast between the grains.

Metallographic specimens were prepared using conventional techniques. After mounting in resin, specimens were mechanically polished to a surface finish of less than 1μm. The specimens were then electro-etched to allow the grain boundaries, precipitates and other microstructural characteristics to be resolved.

Electro-etching was performed at room temperature at 1.5V dc for approximately 90 seconds using a nitric acid solution comprising the following:

1 part nitric acid ($HNO_3$)
1 part water ($H_2O$)

The electro-etching revealed the ferrite grain boundaries, carbonitrides and other precipitates.

## 4.3 SAG TESTING

Sag testing is used as an industry benchmark test for comparing the creep resistance of various alloys (see § 2.7.3). A small frame was constructed with supports 254mm (10") apart, which can accommodate 6 specimens side-by-side and be placed in a standard furnace for the required testing time. Figure 4.1 shows the sag test frame constructed with the specimens placed across the supports.

**Figure 4.1:** Sag test frame with 6 specimens placed across supports. The oxidation on the surface of the specimens is due to annealing in a salt bath.

Measurement of the deflection of the specimens was made using a dial gauge set-up that was modified to accommodate a span of 254mm between the supports. Figure 4.2 shows the dial gauge with a specimen placed on the supports.

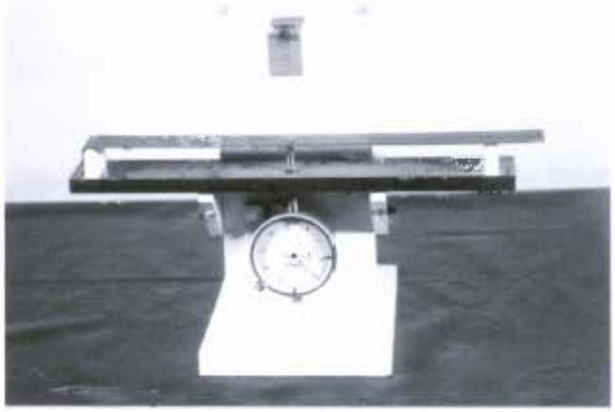

**Figure 4.2:** Dial gauge used for deflection measurement of sag test specimens.

The dial gauge is capable of measuring deflections to an accuracy of ±0.01mm, however, the oxide scale on the specimen surface after sag testing and the error involved in placing the specimen on the supports means that the accuracy is more likely in the region of ±0.05mm.

Each heat of 441 was tested in the various annealed conditions described in table 4.2 for testing times of 5, 30, 60 and 100 hours at 850°C. Under normal conditions, the specimens in a sag test are tested for 100 hours, however, by varying the testing time, it is possible to get an idea of what happens between the start of the test and 100 hours. In general, it is preferable to conduct the sag tests in a furnace with a fan, which minimises any temperature variations within the furnace. Unfortunately, such a furnace was not available for the duration required and therefore the tests were conducted in a furnace where the temperature distribution was measured to be approximately ±20°C. This was obviously not ideal, however specimens were arranged randomly on the test frame to reduce the amount of error involved. Furthermore, two specimens were tested in each condition and an average value of deflection for these two tests was taken as a final result.

## 4.4 CREEP TESTING

Creep tests were conducted in order to obtain continuous strain – time data, which is not possible with a sag test. It was also intended to use the creep test data to investigate the mechanism of deformation in the two heats of 441 stainless steel.

The creep testing apparatus is described in detail in chapter 3. Samples were machined from cold rolled sheet with the tensile axis parallel to the rolling direction (figure 4.3 below). Small tabs on either end of the gauge length provide a means of securely attaching the extensometer.

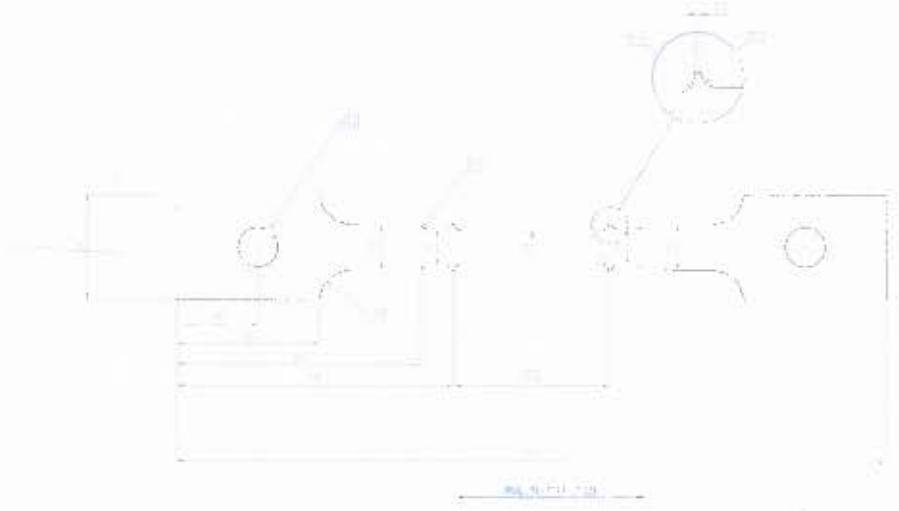

**Figure 4.3:** Creep test sample machined with tensile axis parallel to rolling direction.

Samples were tested under constant load at a temperature of 850°C. The initial load applied to most of the specimens corresponded to a stress of 5MPa, which is about twice the load on a sag test specimen due to its own weight. Unfortunately, due to time constraints, the evaluation of the creep test rigs was done using the test data from the experimental matrix proposed for this investigation. Therefore, it will be noticed that the data obtained for many of the tests is inconsistent and unpredictable as a few teething problems were experienced with the rigs. Nevertheless, certain important conclusions can still be drawn from these data and these are presented and discussed in the chapters following.

Specimens from heat B, annealed at 1050°C, were tested at loads ranging from about 5 to 15 MPa in order to be able to plot the strain rate against stress and hence calculate the stress exponent, $n$. As explained in §2.5.5 the value of $n$ can be used in identifying the prevalent creep deformation mechanism. The experimental matrix for creep testing is summarised in table 4.3.

| Heat | Annealing Temp (°C) | Stress (MPa) |
|---|---|---|
| A | 950 | 5 |
| | 1000 | 5 |
| | 1050 | 5 |
| B | 950 | 5 |
| | 1000 | 5 |
| | 1050 | 5 |
| | | 10 |
| | | 15 |

**Table 4.3:** Experimental matrix for creep testing. This matrix is carried out for both heats and all tests are to be conducted at 850°C.

Further creep testing was done to evaluate the reliability of the creep test rigs. Some of this data is presented in §3.5 of the previous chapter.

CHAPTER 5

# EXPERIMENTAL RESULTS

## 5.1 INITIAL MICROSTRUCTURES

The microstructure of each heat after various final annealing treatments was analysed before testing. Figures 5.1 (a) to (f) show the micrographs of the material in the various annealed conditions.

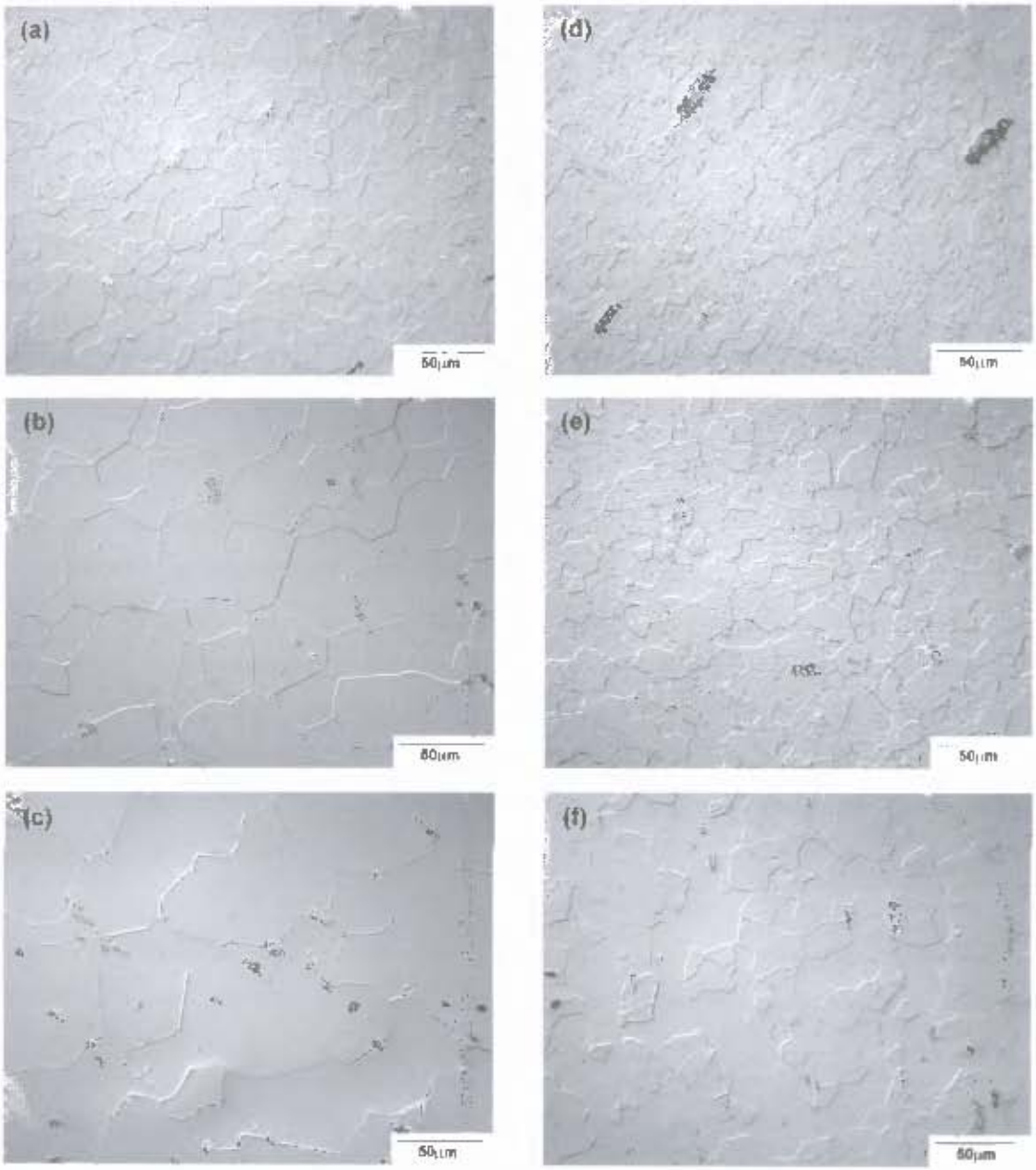


**Figure 5.1:** Micrographs of heat A annealed at (a) 950°C, (b) 1000°C and (c) 1050°C and heat B annealed at (d) 950°C, (e) 1000°C and (f) 1050°C.

It is quite clear from the micrographs in figure 5.1 that the grain size increases with increasing annealing temperature (as would be expected) and that the grain size of heat A is consistently larger than that of heat B. Grain size measurements, obtained using the linear intercept method, are tabulated in table 5.1.

| Annealing Temperature | Average Grain Size | |
|---|---|---|
| | Heat A (μm) | Heat B (μm) |
| 950 °C | 12.2 ± 5.2 | 13.7 ± 4.7 |
| 1000 °C | 30.3 ± 13.2 | 14.0 ± 6.5 |
| 1050 °C | 48.6 ± 20.0 | 18.5 ± 8.3 |

**Table 5.1:** Average grain sizes and standard deviations of annealed samples measured using the linear intercept method.

Other than differences in grain size, the microstructures seem to show no other differences. The large precipitates visible on certain micrographs are likely to be titanium and niobium carbonitrides as are commonly present in wrought stabilised ferritic stainless steels[5,6,63].

## 5.2 SAG TESTING

The sag test produced seemingly consistent results. As could be expected, sag deflection increased with increasing time, and more importantly, the amount of sag decreased for higher annealing temperatures (i.e. high annealing temperatures produce good resistance to creep) as was reported in the literature[6,11]. Figures 5.2 (a) and (b) show the results obtained from heat A and heat B respectively. Each data point represents an average of 2 tests. In general, if the two results obtained differed widely, a third test was conducted on that particular sample to confirm the result. Unfortunately, not all tests could be confirmed in this manner due to a shortage of annealed specimens.

Despite the apparent consistency of results, it should be noted that certain anomalies were also recorded from the sag tests. An example is the decrease in the sag value of Heat A, annealed at 1000°C, between 60 and 100 hours (yellow data points on figure 5.2 (a)).

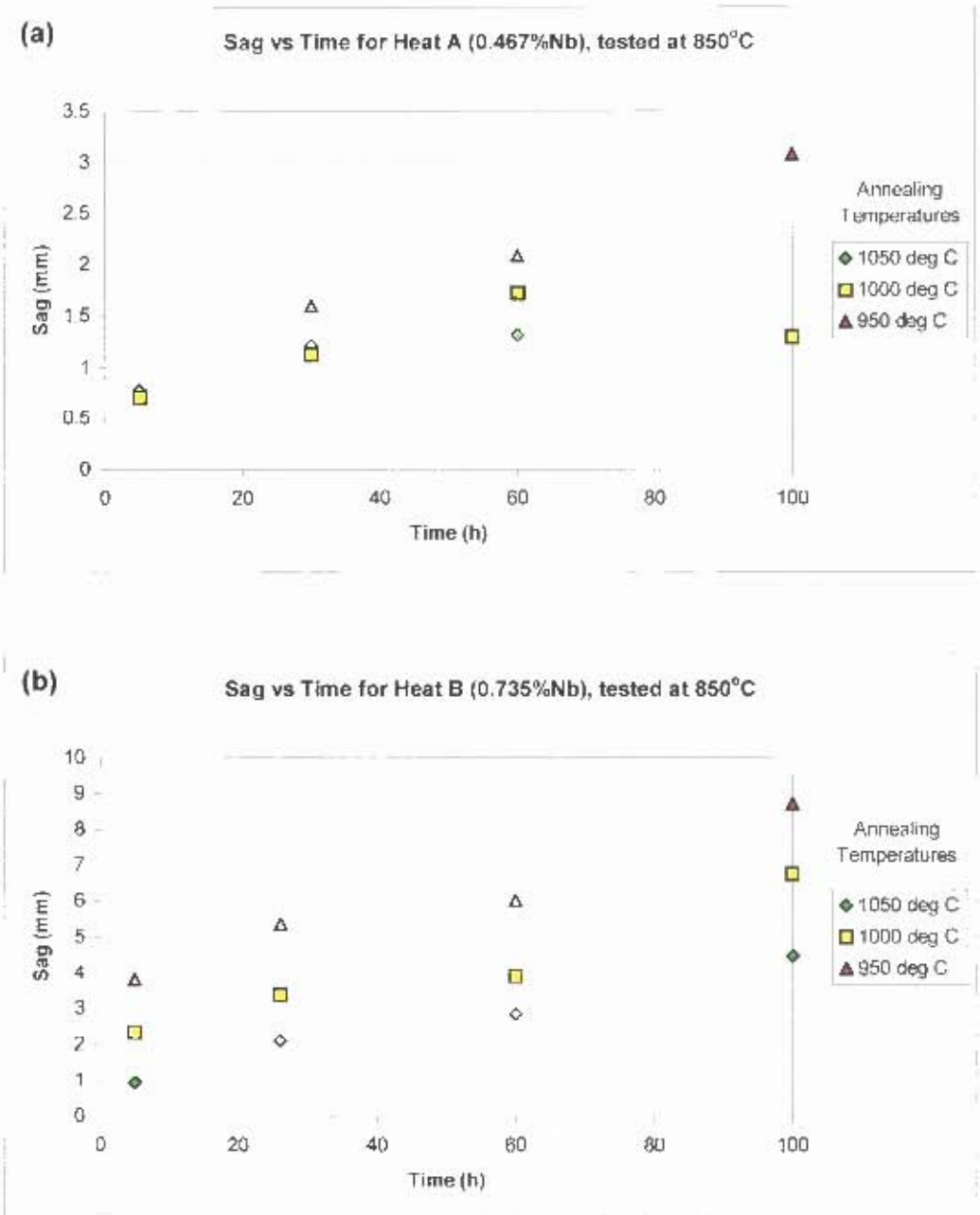


**Figure 5.2:** Sag test deflection plotted as a function of time for heat A (a) and heat B (b) for different annealing temperatures.

It is clear from the figures above that heat A (low Nb content) displays a far greater resistance to sag than does heat B (high Nb content). E.g. considering samples annealed at 1050°C, heat A shows a sag value of approximately 3mm after 100 hours, where the corresponding sample of heat B shows a sag value of approximately 8.5mm. This apparently contradicts reports in the literature that state a higher Nb content is beneficial for creep resistance[6,11].

Evaluation of the microstructures after sag testing reveals an expected increase in grain size and numerous precipitates both within the grains and on grain boundaries can be observed. Figures

5.3 (a) to (f) show the microstructures of heat A ((a) to (c)) and heat B ((d) to (f)) after sag testing for 100 hours at 850°C.

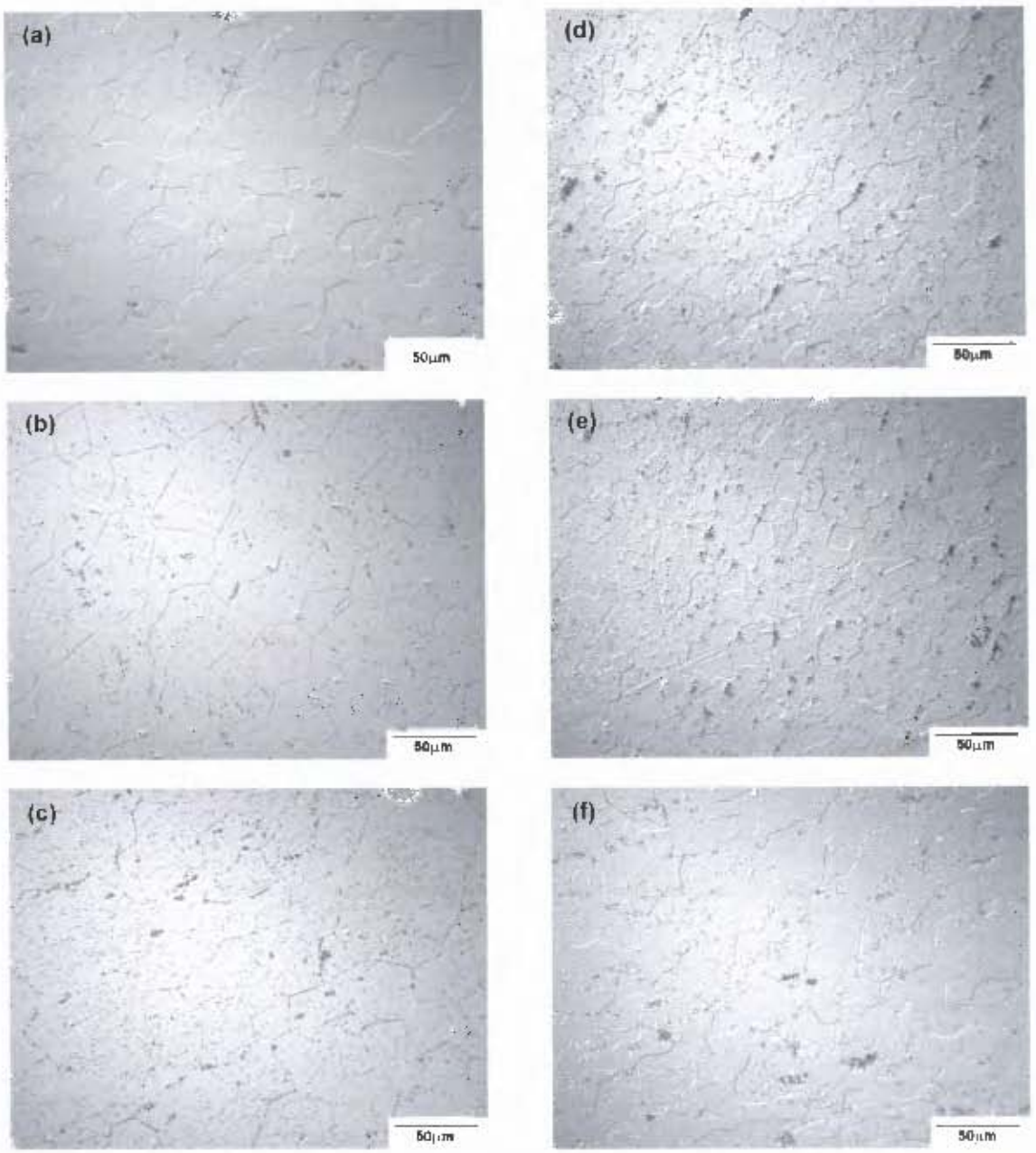


**Figure 5.3:** Post sag test microstructures for heat A ((a) Annealed 950°C; (b) Annealed 1000°C; (c) Annealed 1050°C) and heat B ((d) Annealed 950°C; (e) Annealed 1000°C; (f) Annealed 1050°C).

No analysis was conducted on the composition of the precipitates, however, the literature reviewed indicates that it is likely that Ti,Nb(C,N) is present as well as a Laves phase ($Fe_2Nb$)[65].

## 5.3 CREEP TESTING

Creep tests were conducted in order to gain a broader understanding of the high temperature creep behaviour of 441 stainless steel. In terms of the resistance of each heat to high temperature deformation, the creep tests indicated (as the sag tests had also indicated) that heat A has a greater resistance to high temperature creep than heat B. The creep test results of each heat tested in various annealed conditions at 5 MPa and 850°C are presented in the graphs in figures 5.4 (a) and (b).

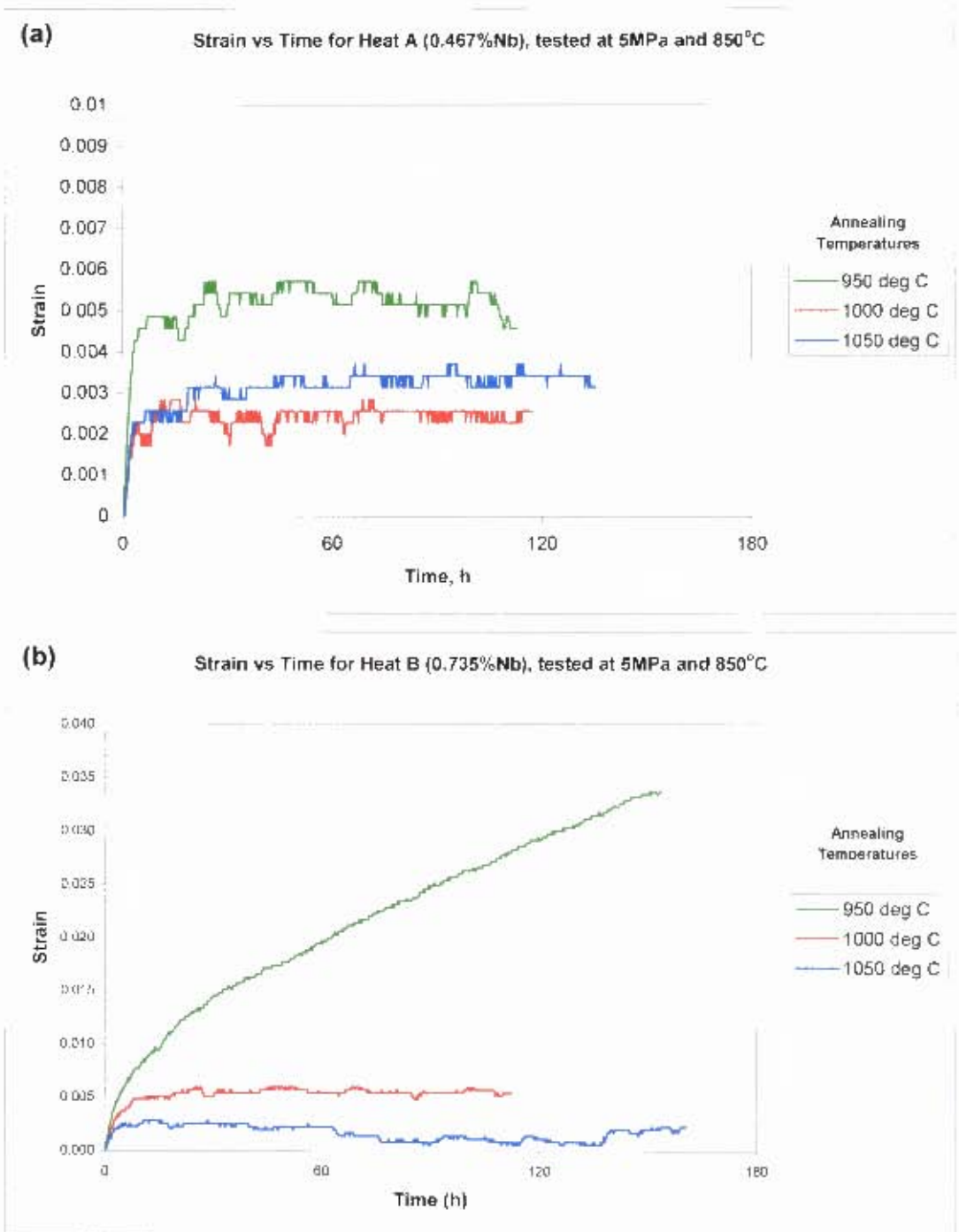


**Figure 5.4:** Creep results for heat A (a) and heat B (b) at 850°C and 5 MPa.

The results shown for heat A look somewhat discontinuous, since the extension values logged from the LVDT are rounded off to the closest 0.01mm (or about $2.9 \times 10^{-4}$ strain in this case). In general, the trends shown by the strain versus time plots seem to be consistent with the literature showing increasing resistance to creep with increasing annealing temperture[6,11]. As with the sag testing, however, there are some inconsistent data, such as the observed decreasing strain with time in some tests, which has already been discussed in more detail in § 3.5.

The microstructures of the creep test samples were examined after testing in order to gain a better understanding of the mechanism of deformation and are presented in figures 5.5 (a) to (f) overleaf. It can be noted again that the grain size increases with increasing annealing temperature and the smaller grain size of heat B is noticeable. Table 5.2 shows the average grain sizes of heat A and B after creep testing.

| Annealing Temperature | Average Grain Size | |
|---|---|---|
| | Heat A (μm) | Heat B (μm) |
| 950 °C | 13.1 ±5.9 | 11.7 ±6.8 |
| 1000 °C | 29.4 ±15.3 | 11.1 ±5.8 |
| 1050 °C | 47.4 ±20.0 | 20.3 ±10.4 |

**Table 5.2:** Average grain sizes and standard deviations after creep testing measured using the linear intercept method.

As with the annealed samples, the grain size measurements yielded a rather high standard deviation indicating a large variation in the grain size.

It is evident from the micrographs in figure 5.5 that there is considerable precipitation on grain boundaries and within the grains. The composition of the precipitates is probably the same as those formed in the sag test samples.

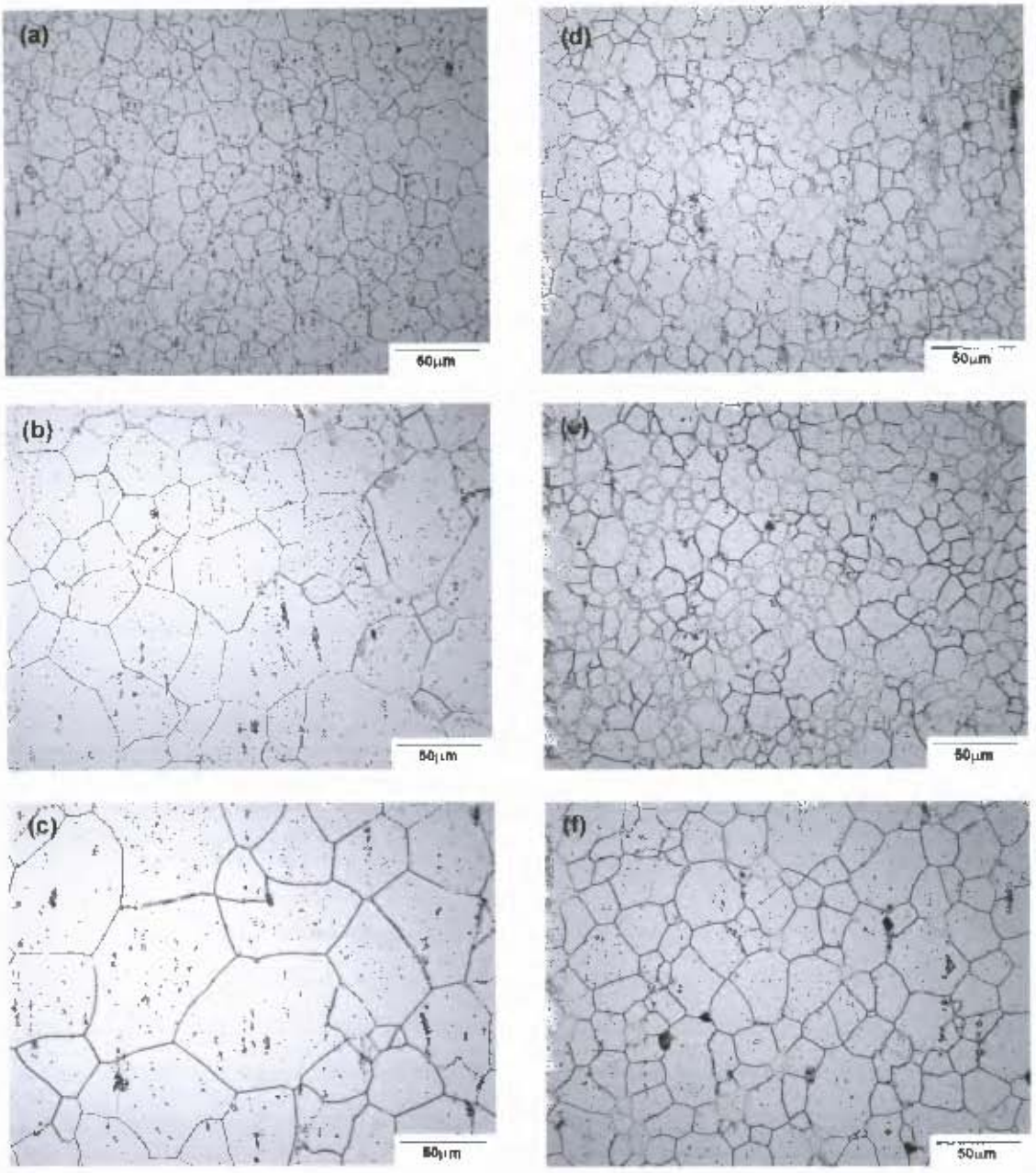


**Figure 5.5:** Post creep micrographs of heat A annealed prior to testing at (a) 950°C, (b) 1000°C and (c) 1050°C and heat B annealed prior to testing at (d) 950°C, (e) 1000°C and (f) 1050°C.

The high definition of the grain boundaries in figure 5.5 is largely due to etching. Further discussion on the composition and nature of the precipitates formed is contained in the following chapter.

Creep tests were also conducted at varying levels of stress, namely: 5, 10 and 15 MPa in order to help identify the predominant creep deformation mechanism. Figure 5.6 shows a plot of the data obtained from these tests.

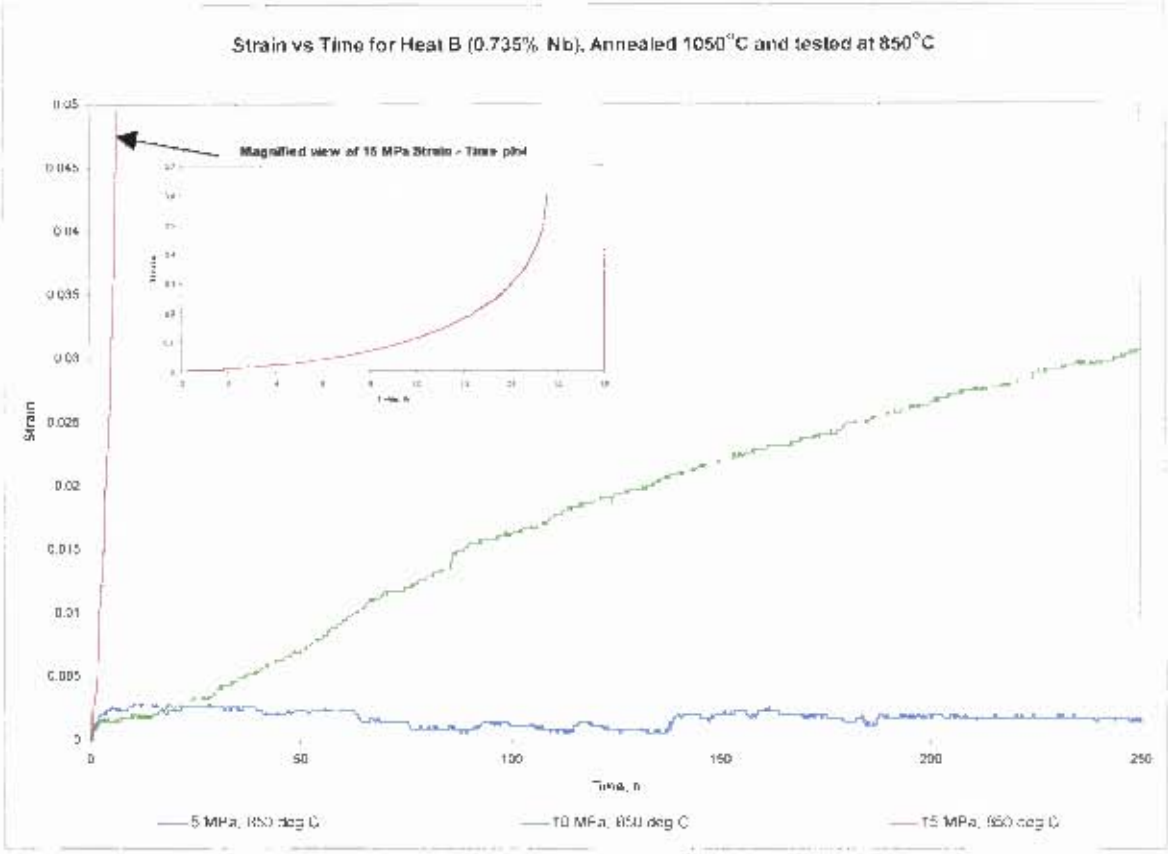


**Figure 5.6:** Strain – time data for heat B annealed at 1050°C. Tests were conducted at 850°C and loads ranging from 5 to 10MPa.

The inset in the above figure shows a full view of the test data for 15MPa. Both the 5MPa and 10MPa test seem to show irregularities (such as negative creep strain) characteristic of load application problems. The details of the load application problems are discussed in Appendix C with recommended solutions. Unfortunately, owing to the inconsistency of this data, very little can be deduced from it in terms of creep mechanisms.

# CHAPTER 6

# DISCUSSION

## 6.1 GENERAL COMMENTS

### 6.1.1 Grain Size Variation

The material supplied in the cold rolled condition was annealed at various temperatures to produce the microstructures shown in figure 5.1. It is clear from these micrographs that there is no longer any evidence of cold rolling in the grains (i.e. recrystallisation has taken place during annealing). Perhaps the only evidence of cold rolling is in the elongated appearance of certain precipitates (probably Ti,Nb(C,N))[5,6,63] that did not dissolve at the lower annealing temperatures.

It is interesting to note that heat B (high Nb) has a noticeably smaller grain size than that of heat A (low Nb), despite having the same thermomechanical history. It has been shown that Nb in solid solution retards recrystallisation, thus reducing the amount of grain growth that can occur[68]. The result of this is that although identical annealing treatments were conducted on both alloys in order to make a quantitative comparison of the effect of Nb content in solution on the creep properties, the results will be skewed by the grain size difference between the two heats. Both high Nb content and large grain size favour good creep resistance. Heat B has a higher Nb content than heat A, but a smaller grain size and vice versa, therefore it is difficult to distinguish between the relative effects of each factor, since neither is constant.

### 6.1.2 The Influence of Sample Design

The measured gauge length was designed to have the smallest cross-sectional area, such that the plastic deformation occurring would proceed between the measured points on the sample. In certain circumstances, plastic deformation outside of the measured gauge length (see figure 3.13) can result in a small amount of error in the measurements. It is better if the head of the sample through which the retaining pin is placed is made wide enough such that no plastic strain occurs there. Allowance must be made for the stress concentration of the pinned joint when deciding on the correct sample head width to use.

Other than the possibility of small errors due to strain outside of the measured length, the effect of sample design seems to be minimal, however, it is advisable, that all samples tested in comparative tests are of the same geometry. The AISI standard for creep testing of metallic

materials recommends that the geometry of the sample is such that it is representative of the material as a whole.

## 6.2 CREEP RESISTANCE OF 441 STAINLESS STEEL

### 6.2.1 Significance of Sag Test Data

The determination of the reliability of the sag test technique was set as an objective for this project. The means by which this objective was to be achieved was to compare the sag of samples after various time intervals with data obtained from continuous creep testing. Given the unreliable nature of the creep test results observed in the previous chapter, it would be senseless to use this data as a measure of reliability for another test (in this case). The general trend of increasing creep resistance with increasing annealing temperature was however observed in both tests. Thus it can be said that the general trend of the data with respect to annealing temperature is most likely correct, but nothing can be stated regarding the absolute values of strain obtained.

The only other benchmark for comparison available is sag test data recorded in literature. Barteri et al.[69] used the sag test to investigate the creep resistance of hot end exhaust component materials. Included in their investigation was 441 stainless steel. Unfortunately, it was not possible to determine the condition of the material prior to testing, but it seems that the average absolute value of sag deflection obtained for 441 stainless steel was 7.5mm[69]. Figure 6.1 shows the sag test data obtained by Barteri et al. for various alloys.

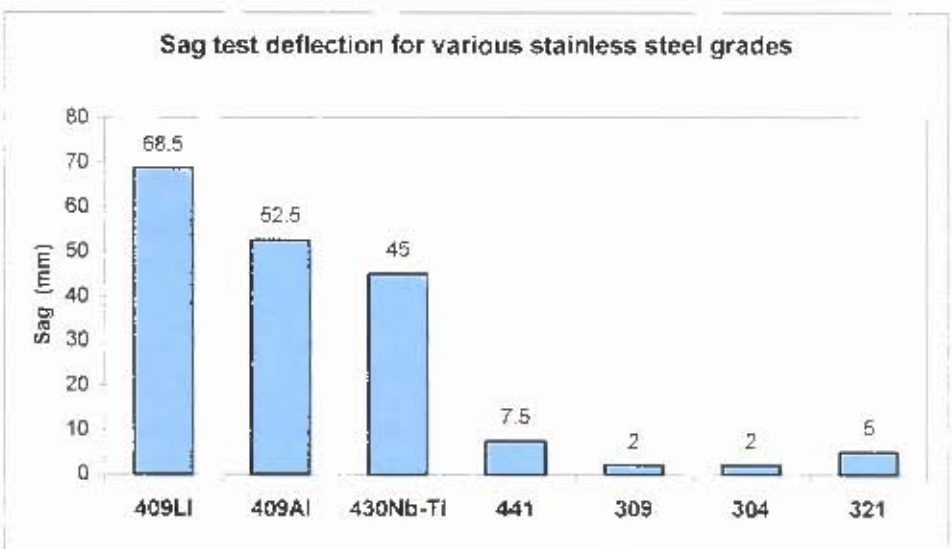


**Figure 6.1:** Sag test data for various grades of stainless steel. After Barteri et al.[69]

The values of sag obtained in the present investigation ranged from approximately 1.3mm to 8.7mm (see figure 5.2). This places the data within the same range as that obtained by Barteri et al. for the same material. Although it may be difficult to place a quantitative measure on the reliability of the data obtained from sag testing, it seems reasonable to suppose that a high level of accuracy could be obtained with regards to ranking alloys in terms of creep resistance and approximating the relative creep strengths of various alloys tested under the same conditions (i.e. being able to state that a particular alloy is 30% stronger than another alloy given a 30% lower sag deflection).

The level of accuracy of data also seems to be highly dependent on the test set up. Variability of the test data can be attributed to one or more of the following factors: temperature variations of approximately 30°C within the furnace (measured), friction between the sample and the supports (exacerbated by the formation of oxide scale) and the limitations of the deflection measurement set up (despite the dial gauge accuracy of 0.01mm, readings varied by up to 0.2mm, depending on how the sample was mounted onto the measurement stand).

### 6.2.2 Interpretation of Creep Test Data

The creep tests described in the experimental matrix (table 4.3) were used in assessing the reliability and reproducibility of the creep test rigs. The main reason for this was to save time since the long duration nature of creep testing would not allow for separate matrices of reliability tests and investigative tests to be carried out within the time period set for this investigation.

Many teething problems were experienced during testing and this is clearly shown by the data (figures 5.4 and 5.6). These problems were expanded upon in § 3.5 and will not be repeated here. Accurate creep data is now obtainable by using the appropriate specimen geometry (limiting deformation to the gauge length only) and by applying a careful technique when setting up a new test. Certain recommendations (see chapter 8) are made to ensure that reliable data is obtained on a consistent basis.

As stated before, the general trend of increasing creep resistance with increasing annealing temperature was observed. In the context of Nb containing ferritic stainless steel, the increased annealing temperature would result in a higher proportion of Nb in solid solution, thus increasing the potential for strengthening by solid solution or by the formation of fine Laves phase and Nb carbide precipitates on grain boundaries and within grains[6,11]. Precipitate formation on grain boundaries impedes both diffusion and dislocation creep mechniasms[14,51]. There is a significant difference in the grain sizes of the samples annealed at different temperatures (table 5.1). This

could pose as an alternative explanation for the observed increasing creep resistance with increasing annealing temperature. A high annealing temperature would produce a coarse grain structure and possibly promote creep resistance if diffusion creep processes are dominant. The problem of distinguishing between the effect of grain size and that of Nb content is therefore encountered as initially described in § 6.1.1. If diffusion creep is not the dominant process, it is likely that the effect is not one of grain size, but rather of Nb content, since it is generally accepted that the effect of grain size on the creep resistance of materials deforming by dislocation creep mechanisms is small[32], if not negligible[36].

### 6.2.3 Microstructural Observations

All post test microstructures, whether sag test or creep test, showed an increasing grain size with increasing annealing temperature and some amount of precipitation both on grain boundaries and within the grains themselves. Figure 6.2 (a) and (b) show heat A and B, both annealed at 1050°C and tested under the same conditions of stress and temperature (5MPa, 850°C).

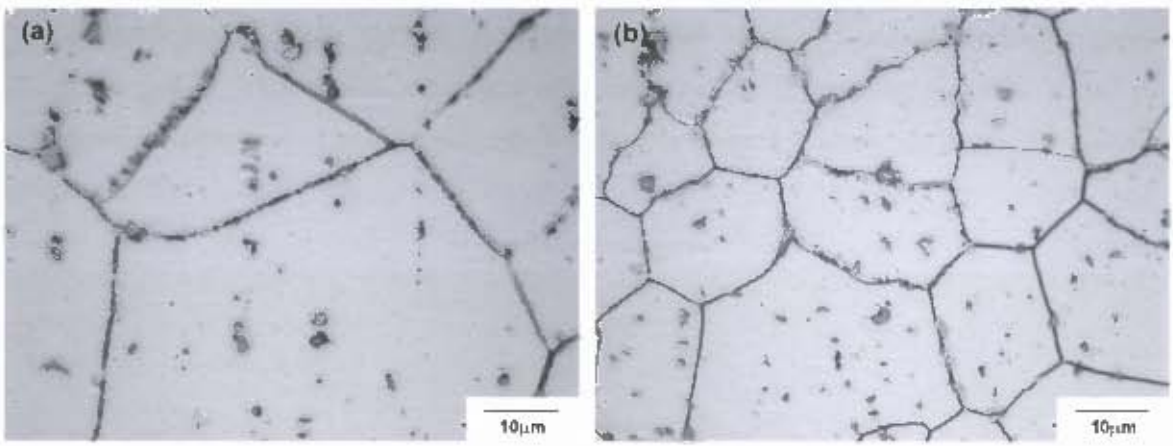


**Figure 6.2:** Post creep micrographs of heats A and B ((a) and (b) respectively) annealed at 1050°C and tested at 5MPa and 850°C. Precipitation within grains and along grain boundaries is visible.

Unfortunately, no analysis of the composition of the precipitates was performed, however, it is clear from the literature that Ti,Nb(C,N) should be present, as well as some Laves phase, given that the material has been held between 820°C and 930°C for extended periods of time[65]. Despite the high magnification of the micrographs above, it is quite clear that heat B has a smaller grain size than heat A, due to the retarding effect of Nb on the rate of recrystallisation and grain growth[67].

### 6.2.4 Operative Creep Mechanisms

The intention of this investigation was to conduct creep tests at a range of stresses in order to be able to calculate the stress exponent, $n$. Although it does not confirm the mechanism of deformation 100%[192], the value of $n$ can be used as a guide to determining the mechanism of creep deformation (see table 2.4). The data presented in figure 5.6 is not suitable for accurate calculation of the creep strain rate and hence the value of $n$. Since calculating $n$ is not a viable option in this case, a careful observation of the microstructure will aid in the determination. It is also possible that the mechanism of deformation will change within the stress range selected. It has been calculated that the stress on a simple sag test sample is approximately 3-4MPa (see Appendix D for calculation), thus the mechanism operating in the 5MPa creep test should be a good indication of the mechanism operating during sag testing, which is probably close to the service stresses that the material will experience.

The shape of a grain will only be changed during conventional diffusion and dislocation creep mechanisms. Grain boundary sliding on the other hand simply results in an increase in the number of grains along the tensile axis, rather than causing any grain elongation. Unfortunately, the sample tested at 5MPa did not show enough creep strain to make any possible grain elongation visible. Thus the microstructure of a sample of heat B (annealed at 950°C) tested at 10MPa was investigated. The microstructure is shown in figure 6.3, alongside that of the sample tested at 5 MPa.

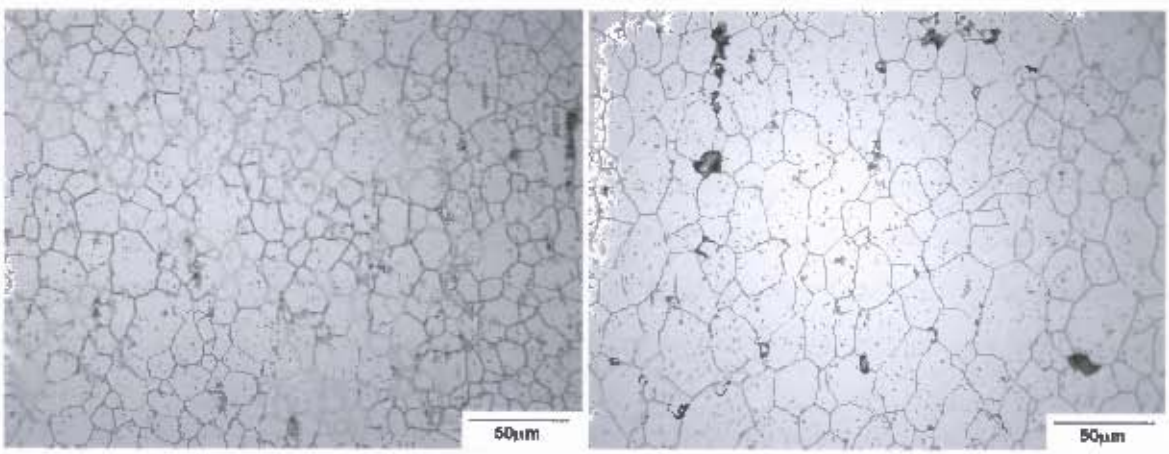


**Figure 6.3:** Microstructure of heat B, annealed at 950°C and tested at 5MPa and 850°C (Left); and annealed at 950°C and tested at 10MPa and 850°C (Right).

The sample tested at 10MPa exhibits a larger grain size and it can be noted that almost every grain is elongated in the vertical direction, which corresponds to the tensile axis.

It is now reasonable to suggest that the deformation mechanism is not grain boundary sliding. It is also certain that Harper-Dorn creep would not take place, since this is a rare mechanism found mostly in high purity aluminium at stresses of the order of 0.1MPa[36].

It is clear that the operative mechanism must be dependent on grain size, since the larger grain size of heat A after annealing gives it significantly better creep resistance than heat B, which has a higher Nb content. The case for diffusion creep is therefore strong. Diffusion creep does lead to grain elongation and it is highly dependent on grain size.[27]

The grain size dependence does not, however, preclude dislocation creep mechanisms. It has been found that the strain rate in dislocation mechanisms is affected by the grain size[32]. Factors in favour of dislocation creep (in particular, recovery-controlled dislocation creep) are: ferritic stainless steel has a high stacking fault energy, meaning that climb and cross-slip of dislocations can occur readily[19] (these processes proceed with the aid of vacancy diffusion[16]), grain elongation in the direction of the tensile axis is observed and the question should be asked whether the creep rates observed at 850°C are able to be accounted for using the diffusion creep model.

The above being said, it is also true that grain elongation was only observed in a sample tested at 10MPa and in general, recovery-controlled creep is said to occur in class II materials. Examples of class II materials are pure metals and single-phase alloys[31], which seems to exclude 441 stainless steel.

Glide-controlled creep requires dislocations to glide through the lattice under an applied stress[22]. A 441 alloy produced by Allegheny Ludlum is said to have a yield strength of approximately 25MPa at 850°C[65]. This does not imply that the applied stress needs to exceed 25MPa, since at the temperature of 850°C there is a large amount of thermal energy available to help dislocations glide. The limiting factor will be the energy required by a dislocation to overcome an obstacle in the lattice[17].

The shape of the creep curves obtained indicated the presence of some amount of primary creep. Primary creep is characteristic of a power law (i.e. dislocation creep) creep curve. During primary creep, the rate of work hardening in the material exceeds the rate of recovery, resulting in a decreasing creep rate[20]. If only diffusion creep were present, there would be no reason for the creep rate to decrease in the initial stage of the test.

Given the high temperature, it is clear that diffusion will play an important role, regardless of the deformation mechanism. There is evidence to suggest that there is some type of dislocation movement within the structure, however only further investigation could possibly identify this for certain.

# CHAPTER 7

# CONCLUSIONS

Two constant load creep test rigs were designed, manufactured and commissioned in accordance with ASTM 139-00 standards for the creep testing of metallic materials. The data acquisition system for the rigs was programmed using Microsoft® Visual Basic 6.0® and is capable of logging extension, load and temperature as a function of testing time. Despite some initial problems, it is now possible to produce accurate creep test data using the rigs, however the reliability of the data is still highly dependent on the users ability to set the tests up correctly. Recommendations are made for the improvement of the rigs to such a level that any user can set up a successful test given a set procedure.

Sag testing was found to be a useful method for comparative testing of the creep resistance of an alloy in different annealed conditions. Other than temperature distributions within the furnace, it seems that the reliability of the test is affected mostly by the friction between the sample and the test rack. Results obtained showed consistent differences between samples of different annealed conditions and once a test method had been established, the consistency of the results obtained improved.

In particular, the results of the sag tests show:

(1) A higher annealing temperature is beneficial for the creep resistance of the material. (A high annealing temperature produces a large grain size and dissolves much of the precipitates present in the microstructure).

(2) Heat A, having a lower niobium content, but a larger average grain size than heat B, displayed superior creep resistance (i.e. lower sag deflections).

(3) The deformation mechanism responsible for causing the sag test samples to creep is dependent on grain size, since a lower niobium content (heat A) should result in poorer creep resistance, but the effect of the grain size overcame the effect of niobium content (for the niobium contents tested).

(4) The data obtained from testing 441 stainless steel, supplied by Columbus Stainless, is comparable to data already published on this material.

Despite the poor quality of the data obtained from creep testing, the trends observed confirmed the first three of the above four points. The effect of the grain size relative to the effect of the niobium content on creep resistance was not resolved, however, it can be said that both factors

are vitally important in controlling the creep characteristics of the steel. In practice, a balance may have to be found where creep properties and properties required for effective processing (such as formability) can be optimised.

The mechanism of creep deformation was not identified, however, certain important characteristics were noted:

(1) The mechanism of deformation results in an elongation of the grains in the microstructure for stresses greater than or equal to 10MPa. It is possible that grain elongation occurs at lower stresses as well, however, no sample was strained to a large enough extent for this to become noticeable.

(2) Most data indicated that primary creep characterised by a decreasing creep rate occurred. This is generally characteristic of dislocation creep models (power law creep).

(3) As mentioned above, the creep rate showed a strong dependence on the grain size. This is generally characteristic of diffusion creep models.

(4) Ferritic stainless steels have a high stacking fault energy resulting in relatively easy cross-slip and climb of dislocations. This could be important with regards to recovery-controlled creep, but perhaps of more significance is the fact that this would aid dislocations in overcoming obstacles in glide-controlled creep.

(5) The temperature at which tests were conducted (850°C) necessarily means that diffusion will play an important role, regardless of the deformation mechanism. (e.g. diffusion of vacancies to dislocation lines resulting in dislocation climb).

# CHAPTER 8

# RECOMMENDATIONS

The influence of microstructure on the creep properties of 441 ferritic stainless steel was investigated, however, due to certain limitations, this objective has not been fully realised.

The creep test results showed a high dependency on the way in which a particular test was set up. In particular, the determination of the exact initial loading conditions of the specimen was found to be difficult due to the nature of the load train. It is recommended that the lower pull rod and the extensometer system be modified to ensure the possibility of precise load application. Technical details of these modifications are included in Appendix C of this report.

A simple modification of the creep test sample is also recommended in order to minimise any plastic deformation outside of the gauge length. These modifications would include a very slight widening of the head of the sample to counter any possibility of deformation around the pin holes.

Besides these minor changes to the apparatus and samples, there are certain suggestions for future work into the investigation of the microstructural influences on the creep properties of 441 ferritic stainless steel.

(1) Based on past literature[8], the influence on the niobium content and grain size are two of the most prevalent microstructural aspects to consider in an investigation of this alloy. For this reason, it is suggested that a wider selection of heats with differing niobium contents be evaluated. Of course the problem encountered in this investigation with the difference in grain size between heats (see §6.1.1) would need to be rectified if a sound analysis was to be made of the relative effect of each factor. This could supposedly be done simply by carefully adjusting the annealing times of each alloy to control the grain growth and obtain a uniform grain size across the entire range of heats. However, care should be taken to establish the amount of '*uncombined*' niobium (as described in §2.6) in each heat after annealing. The reason for this is that by changing the annealing times of each heat, a corresponding change in the amount of uncombined niobium should occur (as further dissolution of precipitates is possible with longer annealing times). The literature shows that it is the uncombined niobium that has a large effect on the creep properties[8].

(2) In terms of determining the creep deformation mechanism, it would be valuable to be able to calculate the steady state strain rate at various levels of stress and to compute the stress exponent, $n$ (see equation 2.15). This should give a good indication of the deformation mechanism, especially if uniform grain size of all samples is achieved. It is advisable that other methods be used in conjunction with this, such as, microstructural observation (grain size and shape) and electron backscattered diffraction (EBSD) for determining the extent of any sub structure (both before and after testing).

(3) The reliability of the sag test could be increased by conducting tests in a furnace fitted with a circulating fan to minimise any temperature distributions, or else a relatively large furnace (relative to the size of the samples and test rig), where temperature variations may not be as pronounced. It may also be useful to take an average of more than 2 tests per result (say 3 to 5 tests).

(2) In terms of determining the creep deformation mechanism, it would be valuable to be able to calculate the steady state strain rate at various levels of stress and to compute the stress exponent, $n$ (see equation 2.15). This should give a good indication of the deformation mechanism, especially if uniform grain size of all samples is achieved. It is advisable that other methods be used in conjunction with this, such as, microstructural observation (grain size and shape) and electron backscattered diffraction (EBSD) for determining the extent of any sub structure (both before and after testing).

(3) The reliability of the sag test could be increased by conducting tests in a furnace fitted with a circulating fan to minimise any temperature distributions, or else a relatively large furnace (relative to the size of the samples and test rig), where temperature variations may not be as pronounced. It may also be useful to take an average of more than 2 tests per result (say 3 to 5 tests).

## CHAPTER 9

# REFERENCES


1 Miyazaki, A. et al., Kawasaki Steel Technical Report, **43**, 21 (2000)

2 Satoh, S. et al., Kawasaki Steel Technical Report, **41**, 30 (1999)

3 ASTM E 139-00, *Standard Practice for Conducting Creep, Creep-Rupture, and Stress-Rupture Tests of Metallic Materials*, American Society for Testing Materials (1990)

4 ASM Speciality Handbook, *Stainless Steels* (1994)

5 Gordon, W. and van Bennekom, A., Mater. Sci. Tech., **12**, 126 (1996)

6 Johnson, J. N., SAE Technical Paper Series, 810035 (1981)

7 Tjong, S. C. and Zhang, J. S., Scripta Metall. et Mater. **30**, 1397 (1994)

8 Barteri, M. et al., "Low Cost Weldable Ferritic Stainless Steel For Hot End of Automobile Exhaust Gas Systems"

9 http://www.ametsoc.org/AMS/sloan/cleanair/cleanairlegisl.html#caa55 (Visited 04/09/02)

10 http://www.sacbee.com/content/news/story/3677199p-4703017c.html (Visited 04/09/02)

11 Fujita, N., et al., Scripta Mater. **35**, 705 (1996)

12 Ashby, M.F. and Jones, D.R.H., Engineering Materials I, Pergamon Press, Oxford (1980)

13 Kennedy, A. J., *Processes of Creep and Fatigue in Metals*, Oliver and Boyd, Edinburgh (1962)

14 Smallman, R.E., *Modern Physical Metallurgy*, Butterworth & Co Publishers Ltd, London (1985)

15 Myers, H. P., *Introductory Solid State Physics*, Taylor and Francis, London (1990)

16 http://www.poco.phy.cam.ac.uk/teaching/A_Donald/ (Visited 03/10/2002)

17 Stouffer, D. and Dame, L., *Inelastic Deformation of Metals*, John Wiley and Sons Inc., New York (1996)

18 Porter and Easterling, *Phase Transformations in Metals and Alloys*, 2nd Ed. Routledge (1992)

19 Humphreys, F. J. and Hatherly, M., *Recrystallisation and Related Annealing Phenomena*, Elsevier Science Ltd, Oxford (1996)

20 Evans, R. W. and Wilshire, B., *Introduction to Creep*, The Institute of Materials, London (1993)

21 Sherby, O.D. and Taleff, E.M. Mater. Sci. Eng. **A322**, 89 (2002)

22 Gittus, J., Creep, *Viscoelasticity and Creep Fracture in Solids*, Applied Science Publishers Ltd, London (1975)

23 Ashby, M. F., Acta Metall. **20**, 887 (1972)

24 Nabarro, F. R. N., Report of a Conference on the Strength of Solids, Physical Society, London, p75 (1948)

25 Herring, C., J. Appl. Phys. **21**, 437 (1949)

26 Wang, J. N., Acta Mater. **48**, 1517 (2000)

27 Langdon, T. G., Mater. Sci. Eng. **A283**, 266 (2000)

28 Coble, R. L., J. Appl. Phys. **34**, 1679 (1963)

29 Langdon, T. G., Scripta Mater. **35**, 733 (1996)

30 Ajaja, O., J. Mater. Sci. Letters, **21**, 3351 (1986)

31 Fagbulu, J. B. and Ajaja, O., J. Mater. Sci. Letters, **6**, 894 (1987)

32 Wilshire, B. and Palmer, C.J. Scripta Mater. **46**, 483 (2002)

33 Blum, W., Mater. Sci. Eng. **A319**, 8 (2001)

34 Wang, J.M. et al., Mater. Sci. Eng. **A334**, 275 (2002)

35 Groisbock, F. and Jeglitsch, F., JOM, **27**, 4365 (1992)

36 Harper, J. G. and Dorn, J. E., Acta Metall. **5**, 654 (1957)

37 Ginter, T. J. et al., Mater. Sci. Eng. **A322**, 148 (2002)

38 Harper, J. G. et al., Acta Metall. **6**, 509 (1958)

39 Fazan, B. et al., J. Metals, NY, **6**, 919 (1954)

40 McLean, D., J. Inst. Met. **81**, 293 (1952)

41 McLean, D., Creep and Fracture of Metals at High Tempertures, p73. National Physical Laboratory Symposium, London (1954)]

42 Ardell, A. J., Acta Mater. **45**, 2971 (1997)

43 Nabarro, F. R. N., Acta Metall. **37**, 2217 (1989)

44 Wang, J.M., Acta Mater. **44**, 855 (1996)

45 Blum, W. and Maier, W., Phys. Stat. Sol. (a) **171**, 467 (1999)

46 Burton, B. and Reynolds, G. L., Mater. Sci. Eng. **A191**, 135 (1995)

47 Ruano, O. A. et al., Mater. Sci. Eng. **A211**, 66 (1996)

48 Ruano, O. A. et al., Scripta Mater. **38**, 1307 (1998)

49 Wadsworth, J. et al., Metall. and Mater. Trans. **33A**, 219 (2002)

50 Wilshire, B., Metall. and Mater. Trans. **33A**, 241 (2002)

51 Nabarro, F. R. N., Metall. and Mater. Trans. **33A**, 213 (2002)

52 Nabarro, F. R. N., Phys. Stat. Sol. (a) **182**, 627 (2000)

53 Matsuo, T., Mater. Sci. Eng. **A146**, 261 (1991)

54 Honeycombe, R.W.K., *The Plastic Deformation of Metals*, Edward Arnold Publishers Ltd, London (1968)

55 Philibert, J., *Atom Movements - Diffusion and Mass Transport in Solids*, Les Editions De Physique, France (1991)

56 Colombier, L. and Hochman, J., *Stainless and Heat Resisting Steels*, Edward Arnold Publishers Ltd., Great Britian (1967)

57 Koppers, M. et al., Acta Mater. **45**, 4181 (1997)

58 Bhandarkar, M. et al., Metall. Trans. **6A**, 1281 (1975)

59 Ueki, M. et al., High Temperature Technology, **3**, 23 (1985)

60 Watanabe, H. et al., Int. J. Plasticity, **17**, 387 (2001)

61 Zhang, W. J. and Deevi, S. C., Intermetallics, **10**, 603 (2002)

62 Langdon, T. G., Metall. and Mater. Trans. **33A**, 249 (2002)

63 Kuzucu, V. et al., J. Mater. Process. Tech. **82**, 165 (1998)

64 http://www.haynesintl.com/mini/230Site/230.htm (Visited 03/10/2002)

65 Allegheny Ludlum, Technical Data Blue Sheet, Stainless Steel, Type 441, AL 441HP™ Alloys

66 ASM Metals Handbook Volume 8, "*Mechanical Testing*", 10th Ed. ASM International, Materials Park, OH (1984)

67 Douthett, J. A., SAE Technical Paper Series, 810036 (1981)

68 Lee, K.J., Scripta Mater. **40**, 837 (1999)

69 Barteri, M. et al., La Metallurgia Italiana, **5**, 31 (1999)

70 McNee, K.R., Scripta Mater. **47**, 619 (2002)

# APPENDIX A

## Creep Test Rig Technical Drawings

| Drawing No. | Drawing |
|---|---|
| 1 | Load Frame |
| 2 | Lever |
| 3 | Fulcrum |
| 4 | Upper base plate |
| 5 | Lower base plate |
| 6 | Hot pull rods |
| 7 | Threaded specimen grips |
| 8 | Extensometer clamps |
| 9 | Lower extensometer plate |
| 10 | Upper extensometer plate |

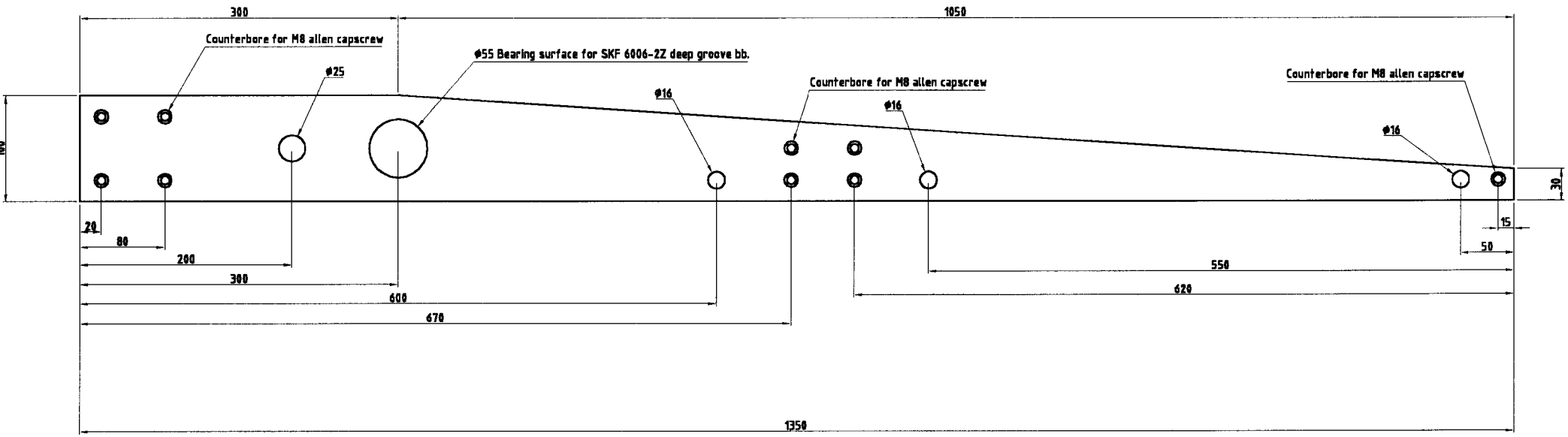


# UNIVERSITY OF CAPE TOWN

CENTRE FOR MATERIALS ENGINEERING

| DRAWING NUMBER: | | All dimensions in mm. All tolerances 0.2mm unless otherwise stated. | TITLE: CREEP TEST RIG LEVER | |
|---|---|---|---|---|
| 2 | | | DRAWN BY: Michael Dollman | DATE: 21/02/2002 |

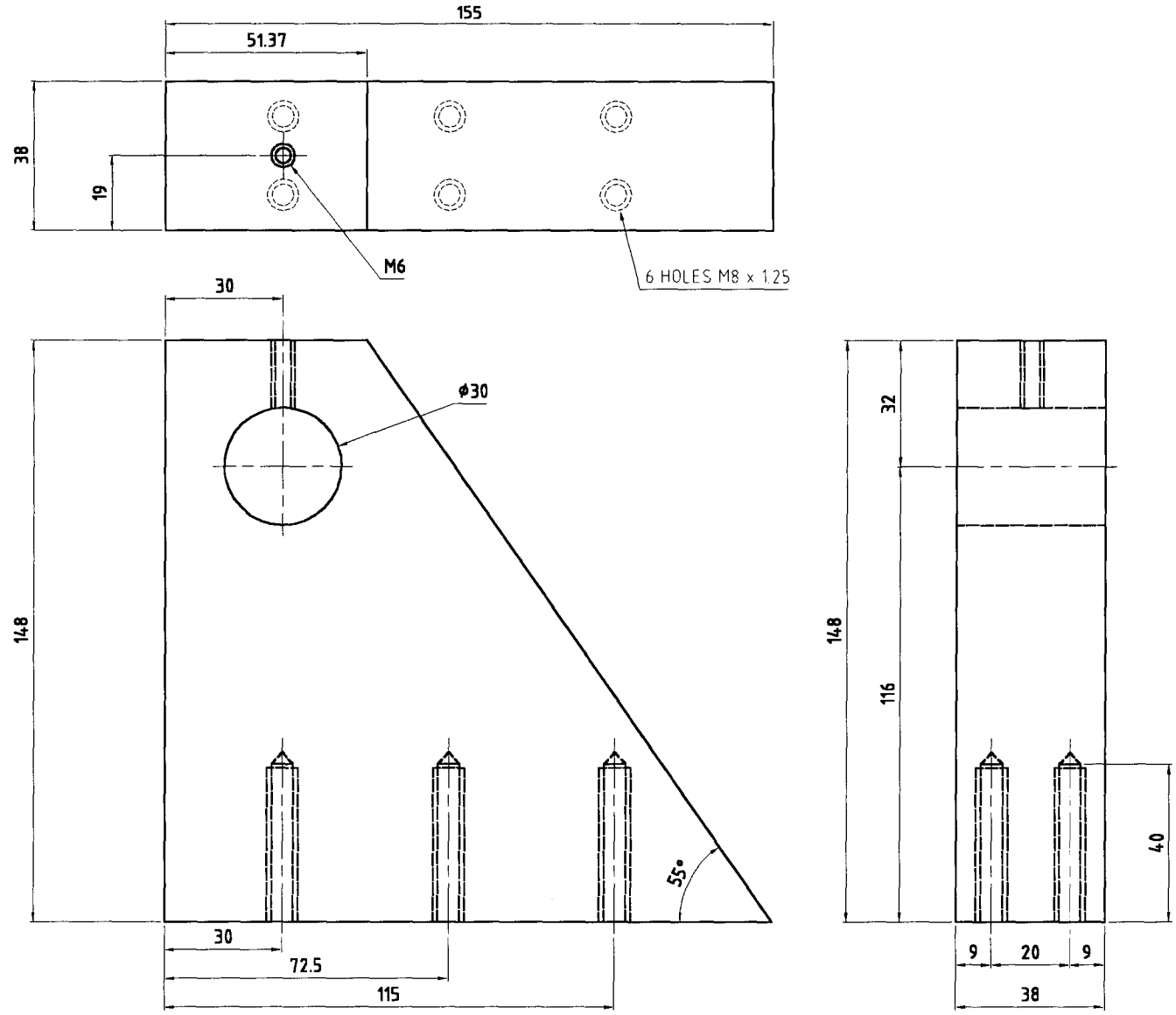


**UNIVERSITY OF CAPE TOWN**
CENTRE FOR MATERIALS ENGINEERING

| DRAWING NUMBER: | | All dimensions in mm. All tolerances 0.2mm unless otherwise stated. | TITLE: CREEP TEST RIG FULCRUM | |
|---|---|---|---|---|
| 3 | | | DRAWN BY: Michael Dollman | DATE: 21/02/2002 |

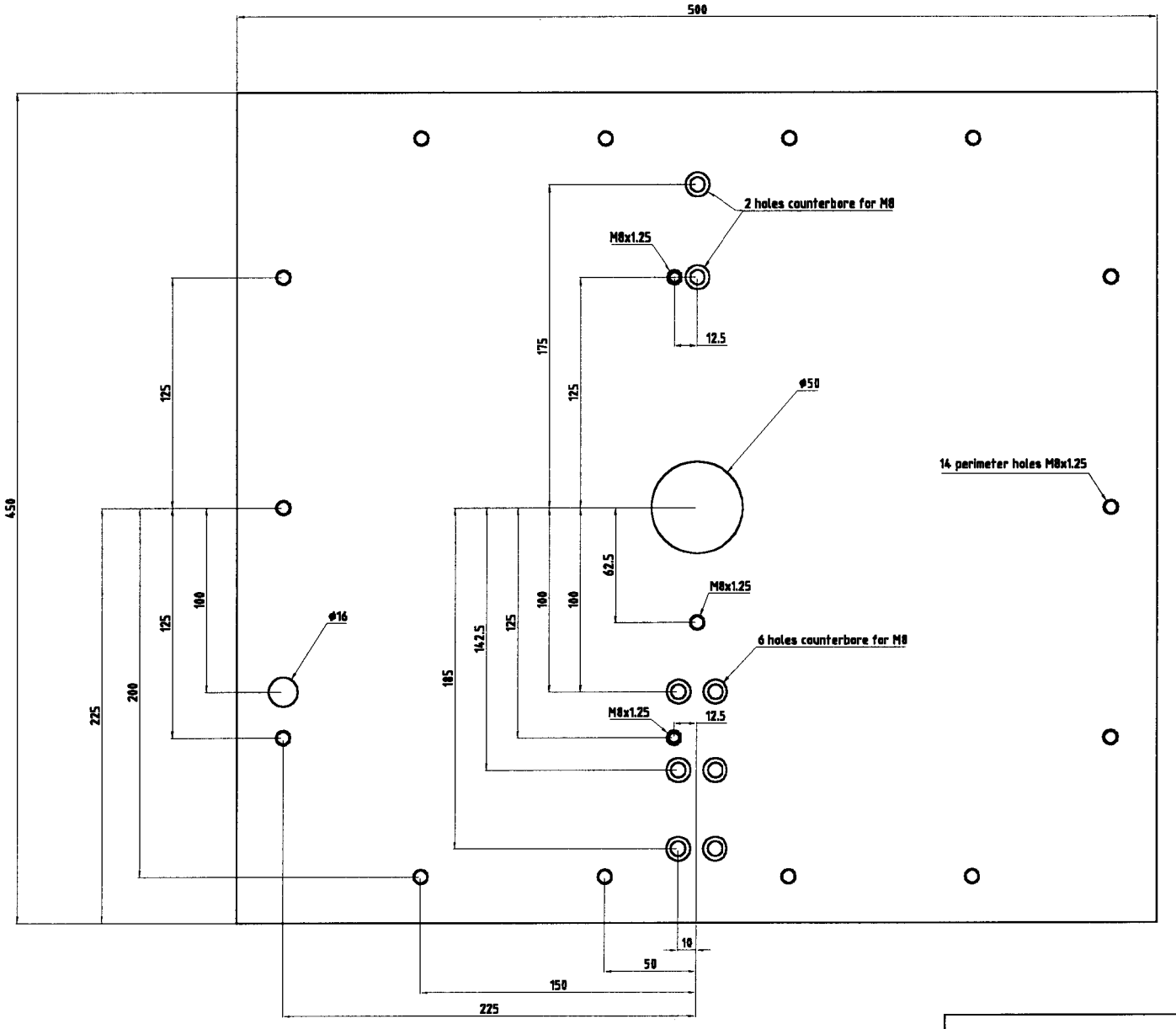


**UNIVERSITY OF CAPE TOWN**

CENTRE FOR MATERIALS ENGINEERING

| DRAWING NUMBER: | | All dimensions in mm. All tolerances 0.2mm unless otherwise stated. | TITLE: CREEP TEST RIG UPPER BASE PLATE | |
|---|---|---|---|---|
| 4 | | | DRAWN BY: Michael Dollman | DATE: 21/02/2002 |

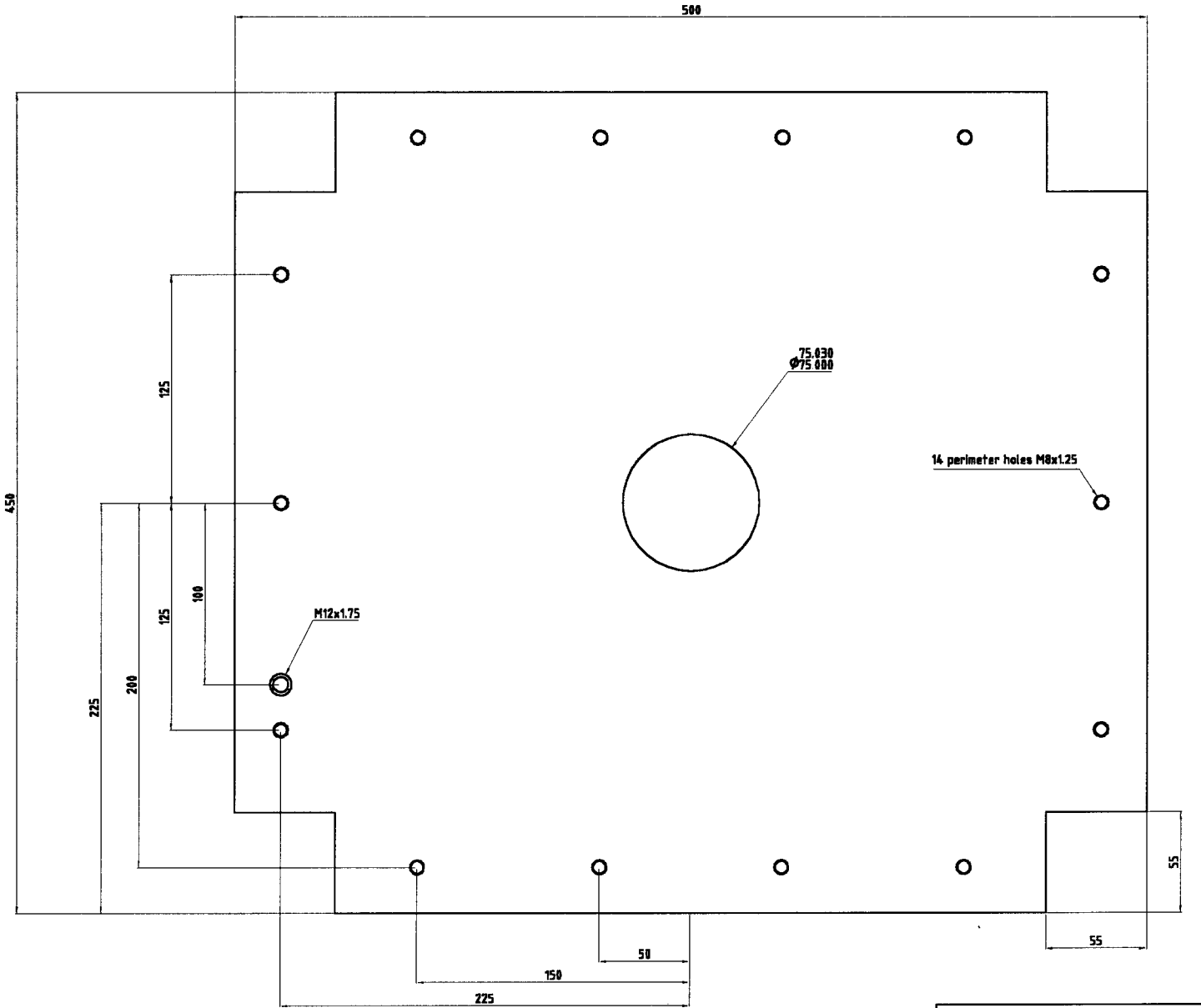


**UNIVERSITY OF CAPE TOWN**

CENTRE FOR MATERIALS ENGINEERING

| DRAWING NUMBER: | | All dimensions in mm. All tolerances 0.2mm unless otherwise stated. | TITLE: CREEP TEST RIG LOWER BASE PLATE | |
|---|---|---|---|---|
| 5 | | | DRAWN BY: Michael Dollman | DATE: 21/02/2002 |

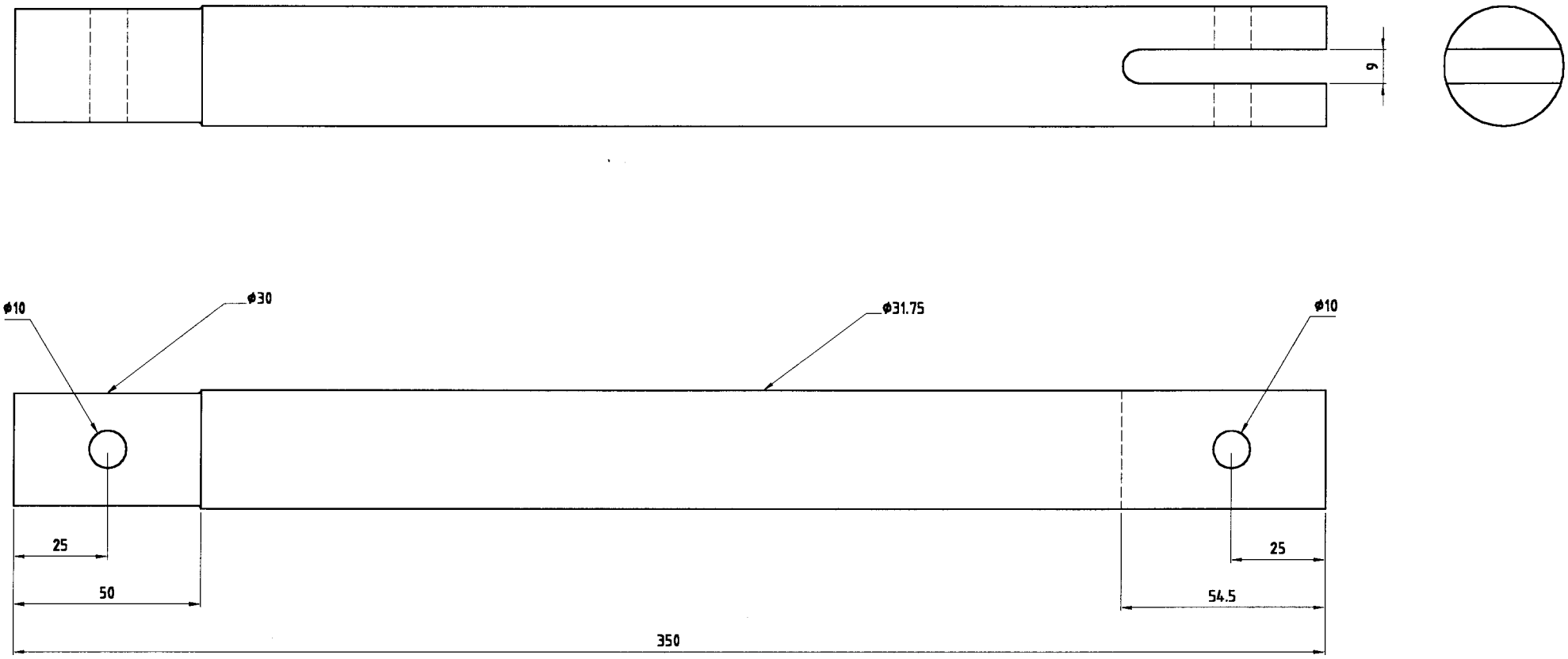


**UNIVERSITY OF CAPE TOWN**
CENTRE FOR MATERIALS ENGINEERING

| DRAWING NUMBER: | | All dimensions in mm. All tolerances 0.2mm unless otherwise stated. | TITLE: CREEP TEST RIG HOT PULL RODS | |
|---|---|---|---|---|
| 6 | | | DRAWN BY: Michael Dollman | DATE: 21/02/2002 |

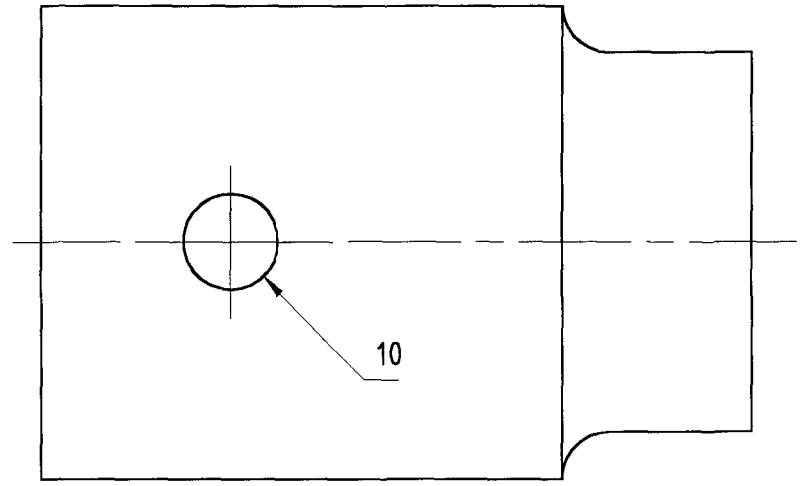


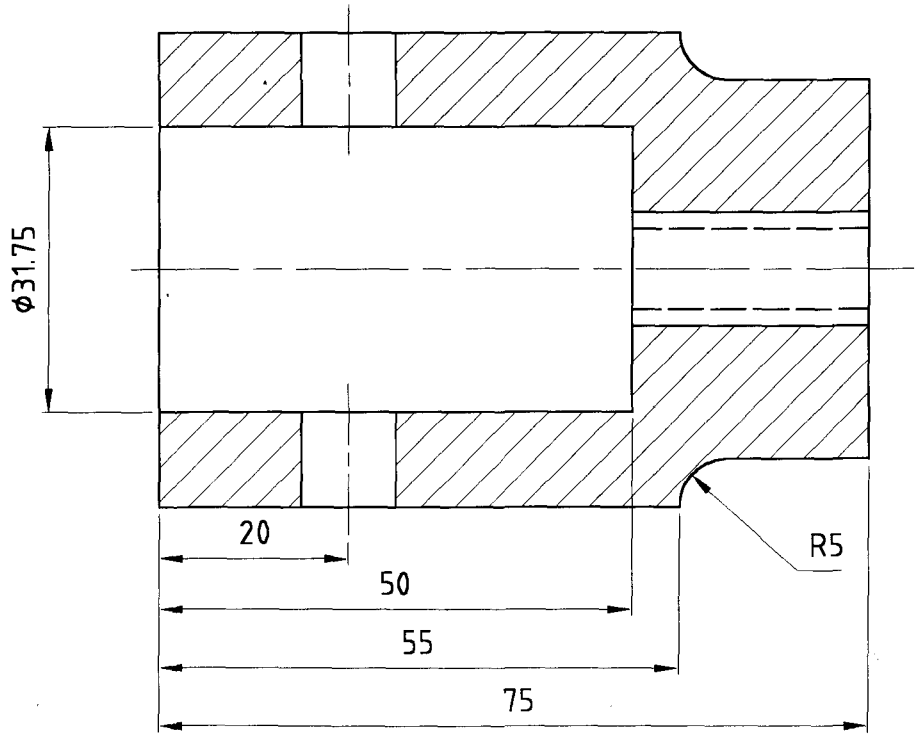


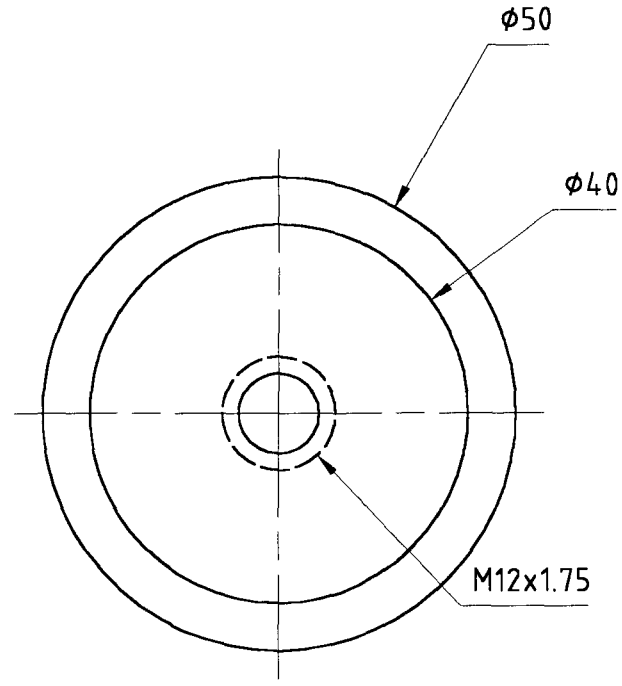


**UNIVERSITY OF CAPE TOWN**
CENTRE FOR MATERIALS ENGINEERING

| DRAWING NUMBER: | | All dimensions in mm. All tolerances 0.2mm unless otherwise stated. | TITLE: CREEP RIG THREADED SPECIMEN GRIPS | |
|---|---|---|---|---|
| 7 | | | DRAWN BY: Michael Dollman | DATE: 21/02/2002 |

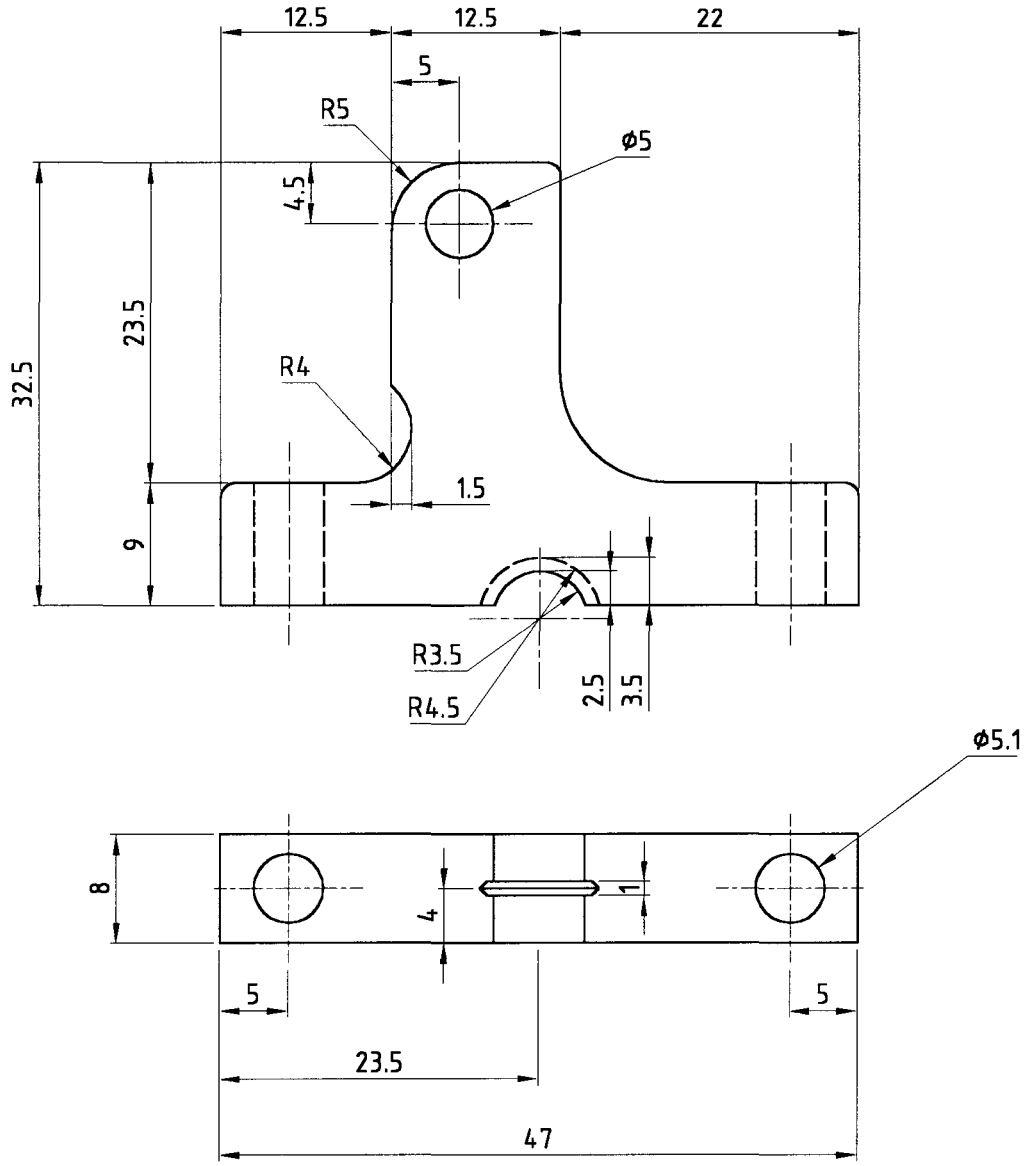


**UNIVERSITY OF CAPE TOWN**

CENTRE FOR MATERIALS ENGINEERING

| | | | |
|---|---|---|---|
| DRAWING NUMBER: 8 | | All dimensions in mm. All tolerances 0.2mm unless otherwise stated. | TITLE: CREEP RIG EXTENSOMETER CLAMPS |
| | | | DRAWN BY: Michael Dollman |
| | | | DATE: 21/02/2002 |

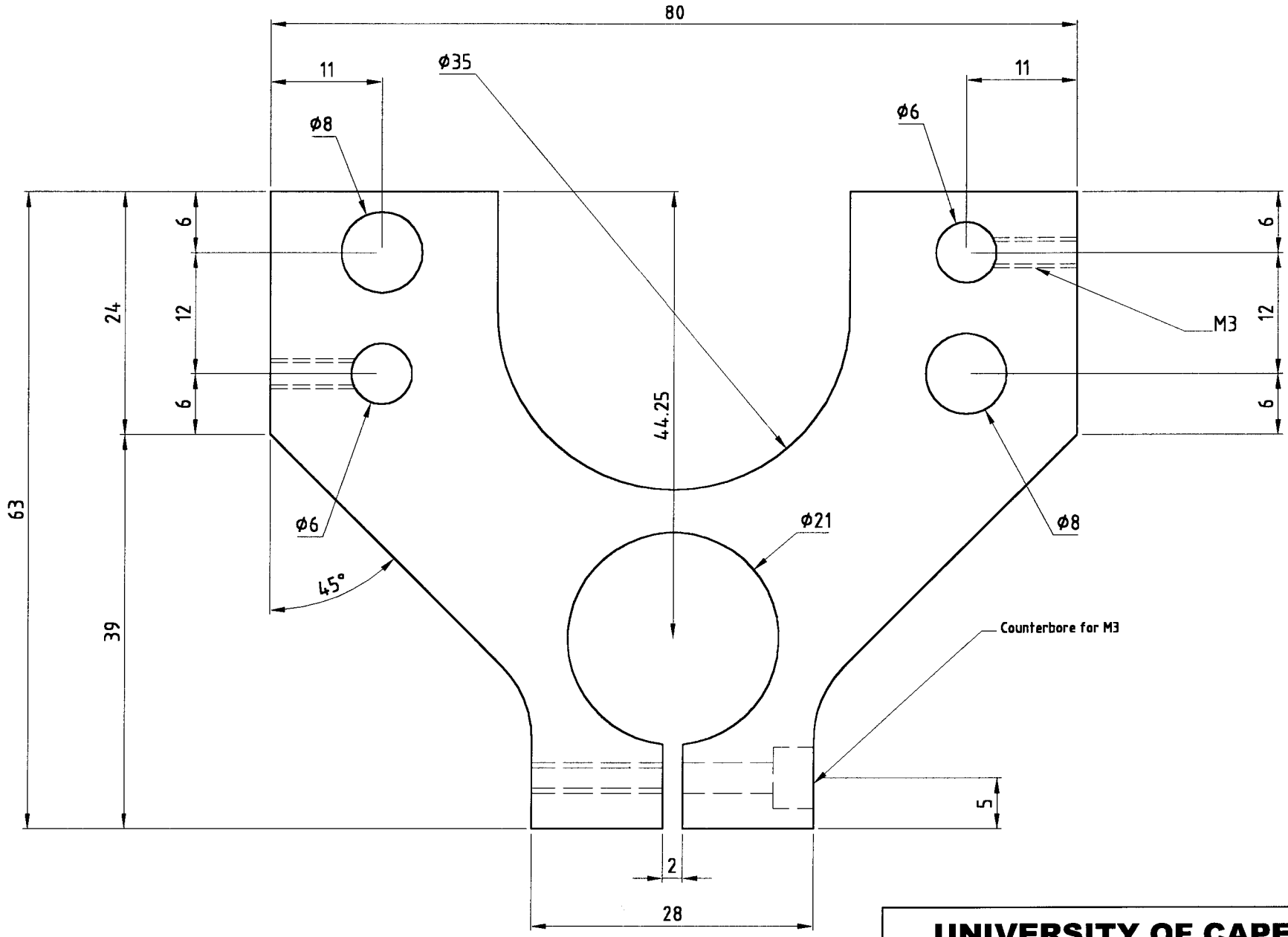


**UNIVERSITY OF CAPE TOWN**

CENTRE FOR MATERIALS ENGINEERING

| DRAWING NUMBER: | | All dimensions in mm. All tolerances 0.2mm unless otherwise stated. | TITLE: LOWER EXTENSOMETER PLATE | |
|---|---|---|---|---|
| 9 | | | DRAWN BY: Michael Dollman | DATE: 21/02/2002 |

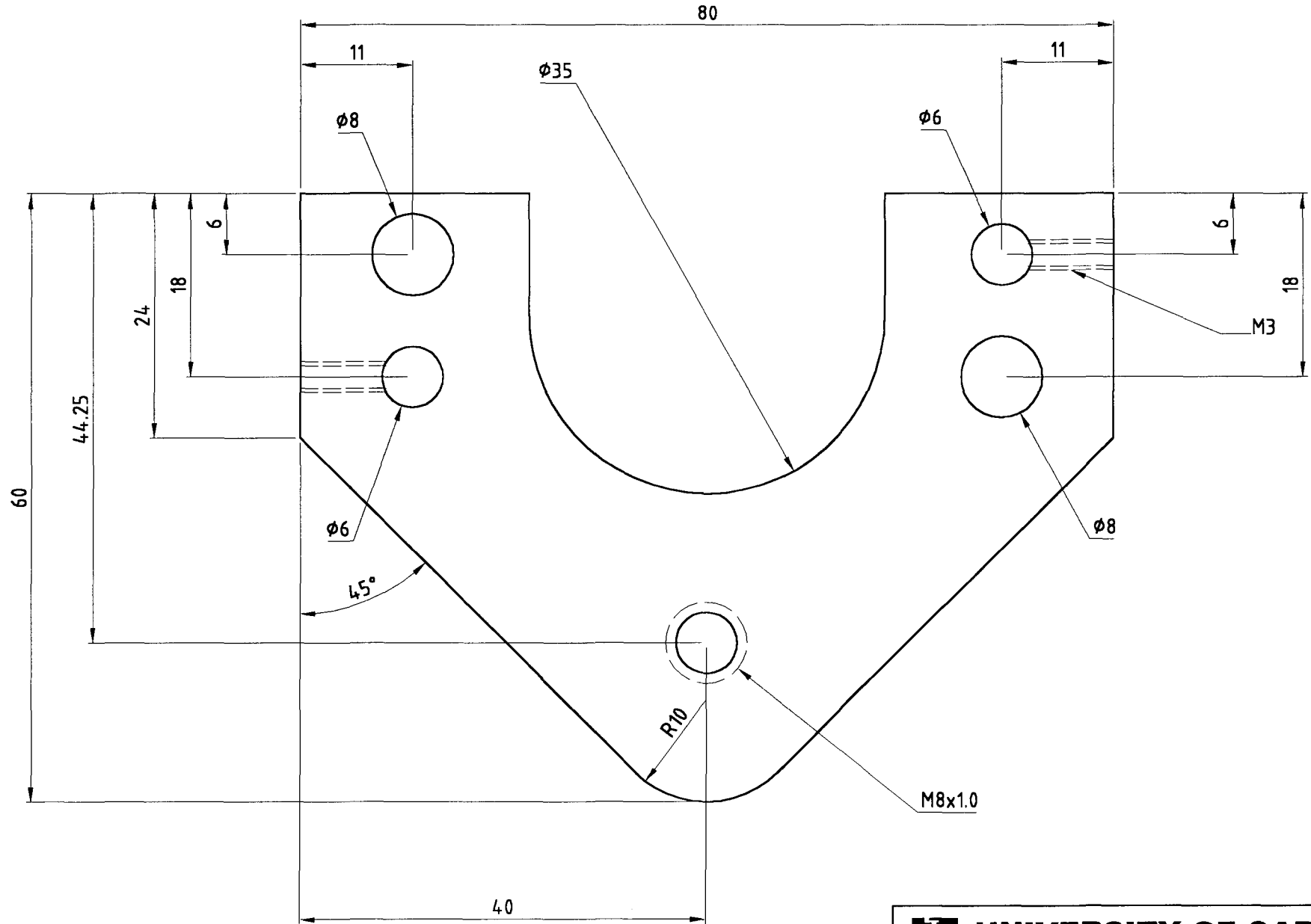


**UNIVERSITY OF CAPE TOWN**
CENTRE FOR MATERIALS ENGINEERING

| DRAWING NUMBER: | | All dimensions in mm. All tolerances 0.2mm unless otherwise stated. | TITLE: UPPER EXTENSOMETER PLATE | |
|---|---|---|---|---|
| 10 | | | DRAWN BY: Michael Dollman | DATE: 21/02/2002 |

# APPENDIX B

## Creep Test Rig Data Acquisition System Code

## MS Visual Basic 6.0®

```
'Centre for Materials Engineering, UCT
'Creep Data Logger - CDL
'July 2002
'Michael Dollman

Option Explicit

Dim SerialNo As Long              'PCI703 16/A Board Serial No
Dim StopW1 As CStopWatch          'New stopwatch 1
Dim StopW2 As CStopWatch          'New stopwatch 2
Dim lngFrequency As Long          'Board Frequency
Const BufSize = 400000            'Max AD buffer size
Const AGND = 4096                 'Ground ref
Dim Value As Long                 'General parameter
Dim error As Long                 'Returned error
Dim chl() As Long                 'Channel list array
Dim gl() As Long                  'Gain list array
Dim uvbuf(BufSize) As Long        'Micro voltage buffer
Dim samples_unread As Long        'Number of samples available in driver buffer
Dim NumChan As Long               'Number of channels
Dim intRange As Integer           'Range
Dim intGain As Integer            'Gain
Dim updatecnt As Long             'Update count variable
Dim updatesec As Long             'Update period
Dim i As Long                     'General variable
Dim intConfirm1 As Integer        'Confirmation for rig 1 stop
Dim intConfirm2 As Integer        'Confirmation for rig 2 stop
Dim intConfirmExit As Integer     'Exit confirmation
Dim dblChannel0 As Double         '
Dim dblChannel1 As Double         '
Dim dblChannel2 As Double         '
Dim dblChannel3 As Double         'Hold channel voltage values during logging
Dim dblChannel4 As Double         '
Dim dblChannel5 As Double         '
Dim dblChannel6 As Double         '
Dim dblChannel7 As Double         '
Dim dblFactor0 As Double          '
Dim dblFactor1 As Double          '
Dim dblFactor2 As Double          '
Dim dblFactor3 As Double          'Hold channel factor values during logging
Dim dblFactor4 As Double          '
Dim dblFactor5 As Double          '
Dim dblFactor6 As Double          '
Dim dblFactor7 As Double          '
Dim strFactor00 As String         '
Dim strFactor01 As String         '
Dim strFactor02 As String         '
Dim strFactor03 As String         'Hold channel factor values on startup
Dim strFactor04 As String         '
Dim strFactor05 As String         '
Dim strFactor06 As String         '
Dim strFactor07 As String         '
Dim dblCH0 As Double              '
Dim dblCH1 As Double              '
Dim dblCH2 As Double              '
Dim dblCH3 As Double              '
Dim dblCH4 As Double              'Hold actual physical values after conversion
Dim dblCH5 As Double              '
Dim dblCH6 As Double              '
Dim dblCH7 As Double              '
Dim strFile1 As String            'File to save rig 1 data
Dim strPath1 As String            'File 1 path
Dim strFile2 As String            'File to save rig 2 data
Dim strPath2 As String            'File 2 path
Dim intCount1 As Integer          'Count variable 1
Dim intCount2 As Integer          'Count variable 2
Dim strPath As String             'CDLFactor.txt path
Dim strFile As String             'CDLFactor.txt
Dim strCalPass As String          'Password for access to Calibration Factors
Dim dblTime1 As Double            'Holds hour time for rig 1
Dim dblTime2 As Double            'Holds hour time for rig 2
Dim DataPoints1 As Integer
Dim DataPoints2 As Integer
Dim intRows1 As Integer
Dim intRows2 As Integer
```

```
Dim dblDisplZero1 As Double      'Holds displacement offset for displacement zeroing
Dim dblDisplZero2 As Double      'Holds displacement offset for displacement zeroing
Dim dblTempConv As Double        '
Dim dblTempAdd As Double         'Conversion Factors for changing units
Dim dblForceConv As Double       '
Dim dblDisplConv As Double       '
Dim dblDisplArray1(100) As Double
Dim intArray1 As Integer
Dim dblDisplAvg1 As Double
Dim dblDisplSum1 As Double
Dim dblDisplArray2(100) As Double
Dim intArray2 As Integer
Dim dblDisplAvg2 As Double
Dim dblDisplSum2 As Double
Dim int30int1 As Integer
Dim int30int2 As Integer


Private Sub cmdChange0_Click()
    'Change factor 0 to user input via inputbox
    txtFactor0.Text = InputBox("Please enter calibration factor for channel 0", "Input calibr
ation factor")

End Sub

Private Sub cmdChange1_Click()
    'Change factor 1 to user input via inputbox
    txtFactor1.Text = InputBox("Please enter calibration factor for channel 1", "Input calibr
ation factor")

End Sub

Private Sub cmdChange2_Click()
    'Change factor 2 to user input via inputbox
    txtFactor2.Text = InputBox("Please enter calibration factor for channel 2", "Input calibr
ation factor")

End Sub

Private Sub cmdChange3_Click()
    'Change factor 3 to user input via inputbox
    txtFactor3.Text = InputBox("Please enter calibration factor for channel 3", "Input calibr
ation factor")

End Sub

Private Sub cmdChange4_Click()
    'Change factor 4 to user input via inputbox
    txtFactor4.Text = InputBox("Please enter calibration factor for channel 4", "Input calibr
ation factor")

End Sub

Private Sub cmdChange5_Click()
    'Change factor 5 to user input via inputbox
    txtFactor5.Text = InputBox("Please enter calibration factor for channel 5", "Input calibr
ation factor")

End Sub

Private Sub cmdChange6_Click()
    'Change factor 6 to user input via inputbox
    txtFactor6.Text = InputBox("Please enter calibration factor for channel 6", "Input calibr
ation factor")

End Sub

Private Sub cmdChange7_Click()
    'Change factor 7 to user input via inputbox
    txtFactor7.Text = InputBox("Please enter calibration factor for channel 7", "Input calibr
ation factor")

End Sub

Private Sub cmdReset1_Click()
```

```
    'Allow time to be reset
    StopW1.Reset
    lblTimer1.Caption = StopW1.Display
    dblTime1 = 0
    txtSeconds1.Text = "0.000"

End Sub

Private Sub cmdReset2_Click()
    'Allow time to be reset
    StopW2.Reset
    lblTimer2.Caption = StopW2.Display
    dblTime2 = 0
    txtSeconds2.Text = "0.000"

End Sub

Private Sub cmdSaveFactors_Click()
    'Remove calibration and voltmeter from user view
    fraMessages.Visible = True
    fraCalibration.Visible = False
    'fraChart.Visible = True

    'Save factors to file
    Open "c:\CDL\CDLFactor0.txt" For Output As #3
    Write #3, txtFactor0.Text
    Close #3

    Open "c:\CDL\CDLFactor1.txt" For Output As #4
    Write #4, txtFactor1.Text
    Close #4

    Open "c:\CDL\CDLFactor2.txt" For Output As #5
    Write #5, txtFactor2.Text
    Close #5

    Open "c:\CDL\CDLFactor3.txt" For Output As #6
    Write #6, txtFactor3.Text
    Close #6

    Open "c:\CDL\CDLFactor4.txt" For Output As #7
    Write #7, txtFactor4.Text
    Close #7

    Open "c:\CDL\CDLFactor5.txt" For Output As #8
    Write #8, txtFactor5.Text
    Close #8

    Open "c:\CDL\CDLFactor6.txt" For Output As #9
    Write #9, txtFactor6.Text
    Close #9

    Open "c:\CDL\CDLFactor7.txt" For Output As #10
    Write #10, txtFactor7.Text
    Close #10

End Sub

Private Sub cmdStart1_Click()
    'If calibration frame is visible, disallow start
    If fraCalibration.Visible = True Then
        imgWarning.Visible = True
        txtAlert.Text = "Please click SAVE AND CLOSE before starting"
        tmrConfirm.Enabled = True
        Exit Sub
    End If

    If txtName1.Text = "" Or txtMat1.Text = "" Or txtSample1.Text = "" Or txtTemp1.Text = ""
Or txtLoad1.Text = "" Or txtFile1.Text = "" Then
        txtAlert.Text = "Please complete all text boxes before starting test"
        imgWarning.Visible = True
        tmrConfirm.Enabled = True
        Exit Sub
    End If
```

```
    If txtInterval1.Text < 2.5 Then
        imgWarning.Visible = True
        txtAlert.Text = "The sampling interval you selected is too low"
        tmrConfirm.Enabled = True
        Exit Sub
    End If

    If txtInterval1.Text > 120 Then
        imgWarning.Visible = True
        txtAlert.Text = "The sampling interval you selected is too high"
        tmrConfirm.Enabled = True
        Exit Sub
    End If
    'Change state of buttons and LED
    EDRELed1.State = True
    cmdStart1.Enabled = False
    cmdStop1.Enabled = True
    cmdReset1.Enabled = False
    txtName1.Enabled = False
    txtMat1.Enabled = False
    txtSample1.Enabled = False
    txtTemp1.Enabled = False
    txtLoad1.Enabled = False
    txtFile1.Enabled = False
    txtSeconds1.Visible = True

    'Zero displacement at start
    If chkDisplZero1.Value = 1 Then
        dblDisplZero1 = Val(txtChannel3)
    Else
        dblDisplZero1 = 0
    End If

    'Display and start stopwatch
    lblTimer1.Caption = StopW1.Display
    tmrStopW1.Enabled = True


    'Create text file to which data will be written
    strFile1 = txtFile1.Text
    strPath1 = "c:\CreepData1\"
    Open strPath1 & strFile1 & ".txt" For Append As #1
    Write #1, "CREEP RIG 1 DATA"
    Write #1,
    Write #1, "Date:  " & Date
    Write #1, "Time Started:  " & Time
    Write #1, "Testers Name:  " & txtName1.Text
    Write #1, "Material tested:  " & txtMat1.Text
    Write #1, "Sample Number:  " & txtSample1.Text
    Write #1, "Test Temperature:  " & txtTemp1.Text
    Write #1, "Test Load:  " & txtLoad1.Text
    Write #1, "FileName:  " & txtFile1.Text
    Write #1,
    Write #1, "Time"; "Displacement"; "Load"; "Temp 1"; "Temp 2"

    Close #1

    'Start timer to begin logging
    tmrWrite1.Interval = 30000
    int30int1 = 2 * Val(txtInterval1.Text)
    txtPerhour1.Text = 60 / Val(txtInterval1.Text)
    txtPerhour1.Visible = True
    tmrWrite1.Enabled = True

End Sub

Private Sub cmdStart2_Click()
    'If calibration frame is visible, disallow start
    If fraCalibration.Visible = True Then
        imgWarning.Visible = True
        txtAlert.Text = "Please click SAVE AND CLOSE before starting"
        tmrConfirm.Enabled = True
        Exit Sub
    End If
```

```
    If intConfirm1 = 0 Then
        imgWarning.Visible = True
        txtAlert.Text = "Click STOP again to confirm"
        tmrConfirm.Enabled = True
        intConfirm1 = intConfirm2 + 1
        Exit Sub
    ElseIf intConfirm1 = 1 Then
        intConfirm1 = 0
        txtAlert.Text = ""
        imgWarning.Visible = False
        tmrWrite1.Enabled = False
    End If

    'Change state of buttons and LED
    EDRELed1.State = False
    cmdStop1.Enabled = False
    cmdStart1.Enabled = True
    cmdReset1.Enabled = True
    txtName1.Enabled = True
    txtMat1.Enabled = True
    txtSample1.Enabled = True
    txtTemp1.Enabled = True
    txtLoad1.Enabled = True
    txtFile1.Enabled = True

    'Stop stopwatch
    tmrStopW1.Enabled = False

End Sub

Private Sub cmdStop2_Click()
    'Ask for confirmation

    If intConfirm2 = 0 Then
        imgWarning.Visible = True
        txtAlert.Text = "Click STOP again to confirm"
        tmrConfirm.Enabled = True
        intConfirm2 = intConfirm2 + 1
        Exit Sub
    ElseIf intConfirm2 = 1 Then
        intConfirm2 = 0
        txtAlert.Text = ""
        imgWarning.Visible = False
        tmrWrite2.Enabled = False
    End If

    'Change state of buttons and LED
    EDRELed2.State = False
    cmdStop2.Enabled = False
    cmdStart2.Enabled = True
    cmdReset2.Enabled = True
    txtName2.Enabled = True
    txtMat2.Enabled = True
    txtSample2.Enabled = True
    txtTemp2.Enabled = True
    txtLoad2.Enabled = True
    txtFile2.Enabled = True

    'Stop stopwatch
    tmrStopW2.Enabled = False

End Sub

Private Sub Command1_Click()
    'Hide Board Status Frame
    fraMessages.Visible = True
    fraStatus.Visible = False

End Sub

Private Sub Form_Load()
    'Load Factors
    strPath = "c:\cdl\"
    strFile = "CDLFactor"
```

```
    Open "c:\CDL\CDLFactor0.txt" For Input As #3
    Input #3, strFactor00
    Close #3
    txtFactor0.Text = strFactor00

    Open "c:\CDL\CDLFactor1.txt" For Input As #4
    Input #4, strFactor01
    Close #4
    txtFactor1.Text = strFactor01

    Open "c:\CDL\CDLFactor2.txt" For Input As #5
    Input #5, strFactor02
    Close #5
    txtFactor2.Text = strFactor02

    Open "c:\CDL\CDLFactor3.txt" For Input As #6
    Input #6, strFactor03
    Close #6
    txtFactor3.Text = strFactor03

    Open "c:\CDL\CDLFactor4.txt" For Input As #7
    Input #7, strFactor04
    Close #7
    txtFactor4.Text = strFactor04

    Open "c:\CDL\CDLFactor5.txt" For Input As #8
    Input #8, strFactor05
    Close #8
    txtFactor5.Text = strFactor05

    Open "c:\CDL\CDLFactor6.txt" For Input As #9
    Input #9, strFactor06
    Close #9
    txtFactor6.Text = strFactor06

    Open "c:\CDL\CDLFactor7.txt" For Input As #10
    Input #10, strFactor07
    Close #10
    txtFactor7.Text = strFactor07

    'Call initialise procedure
    Call Initialise

    'Create new instances of Class Module CStopWatch
    Set StopW1 = New CStopWatch
    Set StopW2 = New CStopWatch

    'Display Stopwatch objects
    lblTimer1.Caption = StopW1.Display
    tmrStopW1.Enabled = False

    lblTimer2.Caption = StopW2.Display
    tmrStopW2.Enabled = False

End Sub

Private Sub Initialise()
    'Initialise board
    EDREUtlX1.SelectDialog
    SerialNo = EDREUtlX1.SerialNumber
    EDREAdX1.SerialNumber = SerialNo

    'Initialise form
    cmdStart1.Enabled = True
    cmdStart2.Enabled = True
    cmdStop1.Enabled = False
    cmdStop2.Enabled = False
    EDRELed1.State = False
    EDRELed2.State = False
    cmdReset1.Enabled = True
    cmdReset2.Enabled = True
    tmrRead.Enabled = False
    fraCalibration.Visible = False
    txtFactor0.Enabled = False
```

```
    txtFactor1.Enabled = False
    txtFactor2.Enabled = False
    txtFactor3.Enabled = False
    txtFactor4.Enabled = False
    txtFactor5.Enabled = False
    txtFactor6.Enabled = False
    txtFactor7.Enabled = False

    'Check if drive is allocated
    chkAlloc.Value = 0
    If EDREAdX1.BufferAllocated Then
        chkAlloc.Value = 1
    End If

    NumChan = 8                 '# of active channels
    lngFrequency = 100          'Set frequency to 100 Hz
    EDREAdX1.Frequency = lngFrequency

    'If serial no is allocated, start
    If SerialNo > 0 Then
        tmrRead.Enabled = True
    End If

    'Set channel list
    Call SetChLst

    'build channel list
    SetChLst

    'Configure
    EDREAdX1.ClockSource = 0
    EDREAdX1.Configure chl(0), gl(0), NumChan
    updatesec = 1
    chkOver.Value = 0

    'start sampling
    EDREAdX1.Stop

    error = EDREAdX1.Start
    tmrRead.Enabled = True
    If (error < EDRE_OK) Then
        MsgBox "AD Start Error! Error = " + Format(error), vbCritical
    Else
        chkOver.Value = 0
    End If

    updatecnt = 0

    'Set Displacement Zeroing variables to 0
    dblDisplZero1 = 0
    dblDisplZero2 = 0

End Sub

Private Sub SetChLst()
Dim i As Long

    'Set range and gain
    intRange = 0
    intGain = 0

    'reset arrays
    Erase chl
    Erase gl
    ReDim chl(NumChan)
    ReDim gl(NumChan)

    'setup gain and channel list
    For i = 0 To NumChan - 1
        chl(i) = i
        gl(i) = 256 * intRange + intGain + AGND
    Next i

End Sub
```

```
Private Sub GetData()

   Value = samples_unread

   'If value > BufSize Then
   '    value = BufSize
   'End If

   If Value > 0 Then
       'get data from driver via buffer
       error = EDREAdX1.GetData(uvbuf(0), Value)
       If (error < EDRE_OK) Then
           MsgBox "Get Data Error! Error = " + Format(error), vbCritical
       End If

       updatecnt = updatecnt + 1

       'If updatecnt = updatesec Then
           Call Updatevalue
           updatecnt = 0
       'End If

   End If

   tmrUpdateText.Enabled = True

End Sub

Private Sub Form_Unload(Cancel As Integer)

    'Confirm application termination
    If intConfirmExit = 0 Then
        imgWarning.Visible = True
        txtAlert.Text = "Logging will be terminated click EXIT again to confirm"
        intConfirmExit = intConfirmExit + 1
        tmrConfirm.Enabled = True
        Cancel = 1
        Exit Sub
    ElseIf intConfirmExit = 1 Then
        intConfirmExit = 0
    End If

    'Stop sampling
    Call StopData

End Sub

Private Sub mnuDisplayPCI_Click()
    'Show Board Status Frame
    fraMessages.Visible = False
    fraStatus.Visible = True

End Sub

Private Sub mnuDisplayUnits_Click()
    frmUnits.Show

End Sub

Private Sub mnuFileExit_Click()
    'unload application
    Unload Me

End Sub

Private Sub mnuFileNewOne_Click()

    If EDRELed1.State = True Then
        txtAlert.Text = "STOP logging before setting up a new test"
        imgWarning.Visible = True
        tmrConfirm.Enabled = True
        Exit Sub
    End If

    'Reset all rig one parameters for new test
```

```
    txtName1.Text = ""
    txtMat1.Text = ""
    txtSample1 = ""
    txtTemp1.Text = ""
    txtLoad1.Text = ""
    txtFile1.Text = ""
    Call cmdReset1_Click
    txtPerhour1.Visible = False

    tmrStopW1.Enabled = False
    tmrWrite1.Enabled = False

    'Variables
    intCount1 = 0
    dblTime1 = 0
    dblDisplZero1 = 0

End Sub

Private Sub mnuFileNewTwo_Click()

    If EDRELed2.State = True Then
        txtAlert.Text = "STOP logging before setting up a new test"
        imgWarning.Visible = True
        tmrConfirm.Enabled = True
        Exit Sub
    End If

    'Reset all rig one parameters for new test
    txtName2.Text = ""
    txtMat2.Text = ""
    txtSample2 = ""
    txtTemp2.Text = ""
    txtLoad2.Text = ""
    txtFile2.Text = ""
    Call cmdReset2_Click
    txtPerhour2.Visible = False

    tmrStopW2.Enabled = False
    tmrWrite2.Enabled = False

    'Variables
    intCount2 = 0
    dblTime2 = 0
    dblDisplZero2 = 0

End Sub

Private Sub mnuHelpAbout_Click()
    frmAbout.Show

End Sub

Private Sub mnuSettingsCal_Click()
    'If data logging is in progress, deny access to calibration
    If EDRELed1.State = True Or EDRELed2.State = True Then
        imgWarning.Visible = True
        txtAlert.Text = "NO ACCESS with data logging in progress"
        tmrConfirm.Enabled = True
        Exit Sub
    End If

    Open "c:\CDL\CalPass.txt" For Input As #12
        Input #12, strCalPass
    Close #12

    Dim strPassword As String
    strPassword = InputBox("Please enter password", "Password verification")
    If strPassword = strCalPass Then
        fraMessages.Visible = False
        fraCalibration.Visible = True
    Else
        MsgBox "Incorrect password", vbCritical, "Access Denied"
        Exit Sub
    End If
```

```
End Sub

Private Sub mnuSettingsCalculate_Click()
    frmCalculate.Show

End Sub

Private Sub mnuSettingsPassword_Click()
    'If data logging is in progress, deny access to password setting
    If EDRELed1.State = True Or EDRELed2.State = True Then
        imgWarning.Visible = True
        txtAlert.Text = "NO ACCESS with data logging in progress"
        tmrConfirm.Enabled = True
        Exit Sub
    End If

    frmPassword.Show

End Sub

Private Sub tmrConfirm_Timer()
    'Reset confirmation procedures
    intConfirm1 = 0
    intConfirm2 = 0
    intConfirmExit = 0
    imgWarning.Visible = False
    txtAlert.Text = ""

    tmrConfirm.Enabled = False

End Sub

Private Sub tmrRead_Timer()

'get status information from the board

    'Reset
    chkBusy.Value = 0
    chkOver.Value = 0

    'check if busy
    If EDREUtlX1.Query(103, 0) > 0 Then chkBusy.Value = 1

    'check if there was a buffer overrun
    If EDREUtlX1.Query(107, 0) > 0 Then chkOver.Value = 1

    'check number of samples available
    samples_unread = EDREAdX1.GetUnread()
    If (error < EDRE_OK) Then
        imgWarning.Visible = True
        txtAlert.Text = "Error: " + Format(error)
    Else
        txtUnread.Text = Format(samples_unread)
    End If

    'Check for errors
    'If (error < EDRE_OK) Then
     '   MsgBox "Error: " + Format(error), vbCritical, "Error"
    'End If

    'Get voltages from driver
    Call GetData

End Sub

Private Sub tmrStopW1_Timer()
    'Tell stopwatch to increment itself
    StopW1.Increment

    'Give the statement that tells the object to display itself
    lblTimer1.Caption = StopW1.Display

    'Increment dbltime1
    dblTime1 = dblTime1 + (1 / 3600)
```

```
    Select Case intForce
        Case Is = 0
            dblForceConv = 1 * 9.81
            j = 3
            For z = 0 To 3
                lblN1(z).Caption = "N"
            Next
        Case Is = 1
            dblForceConv = 1
            j = 3
            For z = 0 To 3
                lblN1(z).Caption = "kg"
            Next
        Case Is = 2
            dblForceConv = 1000
            j = 0
            For z = 0 To 3
                lblN1(z).Caption = "g"
            Next
    End Select

    Select Case intDispl
        Case Is = 0
            dblDisplConv = 1
            k = 2
            For z = 0 To 1
                lblmm1(z).Font = "MS Sans Serif"
                lblmm1(z).Caption = "mm"
                lblMicron(z).Visible = False
            Next
        Case Is = 1
            dblDisplConv = 1000
            k = 0
            For z = 0 To 1
                lblmm1(z).Caption = "m"
                lblmm1(z).Font = "Symbol"
                lblMicron(z).Visible = True
            Next
        Case Is = 2
            dblDisplConv = 1 / 1000
            k = 5
            For z = 0 To 1
                lblmm1(z).Font = "MS Sans Serif"
                lblmm1(z).Caption = "m"
                lblMicron(z).Visible = False
            Next
    End Select
    'Put voltage into variable
    dblChannel0 = txtChannel(0).Text
    dblChannel1 = txtChannel(1).Text
    dblChannel2 = txtChannel(2).Text
    dblChannel3 = txtChannel(3).Text
    dblChannel4 = txtChannel(4).Text
    dblChannel5 = txtChannel(5).Text
    dblChannel6 = txtChannel(6).Text
    dblChannel7 = txtChannel(7).Text

    'Put factor into variable
    dblFactor0 = txtFactor0.Text
    dblFactor1 = txtFactor1.Text
    dblFactor2 = txtFactor2.Text
    dblFactor3 = txtFactor3.Text
    dblFactor4 = txtFactor4.Text
    dblFactor5 = txtFactor5.Text
    dblFactor6 = txtFactor6.Text
    dblFactor7 = txtFactor7.Text

    'Put product of factor and voltage into text box
    dblCH0 = dblChannel0 * dblFactor0
    dblCH1 = dblChannel1 * dblFactor1
    dblCH2 = dblChannel2 * dblFactor2
    dblCH3 = dblChannel3 * dblFactor3
    dblCH4 = dblChannel4 * dblFactor4
    dblCH5 = dblChannel5 * dblFactor5
    dblCH6 = dblChannel6 * dblFactor6
```

```
    dblCH7 = dblChannel7 * dblFactor7

    'Assign variables to text boxes for display in selected units
    txtChannel0.Text = Round((dblTempConv * dblCH0) + dblTempAdd, 0)
    txtChannel1.Text = Round((dblTempConv * dblCH1) + dblTempAdd, 0)
    txtChannel2.Text = Round(dblForceConv * dblCH2, j)
    Call Average1 'To display displacement 1
    txtChannel4.Text = Round((dblTempConv * dblCH4) + dblTempAdd, 0)
    txtChannel5.Text = Round((dblTempConv * dblCH5) + dblTempAdd, 0)
    txtChannel6.Text = Round(dblForceConv * dblCH6, j)
    Call Average2 'To display displacement 2

End Sub

Private Sub tmrWrite1_Timer()

    intCount1 = intCount1 + 1

    'Open file to write data
    If intCount1 = int30int1 Then
        Open strPath1 & strFile1 & ".txt" For Append As #1
        Write #1, Round(dblTime1, 3); txtChannel3.Text; txtChannel2.Text; txtChannel0.Text; t
xtChannel1.Text
        Close #1
        intCount1 = 0
    End If

    tmrWrite1.Enabled = False
    tmrWrite1.Enabled = True

End Sub

Private Sub tmrWrite2_Timer()

    intCount2 = intCount2 + 1

    'Open file to write data
    If intCount2 = int30int2 Then
        Open strPath2 & strFile2 & ".txt" For Append As #2
        Write #2, Round(dblTime2, 3); txtChannel7.Text; txtChannel6.Text; txtChannel4.Text; t
xtChannel5.Text
        Close #2
        intCount2 = 0
    End If

    tmrWrite2.Enabled = False
    tmrWrite2.Enabled = True

End Sub

Private Sub txtChannel2_Change()
    'Check load cell
    If Val(txtChannel2.Text) > 981 Then
        txtAlert.Text = "Make sure 0-1000 kg load cell is in use"
        imgWarning.Visible = True
        tmrConfirm.Enabled = True
    ElseIf Val(txtChannel2) > 9810 Then
        txtAlert.Text = "Load cell limit exceeded. REMOVE load now!"
        imgWarning.Visible = True
        tmrConfirm.Enabled = True
    End If

End Sub

Private Sub txtChannel6_Change()
    'Check load cell
    If Val(txtChannel6.Text) > 981 Then
        txtAlert.Text = "Make sure 0-1000 kg load cell is in use"
        imgWarning.Visible = True
        tmrConfirm.Enabled = True
    ElseIf Val(txtChannel6) > 9810 Then
        txtAlert.Text = "Load cell limit exceeded. REMOVE load now!"
        imgWarning.Visible = True
        tmrConfirm.Enabled = True
    End If
```

```
End Sub

Private Sub Average1()
    Dim i As Integer

    If intArray1 = 100 Then
        intArray1 = 0
    End If

    intArray1 = intArray1 + 1

    dblDisplArray1(intArray1) = dblCH3
    dblDisplSum1 = 0

    For i = 0 To 99
        dblDisplSum1 = dblDisplSum1 + dblDisplArray1(i)
    Next

    dblDisplAvg1 = dblDisplSum1 / 100

    txtChannel3.Text = Round(dblDisplAvg1 - dblDisplZero1, 2)

End Sub

Private Sub Average2()
    Dim j As Integer

    If intArray2 = 100 Then
        intArray2 = 0
    End If

    intArray2 = intArray2 + 1

    dblDisplArray2(intArray2) = dblCH7
    dblDisplSum2 = 0

    For j = 0 To 99
        dblDisplSum2 = dblDisplSum2 + dblDisplArray2(j)
    Next

    dblDisplAvg2 = dblDisplSum2 / 100

    txtChannel7.Text = Round(dblDisplAvg2 - dblDisplZero2, 2)

End Sub
```

# APPENDIX C

## Technical Information Regarding Creep Rig Recommendations

**Defining the Current Problem**

At present, the ability of the user to accurately determine the force exerted on the specimen is hampered. The reasons for this are two-fold. Firstly, the insulation packed at the top and bottom ends of the furnace can result in a frictional force if packed too tightly. This frictional force results in inaccurate force measurements. Secondly, and more significantly, when the load on the sample is zeroed at the beginning of a test, part of the load train experiences a compressive force. This is a problem since the load train is mounted between rod end bearings (which ensure axiality of loading during testing), which cause the load train to buckle sideways and rest slightly on the insulation and/ or the inner tube of the furnace. This effectively means that the resultant force measured by the laod cell is erroneous.

Consider the schematic diagram of the load train in figure C1. Note that the red arrows represent various forces.

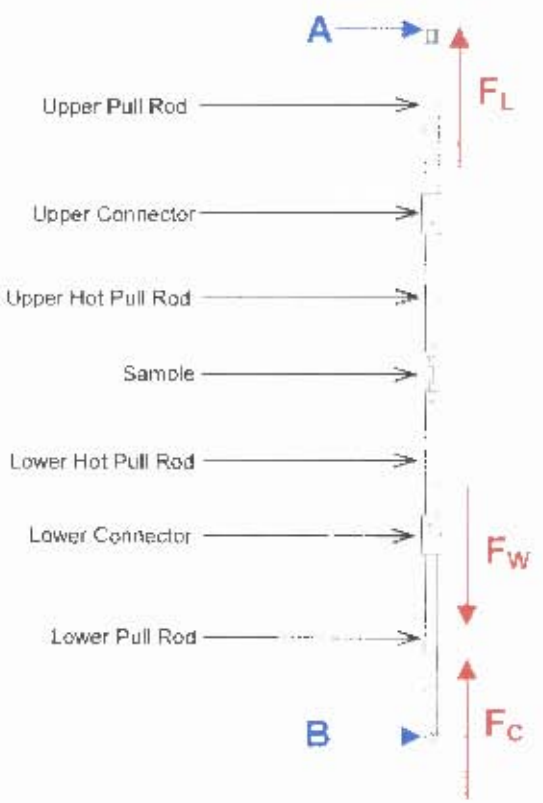


**Figure C1:** Schematic of current load train. A and B represent the positions of the pivot points (rod end bearings). The directions of the forces are drawn for the condition where the load on the sample is zero.

The forces depicted in figure C1 are as follows:

$F_L$ is the force applied to the load train via the lever.

$F_W$ is the weight of the lower hot pull rod, connector, pull rod and extensometer (not shown)

$F_C$ is the reaction force at the load cell situated just beneath point B.

It can be seen that the lower portion of the load train is in compression, allowing the load train to swing sideways about point B.

The proposed recommendations include moving the pivot from point B to approximately the position of the lower connector and redesigning the lower pull rod. The load cell is removed from the load train altogether and placed on the weight pan assembly. These recommendations require minimum cost and time of production to complete and will therefore not hinder any further projects greatly.

## Details of the Proposed Design Recommendations

**(i) Lower Pivot Point**

It is recommended that the lower pivot point be moved from point B (in figure C1) to the lower end of the lower hot pull rod. This enables tests to be set up with minimal weight 'hanging' from the sample. This weight will equal that of the lower hot pull rod and the extensometer system (about 2MPa using the sample design of the current investigation) and will have to be tolerated while setting up a test (i.e. the load on the sample cannot be zeroed, but rather minimized to a value which will be constant for every test conducted). It should be noted that this is the case with many commercial constant load creep test rigs.

**(ii) Lower Pull Rod**

It is recommended that the lower pull rod be modified from a single rod to two smaller rods side-by-side and joined by braces at the top and bottom. This will enable the center of weight of the extensometer system to be directly in line with the axis of loading, ensuring that no loading eccentricities occur due to the presence of the extensometer system.

**(iii) Extensometer**

Since the lower pull rod is to be modified to allow the extensometer to be properly aligned with the tensile axis, the existing aluminium extensometer plates, which house the LVDT, need to be replaced with similar plates that allow the LVDT to be positioned along the tensile axis of the load train.

**(iv) Load Cell Placement and Use**

If the weight of the lower hot pull rod and extensometer system is known, then the force on the sample before testing is known ***exactly***. If the mass of the weights placed on the weight

pan are carefully measured before applying the load and the lever ratio is applied, the constant load on the sample can be calculated accurately without the use of the load cell. Thus the load cell is essentially made redundant in this case. It may be possible to include the load cell in the weight pan assembly, in which case it would function as a scale, measuring the mass of the weights placed on the weight pan, otherwise, the possibility of keeping the load cell in the load train assembly could be investigated ***changes*** in the sample load were to be monitored. Of course no changes in the sample load should be expected between the application of the load and the termination of a test.

Figure C2 shows a schematic assembly of the proposed modified load train. Technical drawings for new and modified parts required are also included.

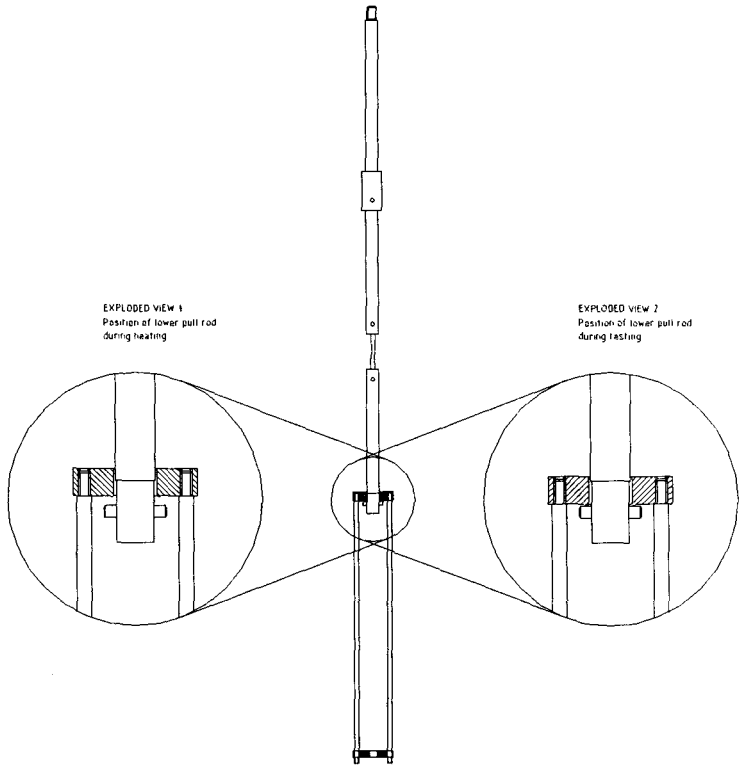


**Figure C2:** Schematic of recommended load train modifications. Note that the lower pull rod assembly is fixed and can move up and down on the screw jack.

During heating, the screw jack is raised to ensure that only the lower hot pull rod and pin are weighing on the sample (see exploded view 1 in figure C2). The screw jack is lowered just prior to application of the load to ensure that the load train is taut and that the applied load is accurate (see exploded view 2 in figure C2).

## Creep Test Set-up Procedure

The basic procedure to follow in setting up a creep test using the modified design is as follows.

1. Insert sample into grips.
2. Attach extensometer clamps to sample gauge length (see figure 3.5 in § 3.4.4). Ensure that clamps are secure to prevent slippage during testing.
3. Insert monitoring thermocouples into furnace from the top and position one as close to the top of the gauge length as possible and one as close to the bottom of the gauge length as possible. Ensure that thermocouples are securely attached to upper pull rod assembly.
4. Adjust the counter weight on the lever (see figure 3.4 in § 3.4.2) until the lever is more or less horizontal.
5. Adjust the screw jack such that the lower hot pull rod and pin are hanging completely free from the lower pull rod assembly (see figure C2, exploded view 1).
6. Gently lower the furnace over the sample making sure that nothing clashes with the brittle furnace tube.
7. Check that the load train is hanging completely free from the furnace and other components.
8. Pack insulation very gently into the open ends of the furnace. Tight packing (in the radial direction of the furnace tube) of the insulation will result in friction on the load train and change the desired applied load. Check that the insulation does not move the lower hot pull rod and pin into contact with the lower pull rod assembly (see figure C2, exploded view 1).
9. Switch on furnace and set all three zones of the furnace to the desired testing temperature.
10. When the set temperature has been reached on the furnace temperature controllers, check that the temperature distribution shown by the monitoring thermocouples is within acceptable limits.
11. Using the screw jack, slowly adjust the lower pull rod assembly downwards until the top brace of the lower pull rod assembly is just touching the pin through the lower hot pull rod (see figure C2, exploded view 2).
12. Ensure all the information entered into the data acquisition system is correct and start logging.
13. Gently load the required weight onto the weight pan. (Remember to take into account the correct lever ratio when calculating the required weight pan load.)

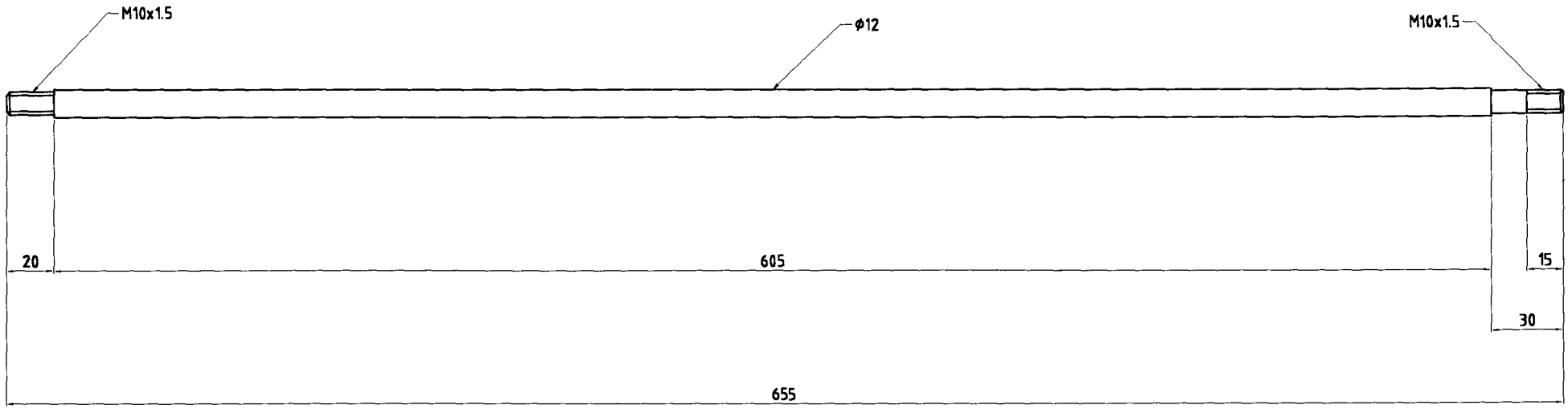


**UNIVERSITY OF CAPE TOWN**
CENTRE FOR MATERIALS ENGINEERING

NOTES:
Quantity: 2 parts per assembly
Material: AISI 316 Stainless Steel

DRAWING NUMBER: C1

All dimensions in mm.
All tolerances 0.2mm unless otherwise stated.

TITLE: MODIFIED LOWER PULL RODS

DRAWN BY: Michael Dollman

DATE: 19/03/2003

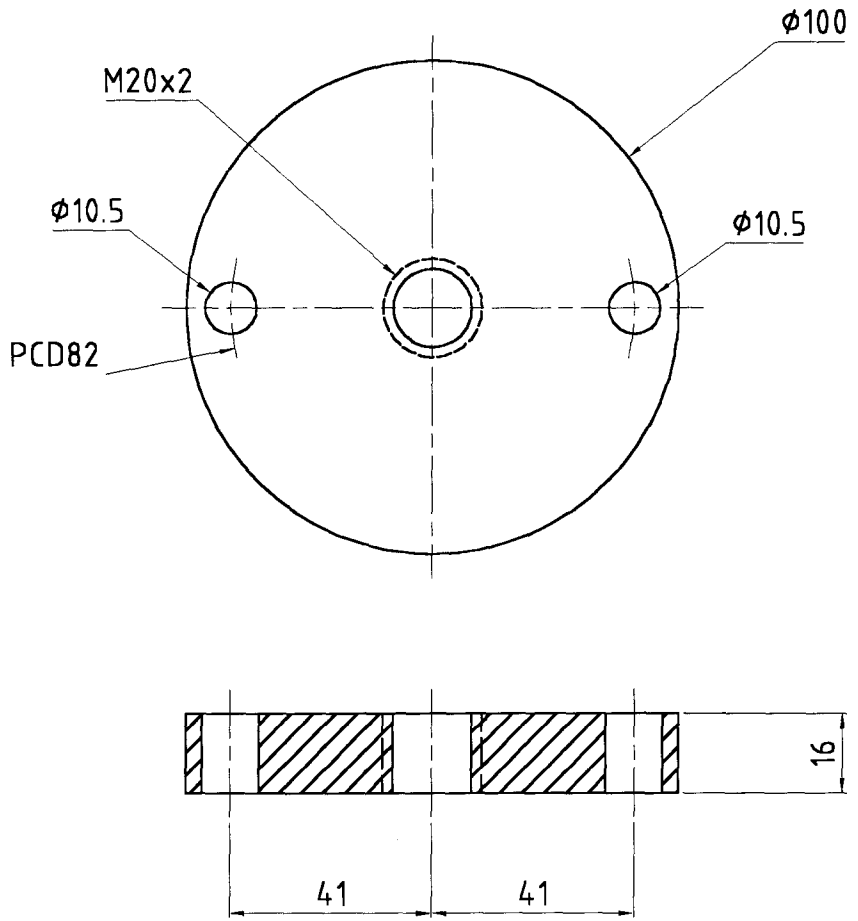


**UNIVERSITY OF CAPE TOWN**
CENTRE FOR MATERIALS ENGINEERING

NOTES:

Quantity: 1 per assembly

Material: AISI 304 or 316 Stainless Steel

DRAWING NUMBER: C2

All dimensions in mm.
All tolerances 0.2mm unless otherwise stated.

TITLE: LOWER PULL ROD BRACE

DRAWN BY: Michael Dollman

DATE: 19/03/2003

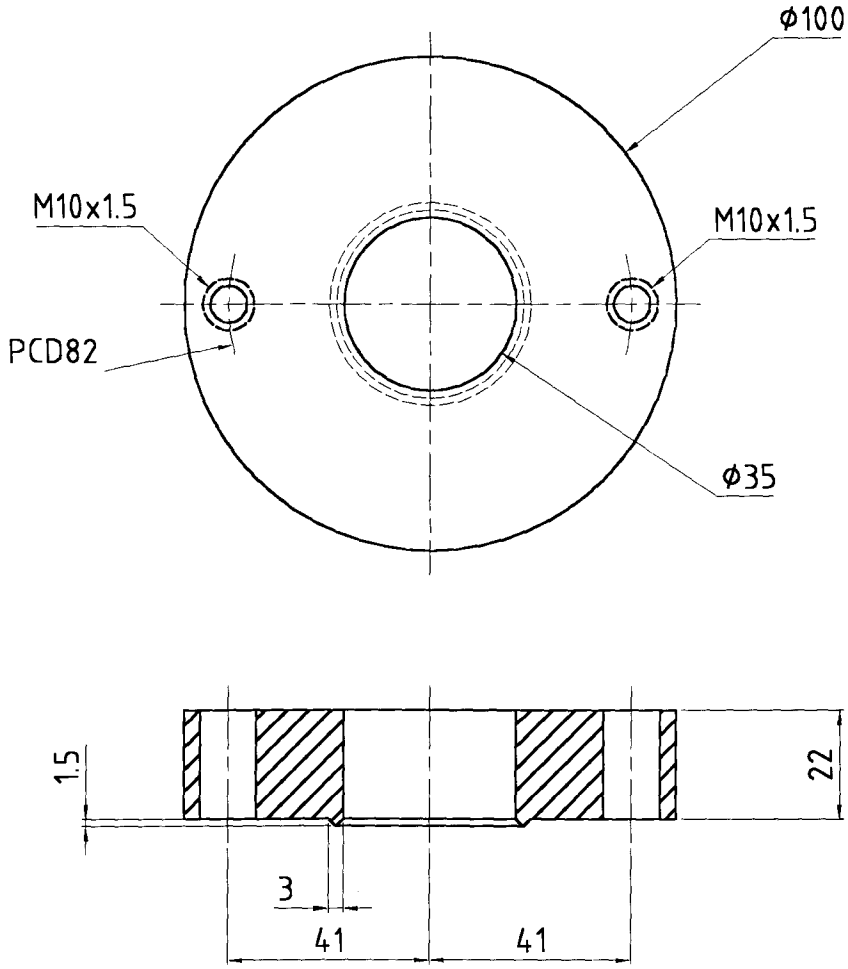


**UNIVERSITY OF CAPE TOWN**
CENTRE FOR MATERIALS ENGINEERING

NOTES:
Quantity: 1 per assembly
Material: AISI 310 or 316 Stainless Steel

DRAWING NUMBER: C3

All dimensions in mm.
All tolerances 0.2mm unless otherwise stated.

TITLE: UPPER PULL ROD BRACE

DRAWN BY: Michael Dollman

DATE: 19/03/2003

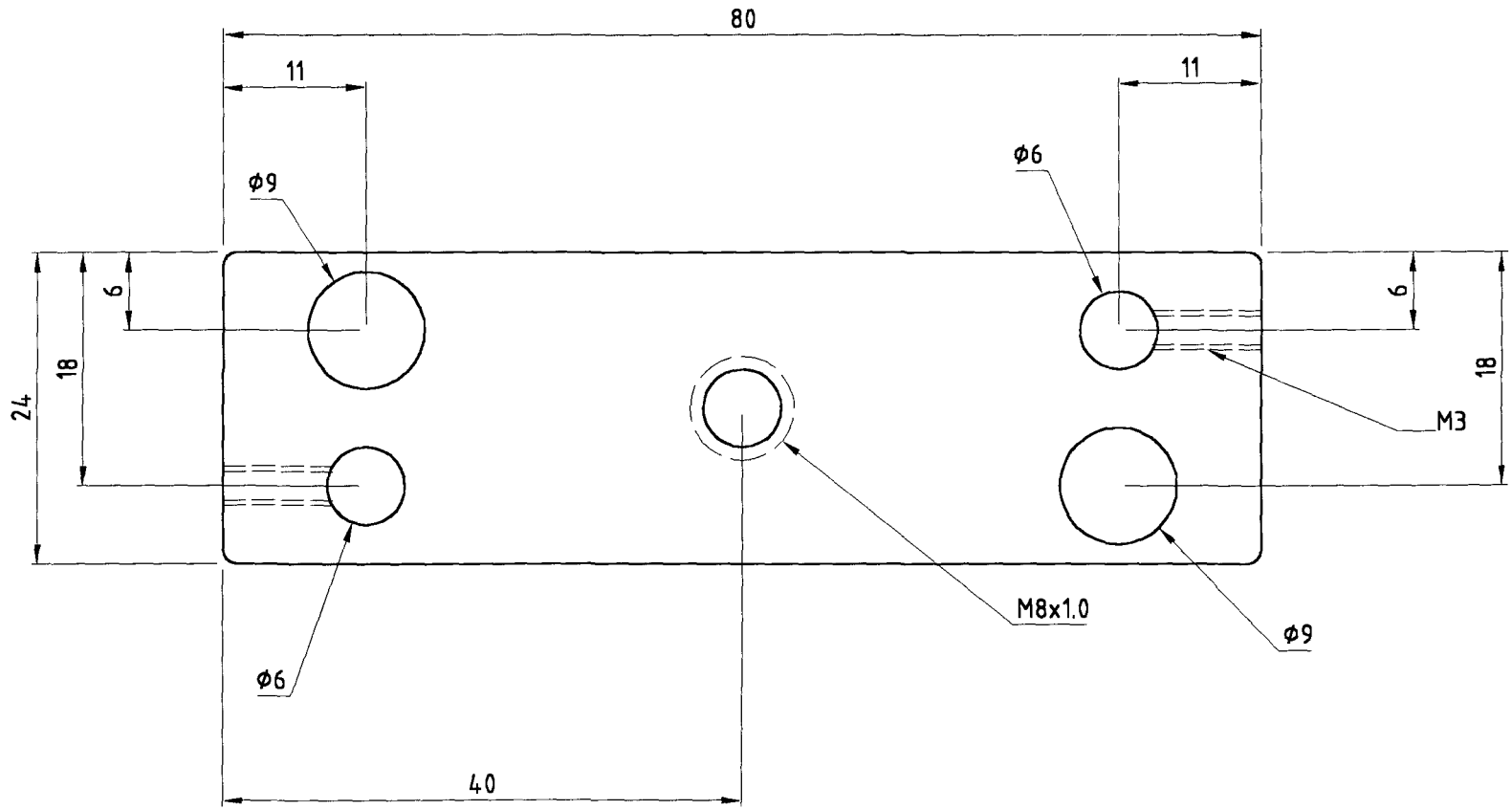


**UNIVERSITY OF CAPE TOWN**
CENTRE FOR MATERIALS ENGINEERING

NOTES:
Quantity: 1 per assembly
Material: 6061 Aluminium
Material Thickness: 6 mm

DRAWING NUMBER: C4

All dimensions in mm.
All tolerances 0.2mm unless otherwise stated.

TITLE: UPPER EXTENSOMETER PLATE

DRAWN BY: Michael Dollman

DATE: 19/03/2003

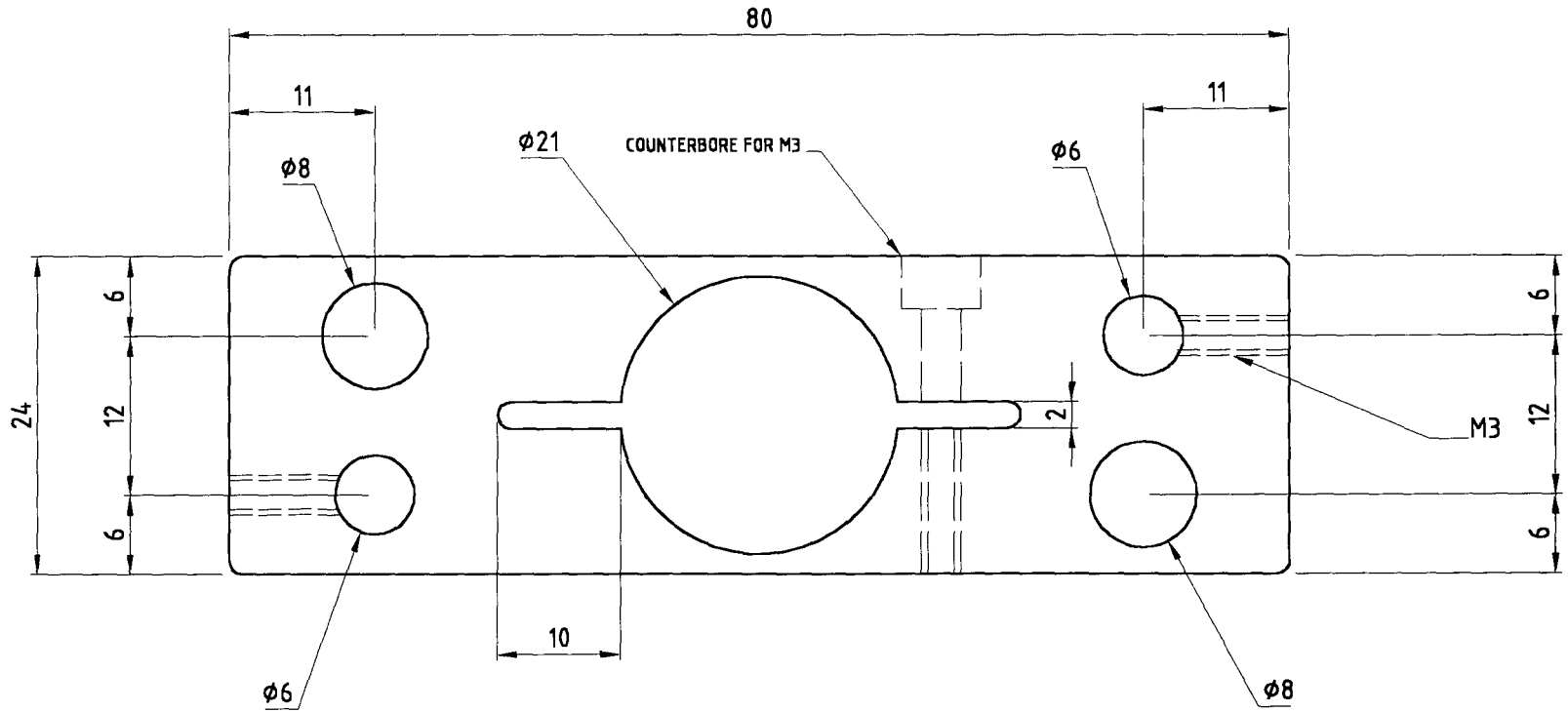


**UNIVERSITY OF CAPE TOWN**
CENTRE FOR MATERIALS ENGINEERING

NOTES:
Quantity: 1 per assembly
Material: 6061 Aluminium
Material Thickness: 6 mm

DRAWING NUMBER: C5

All dimensions in mm.
All tolerances 0.2mm unless otherwise stated.

TITLE: LOWER EXTENSOMETER PLATE

DRAWN BY: Michael Dollman

DATE: 19/03/2003

# APPENDIX D

## Calculation of Approximate Stress in Sag Test Sample

The details of a rough approximation to the stress on a sag test sample are shown below. The sample was assumed to be a straight, flat, simply supported beam, the weight of which was taken to be a uniform distributed load, $w$.

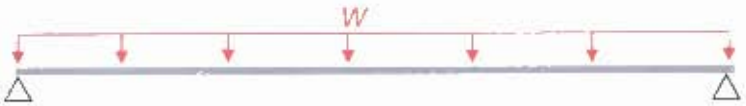


The distributed load was calculated as follows:

$$w = \frac{\rho bdlg}{l} = \frac{(7800)(0.0254)(0.0015)(0.254)(9.81)}{0.254} = 2.915Nm$$

where,

$w$ is the uniformly distributed weight of the sample

$\rho$ is the density of the sample

$b$ is the width of the sample

$d$ is the thickness of the sample

$l$ is the length of the sample

$g$ is the gravitational acceleration constant.

The maximum bending moment can be found by the following formula:

$$M_{MAX} = \frac{wl^2}{8} = \frac{(2.915)(0.254)^2}{8} = 0.0235Nm$$

The bending stress is found as follows:

$$\sigma = \frac{My}{I} = \frac{(0.0235)(0.00075)}{3.175 \times 10^{-6}} = 5.6MPa$$

where,

$M_{MAX}$ is the maximum bending moment experienced by the sample

$y$ is the distance from the neutral axis

$I$ is the moment of inertia given by $I = bd^3/12$ for rectangular samples.

It is important to note that this calculation neglects certain effects, such as:

- One end of the sample hangs over the one support by approximately 35mm reducing the overall stress in the tested section of the sample.

- The sample experiences a frictional force at the supports, which has not been taken into account.
- The samples are usually slightly bent before testing starts, thus the assumption that the samples are straight and flat is not necessarily true.

For the above reasons, it might be expected that the value of 5.6 MPa is slightly exaggerated, however it would be fair to guess that the actual stress in the sample during testing is approximately in the region of 3 – 4 MPa.